

**Seismic and Hydroacoustic Studies
of Surficial Sediment Tectonics
along the Northern Red Sea Rift
and the Dead Sea Transform Fault**

Dissertation

zur Erlangung des Doktorgrades
der Naturwissenschaften im Fachbereich

Geowissenschaften

der Universität Hamburg

vorgelegt

von

Lutz Axel Ehrhardt

aus

Köln–Porz

Hamburg, 2004

Als Dissertation angenommen vom Fachbereich
Geowissenschaften der Universität Hamburg
auf Grund der Gutachten von Prof. Dr. Dirk Gajewski
und Dr. Christian Hübscher

Hamburg, den 12.11.2004

Prof. Dr. H. Schleicher
Dekan
des Fachbereichs Geowissenschaften

Contents

1	Introduction	1
2	Data Acquisition and Processing	7
2.1	HYDROSWEEP Swath Echosounder	7
2.2	PARASOUND Sediment Echosounder	8
2.3	Multichannel Seismic Data Acquisition	9
2.3.1	Seismic Source	10
2.3.2	Acquisition Geometry	10
2.3.3	Data Processing	11
3	Evaporites in the Red Sea Rift	15
3.1	Deposition of Evaporites	15
3.2	Stratigraphic Evolution of Evaporite Basins	15
3.3	Physical Properties of Salt Systems	16
3.4	Physical Properties of Rock Salt and its Implications to Seismic Measurements	17
4	Seismic Study of Pull–Apart Induced Sedimentation and Deformation in the Northern Gulf of Aqaba (Elat)	19
	<i>by A. Ehrhardt, C. Hübscher, Z. Ben-Avraham and D. Gajewski in Press, Tectonophysics, 2005</i>	
4.1	Abstract	19
4.2	Introduction	20
4.3	Geological Setting	22
4.4	Previous Work	23
4.5	Geophysical Data	26
4.5.1	Bathymetric Data	26
4.5.2	Reflection Seismic Data	27
4.6	Fault System and Seismic Stratigraphy	36
4.7	Discussion	43
4.7.1	Comparison to Previous Results	43
4.7.2	Comparison to Analog Models	45
4.8	Conclusion	46
4.9	Acknowledgments	48

5 Conrad Ocean Deep, Northern Red Sea: Transtension Basin within the Axial Depression	49
<i>by A. Ehrhardt, C. Hübscher and D. Gajewski</i>	
<i>submitted to Tectonophysics, 04/2004</i>	
5.1 Abstract	49
5.2 Introduction	50
5.3 Geological Setting	51
5.4 Previous Work in the Northern Red Sea	56
5.5 Methods and Results	58
5.5.1 Bathymetry	58
5.5.2 Seismic Data	59
5.5.3 Results	63
5.6 Interpretation and Discussion	71
5.7 Conclusions	77
5.8 Acknowledgements	78
6 Development of the Conrad–, Shaban– and Kebrit Deeps, northern Red Sea, based on Seismic and Hydroacoustic Data	79
<i>by A. Ehrhardt, C. Hübscher and D. Gajewski</i>	
<i>submitted to Marine Geology, 07/2004</i>	
6.1 Abstract	79
6.2 Introduction	80
6.3 Geological Setting	80
6.3.1 The Northern Red Sea	80
6.3.2 The Deeps	84
6.4 Methods and Results	86
6.4.1 Bathymetry	87
6.4.2 Seismic Data	90
6.5 Discussion	101
6.5.1 Conrad– and Shaban Deeps	101
6.5.2 Kebrit Deep	103
6.5.3 Segmentation controlled development	105
6.6 Conclusions	105
6.7 Acknowledgements	109
7 Summary and Conclusions	111
References	117
Acknowledgements	125

1 Introduction

The Red Sea Rift and the Dead Sea Transform are the main tectonic structures in the Middle East. Since the onset of the Red Sea rifting in the Oligocene (Pircard, 1987), when the formerly continuous African-Arabian Plate was fragmented, the Red Sea Rift controls the tectonic development in the Middle East. The Euler pole of the Red Sea Rift is located in the eastern Mediterranean region (Joffe and Garfunkel, 1987) (Fig. 1.1). Because of the close distance between the Euler pole and the Red Sea, the rifting velocity becomes significantly faster towards the south. As a result of this reasonable gradient in the rifting velocity, different stages of evolution have been established along the 2000 km long Red Sea Rift. The northern part of the Red Sea is in the late stage of continental rifting (Cochran et al., 1986), whereas the southern part exhibits already organized seafloor spreading for the past 5 Ma (Röser, 1975); the central part is in a transition stage from rifting to drifting. This makes the Red Sea a unique place in the world to study the evolution from continental rifting to seafloor spreading. In the Miocene, about 20 Ma ago (Courtilot et al., 1987), a major change occurred in the Red Sea Rift. The extension was no longer compensated in the north by the Gulf of Suez, but by the newly developing left lateral Dead Sea Transform (DST). The DST forms a continental transform fault that extends over a distance of 1200 km from the triple point in the Red Sea to the Taurus Zagros Orogenic Belt (Fig. 1.1). 105 km of left lateral displacement were compensated along the DST and subparallel faults until now. On its southern extension, three major pull-apart basins are arranged in an en-echelon pattern and form the Gulf of Aqaba (Fig. 1.2). Because the Gulf is connected to the Red Sea, the continental transform fault runs into a marine environment. This is one of two locations worldwide (the other is the Gulf of California, Imperial Valley) (Ben-Avraham, 1985) to study a continental transform fault with marine geophysical methods.

So, the Red Sea Rift and the DST provide an excellent tectonic framework to study the progression from rifting to seafloor spreading and the development of pull-apart basins, but the necessary basement observations to validate the status of the rift or the transform fault are missing. For the Red Sea, the crucial point are the massive evaporites that were deposited during the Miocene (Searle and Ross, 1975; Guennoc et al., 1988; Gaulier et al., 1988; Martinez and Cochran, 1989) in the main trough of the Red Sea (Fig. 1.2). The special physical properties of the evaporites, which consists mostly out of precipitated salt hinder the observation of the basement structure in two ways. (I) The significantly lower viscosity of the salt has led to a decoupling of the basement from the overburden so that basement structures like faults are not necessarily reflected in the surficial sediments. (II) The high seismic velocity of the evaporites in comparison

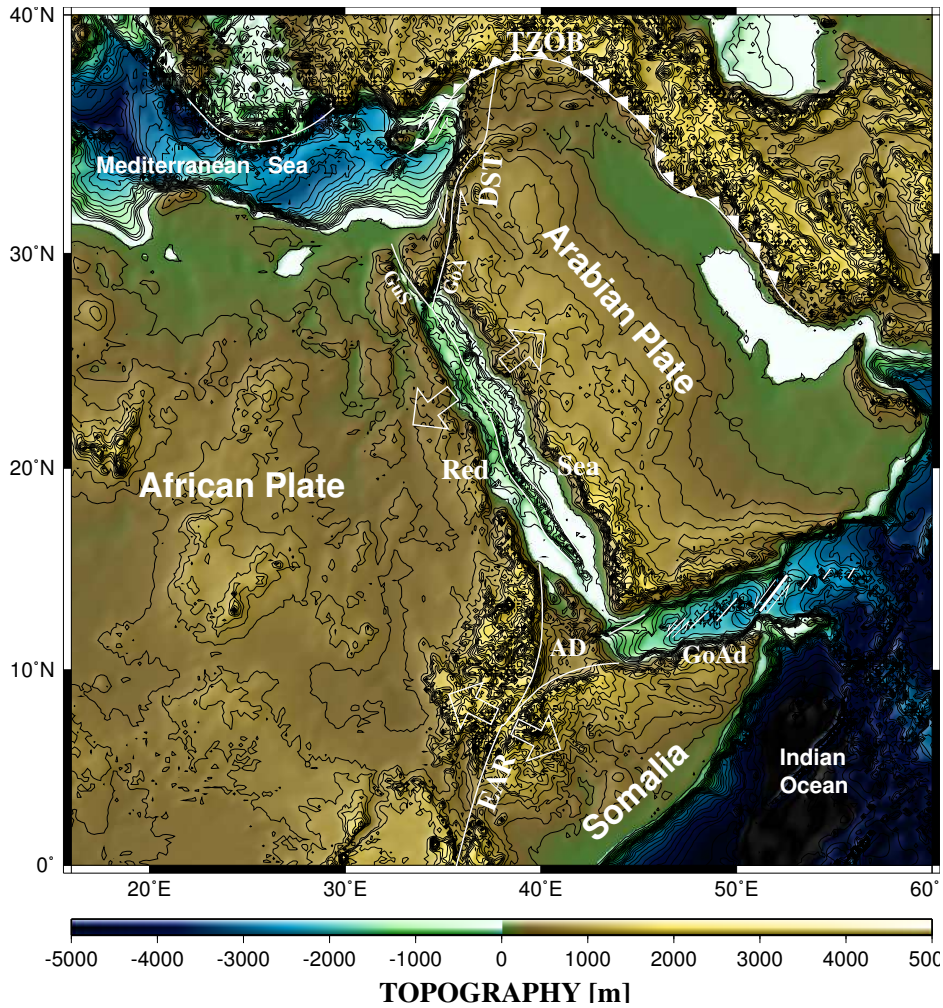


Fig. 1.1: The rift system includes, starting from the south, the East African Rift (EAR), the Gulf of Aden (GoAd) and Afar Depression (AD), the Red Sea, the Gulf of Suez (GoS), the Gulf of Aqaba (GoA) and the Dead Sea Transform. It terminates in the north against the Taurus Zagros Orogenic Belt (TZOB). The main faults are marked with white bold lines (after Joffe and Garfunkel, 1987; Rihm, 1989); rifting and transform motion are indicated by the white arrows. The location of the Red Sea poles is inserted (after Joffe and Garfunkel, 1987). The basic topography and bathymetry are extracted from the Gebco dataset (Gebco-Atlas, 2004)

to the overlying sediments, yield a remarkable high impedance contrast. For these reasons the evaporite layer is difficult to penetrate with seismic methods. As a matter of fact, direct basement observations by seismic methods are very rare in the northern Red Sea and the nature of the basement type is still being discussed.

As experienced previously in the northern Red Sea, imaging of the basement in the Gulf of Aqaba failed. The obstacle lies in the narrow shape of the Gulf that is only about 5 km across at its top end. In addition, the basement is covered

by a considerable amount of sediments that has been deposited in the Gulf. Because of the narrow shape of the Gulf only a small streamer offset could be used for the data acquisition which had a negative impact on the data quality. Another obstacle might potentially turn out to be the major reason why so little is known about the fascinating and unequaled study areas of the Red Sea Rift and the Gulf of Aqaba. The entire region belongs to the territorial waters of the abutting states. Some of the small ocean deeps are even split between two states. To obtain research permits for all of the territorial waters is difficult and so in some cases we were forced to stop the acquisition over crucial points of the area. Nevertheless, during M44/3 we had the unparalleled chance to acquire data in the territorial waters of Jordan, Egypt and Israel, which led to an unique dataset of the northern Gulf of Aqaba.

Because of the lack of direct basement observation, surficial structures were analyzed to draw conclusions about the basement. The most conspicuous surficial structures in the Red Sea are the Red Sea Ocean Deeps. These deeps are mostly located in the axial trough or depression of the Red Sea (Fig. 1.2), often accompanied by magmatic intrusions or extrusions (Cochran et al., 1986; Martinez and Cochran, 1988; Coutelle et al., 1991). Bonatti (1985) proposed that the deeps form initial seafloor spreading cells. In the central Red Sea, seafloor spreading

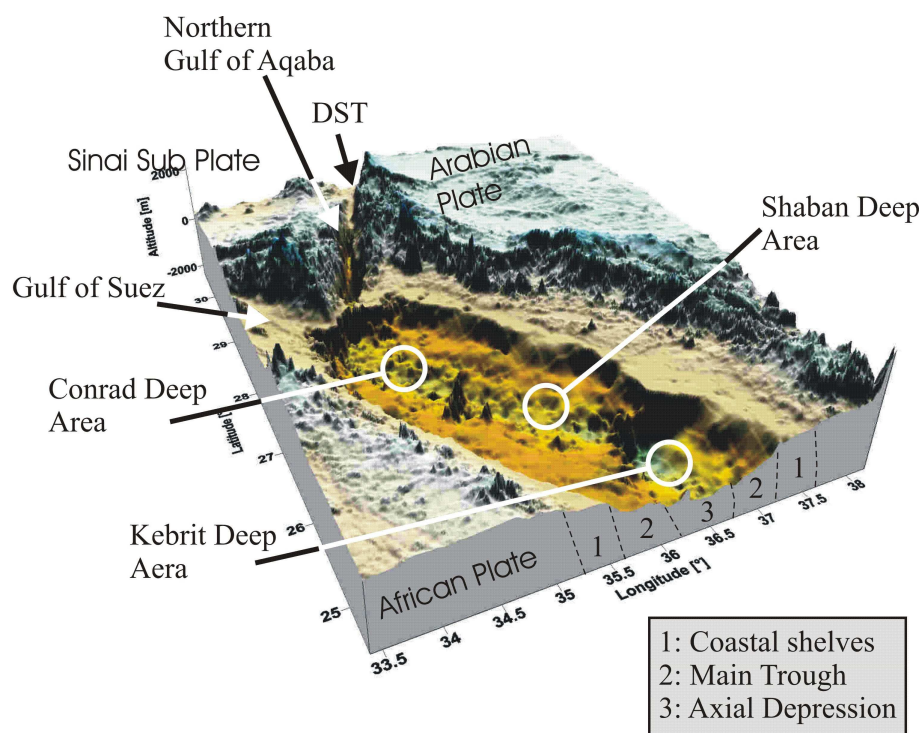


Fig. 1.2: 3D-blockimage of the northern Red Sea and the Gulf of Aqaba. The survey areas are located in the axial depression and the northern Gulf of Aqaba. These are the most active areas regarding the latest development of the Red Sea rift and Dead Sea Transform.

has been active since 1.7 Ma ago (Searle and Ross, 1975) within some deeps, but the northern deeps are less developed and only occasionally associated with isolated magmatic intrusions. These deeps probably provide the only possibility to derive information about the dynamics of the northern Red Sea rift, but until now the development of the deeps is not fully understood.

Similar to the rift structures of the Red Sea, the basement below the Gulf of Aqaba is not yet imaged; additionally, the political borders so far prevented the acquisition of a continuous dataset of this area. Because of the insufficient information about the eastern part of the northern Gulf, the derivation of models was not completely based on data but also on speculation. The investigation of the surficial structures of the entire northern Gulf could lead to a new model of this area that could also provide information about the deeper crustal dynamics of the northern Gulf.

A new approach to investigate the development of surficial structures like pull-apart basins and ocean deeps was started with the R/V Meteor cruises M44/3 and M52/3 in the northern Gulf of Aqaba and the northern Red Sea. These investigations might lead to models describing the crustal dynamics. Following a new strategy, only specifically selected structures were investigated by multi-channel seismic and hydroacoustic methods. The extension of the survey area was reduced in favor of a dense and complete coverage within the survey area. The spacing of the high resolution multichannel seismic lines was close enough for the interpolation of subsurface structures. Swath echosounder and sediment echograph (Hydrosweep and Parasound) data completed the data acquisition. Thus far, nine ocean deeps were discovered in the northern Red Sea. The most conspicuous deep is the Conrad Deep, because of its elongated shape parallel to the Dead Sea Transform and its location between two magnetic anomalies. These magnetic anomalies point to magmatic intrusions that might have affected the development. The apparent morphology of the Conrad Deep constricts the theories for its development; therefore this deep provides a good opportunity to derive a general model for the development of ocean deeps. In a next step this model must be confirmed at other deeps. In order to apply this model to other deeps, the Shaban- and Kebrit Deep were investigated. The Shaban Deep is also affected by magmatic activity. A single volcanic edifice builds a central ridge within the Deep. The Kebrit Deep shows no evidence for magmatic activities that could have influenced its development.

In the Gulf of Aqaba the northern part of the Elat Deep and its transition to the onshore Arava Valley was observed in order to identify and map the step over of the Dead Sea transform. In this area the Elat Deep pull-apart basin terminates against the transition zone, which is also potentially affected by a Miocene graben structure. During the cruise M44/3 in 1999 a unique opportunity to collect a dataset of the entire northern Gulf of Aqaba occurred. This new evidence about the eastern part of the northern Gulf contributes to a detailed map of the surficial fault system and sedimentary pattern.

Agenda

The objectives of this study are the reconstruction of recent basin formations along the DST and the axial depression of the northern Red Sea, as they are both linked to the rifting between the African- and Arabian Plates. The inherent structures of the studied basins provide evidence for the driving forces for their development and possible conclusions for the deeper crustal processes that are masked by the sedimentary cover.

This work is structured as follows:

1. The geological and tectonic setting of the northern Red Sea, the Gulf of Aqaba and the DST will be introduced.
2. Description of the data acquisition and processing, as the results of this study are mainly based on the seismic and hydroacoustic data.
3. The deposition of salt and its special physical properties, since they play a key role in the recent basin building processes in the Red Sea and the northern Gulf of Aqaba.

The results of the work on the geophysical datasets will be presented in the following three chapters. Every chapter is composed of an article that has been submitted or is close to submission to an appropriate scientific journal:

4. Seismic study of pull-apart induced sediment tectonics in the northern Gulf of Aqaba (Elat)

(Ehrhardt, A., Hübscher C., Ben-Avraham Z. and Gajewski D., submitted to *Tectonophysics* 12/2003)

This chapter describes the bathymetric and seismic structure of the Gulf's Head and the northern part of the Elat Deep. The surface expression of the DST was mapped for the first time. The inherent structure of the northern Elat Deep and the Gulf's Head lead to new theories concerning the pull-apart history of the Elat Deep.

5. Conrad Ocean Deep, Northern Red Sea: Transtension Basin within the Axial Depression.

(Ehrhardt, A., Hübscher C. and Gajewski D., submitted to *Tectonophysics* 05/2004)

The Conrad Deep, as one of the northernmost Red Sea Deeps was investigated regarding its structure and the driving forces that caused its formation. Because it is a very young basin, the formation induced faults and folds within the sediments are not overprinted by the continuous extension of the Red Sea. With these results a model for the development of the Conrad Deep was derived.

6. Comparison of three northern Red Sea Deeps.

(Ehrhardt, A., Hübscher C. and Gajewski D., submitted to *Marine Geology*)

The Conrad-, Shaban- and Kebrit Deeps will be compared concerning their formation mechanisms. All three deeps are in the northern part of the Red Sea and are in an early stage of their development. The analysis of the internal structure gives evidence that there is a common pattern for their development.

7. A chapter 'Summary and Conclusions' will recapitulate the results of the main chapters and figure out the similarities of surficial basins in active tectonic regions and their implications to crustal processes.

2 Data Acquisition and Processing

In this work multichannel seismic, bathymetric and sediment echosounder data will be presented. The data acquisition was conducted during two cruises of R/V Meteor in 1999 and 2002 (see M44/3 by Hübscher et al., 2000) and (M52/3 by Ehrhardt & Hübscher, 2003). Whereas the multichannel seismic equipment was different, related to the participating Institutes, the bathymetric (HYDROSWEEP) and sediment echograph (PARASOUND) devices were installed on board of the research vessel.

Survey Areas and Base Maps

In this work four different survey areas are processed that are located in the northern Gulf of Aqaba and the northern Red Sea. In the Red Sea the Conrad-, Shaban- and Kebrit deeps were investigated, as well as the northernmost Gulf of Aqaba (see Fig. 2.1). For the number of lines and their total length, please refer to Table 2.1. The planning of the survey areas was done with special emphasis on a close lines spacing, in order to enable the interpolation of subbottom structures, and to achieve a complete coverage of the seafloor topography by the swath echosounder.

All survey areas are located in the territorial waters of the abutting states of Jordan, Egypt, Israel and Saudi Arabia. The research permits during the cruises M44/3 and M52/3 were different and not always sufficient for the entire extension of geologic interrelated regions. For this reason the survey areas are limited in some cases, especially the Shaban Deep belongs to the territorial waters of Egypt and Saudi Arabia. Since we had only one research permit at a time during the cruises M44/3 and M52/3, it was unfortunately not possible to acquire data crossing the deep from west to east.

2.1 HYDROSWEEP Swath Echosounder

The swath echosounder worked continuous in 24 hour modus, monitored by the vessel staff. A swath width of twice the water depth and a dense line spacing in the survey areas led to a complete coverage of the seafloor topography. Owing

	Gulf of Aqaba	Conrad Deep	Shaban Deep	Kebrit Deep
Cruise	M44/3	M44/3	M44/3, M52/3	M52/3
No. of lines	16	13	24	17
Total	143 km	135 km	250 km	125 km

Table 2.1: General informations about the seismic survey areas

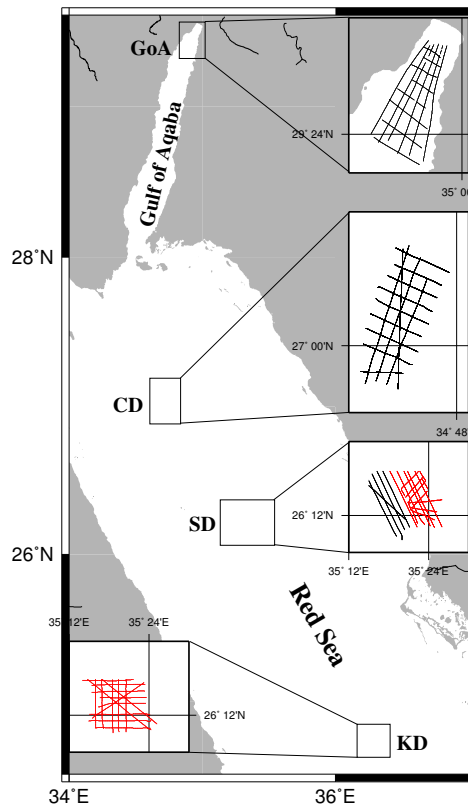


Fig. 2.1: Survey area of the Cruises M44/3 and M52/3. GoA: Gulf of Aqaba; CD: Conrad Deep; SD: Shaban Deep; KD: Kebrit Deep. The lines of cruise M52/3 are in red, M44/3 in black.

to the variations in the velocity depth function of the water column and the compensation of the sea state the vertical error is in the order of 1% - 3%.

The processing of the swath echosounder data was performed with MB-Systems software. After the transformation of the data from Hydrosweep format (by STN ATLAS) into a MB-Systems internal format, bad traces or complete bad beams were edited by different filter tools and finally by a complete check of every single beam using an interactive graphical user interface. The resulting datasets were gridded with GMT¹ for further use. In the following, the presented bathymetric maps were computed and produced with GMT.

2.2 PARASOUND Sediment Echosounder

The sediment echosounder worked also in 24 hour modus and was operated by the scientific staff. It worked both, as high frequency navigation echosounder

¹Generic Mapping Tools (see <http://gmt.soest.hawaii.edu>)

	M44/3	M52/3
Source	1 GI-Gun	2 GI-Guns
Volume	2 x 0.4 l	2 x 0.7 l/Gun
Dominant Frequency Bandwidth	20 Hz – 350 Hz	20 Hz – 300 Hz
Time Shot Interval	10 s	8 s
Spatial Shot Interval	approx. 25 m	approx. 20 m
	(Ship velocity 4.9 knots)	
Streamer	SYNTRON	Prakla
No. of Channels	24	
Active Length	300 m	150 m
Sampling Interval	0.5 ms	1 ms
Group Interval	12.5 m	6.25 m
CMP Interval ¹	12.5 m	6.25 m
Average Fold ¹	12	6

Table 2.2: Seismic Acquisition Parameters **M44/3** and **M52/3**. Explanation of the parameters in the text

and as low frequency subbottom profiler. The Parasound system takes advantage from the parametric effect. Two frequencies are emitted (18 and 22 kHz) with a rate of 400 ms. Within a narrow emitting cone of 4° a difference signal is generated within the upper meters of the water column owing to the non linear terms of the wave equation. Therefore the foot print is approximately 7% of the water depth which omits generally the existence of diffraction hyperbola. Thus the Parasound data yield an excellent lateral and vertical resolution. The main processing steps include subtraction of mean noise, frequency filtering (2.5 - 5.5 kHz), and trace scaling. Amplitudes above a defined threshold are clipped. Subsequently amplitudes are converted into grey scale images. Since the resolution of the print media (expressed in dpi) is often less than the seismic resolution, mean amplitudes are calculated for each dot to print.

2.3 Multichannel Seismic Data Acquisition

The seismic measurements were conducted with two different setups, according to the different cruises (see Table 2.2). The surveys of the northern Gulf of Aqaba, the Conrad Deep and the western side of the Shaban Deep were performed during the cruise M44/3; the eastern side of the Shaban Deep and the Kebrit Deep were investigated during the cruise M52/3.

¹The regular CMP distance was doubled in order to increase the fold

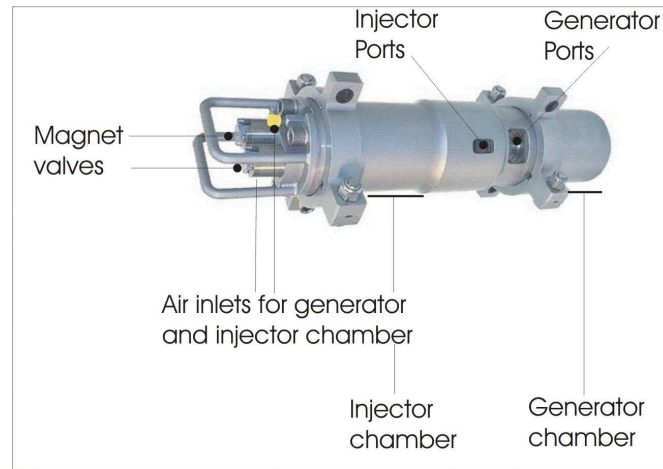


Fig. 2.2: GI-Gun (Generator/Injector): Marine seismic source with two chamber system in order to suppress the bubble energy.

2.3.1 Seismic Source

GI-Gun (Generator/Injector): The GI-Gun is a two chamber airgun that was designed to reduce or even to eliminate the bubble of the seismic signal (see Fig. 2.2). Therefore the generator chamber will be released to create a signal. After a determined period of time, the injector chamber will be released into the bubble of the generator signal in order to reduce or prevent the oscillation of the bubble. The chamber volumes are variable; please refer to Table 2.2 for the source details for the individual cruises. The arrangement of the seismic sources differed between both cruises. During the cruise M44/3, a single GI-Gun with reduced chamber volume was used, in order to resolve the structure of the Plio-Quaternary sediments above the Miocene evaporites. Figure 2.3 shows shot-gathers and the corresponding frequency content extracted from a representative line of M44/3. An array of two GI-Guns was used during the cruise M52/3. With the enhanced signal energy possible intra-evaporitic structures should be imaged.

2.3.2 Acquisition Geometry

During the cruise M44/3 the streamer length was reduced to 300 m and 24 channels, because of the narrow survey areas in the northern Gulf of Aqaba and northern Red Sea (Fig. 2.4). Because of the small streamer length the vessels flexibility was good enough to run a dense grid of seismic lines in a minimum amount of time.

During the cruise M52/3 only a mini-streamer with an active length of 150 m, was available. Again, the flexibility of the vessel was very good and a dense grid of seismic lines was measured. Unfortunately, the small offsets led to an insufficient hyperbolic moveout of events within the CMP gathers, so that velocity

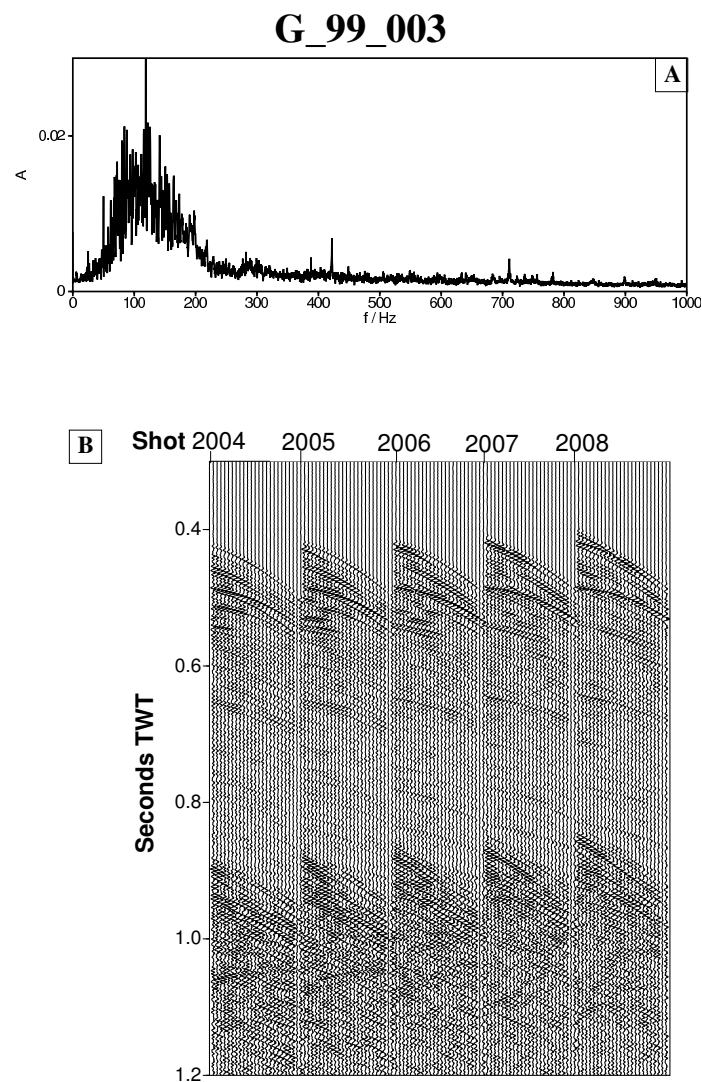


Fig. 2.3: A: Spectrum of a stacked trace of the cruise M44/3, line G_99_003 (one GI-Gun, volume reduced). Frequencies above 300 Hz were filtered because of spatial aliasing. B: Associated shot gathers. The data quality is reasonable good; weak points are the small streamer offset and only 24 channels.

analysis was reliable only for the seafloor and uppermost reflections.

2.3.3 Data Processing

The processing of the seismic data was realized with the Focus/DISCO seismic data processing system (PARADIGM). Beyond the standard processing a static correction of the CMP gathers was conducted in order to consider the high frequency bandwidth of the source signal. The following main processing steps

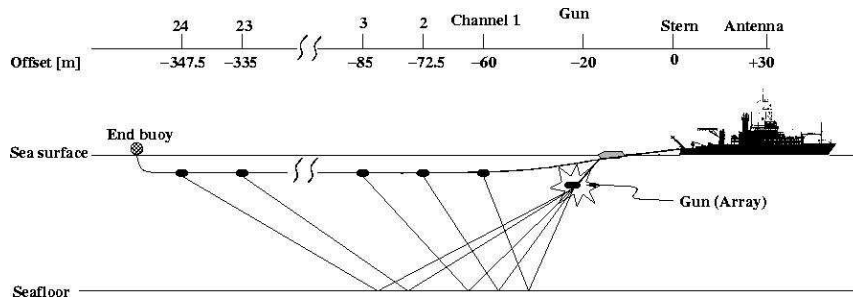


Fig. 2.4: Acquisition geometry for the cruise M44/3. A 300 m active streamer with 24 channels was towed with an initial offset of 60 m.

were applied to the seismic data:

- Geometry Processing
- Editing of bad traces
- Bandpass filtering
- Deconvolution
- CMP sorting
- First velocity analysis
- Static correction by cross-correlation with pilot trace
- Second velocity analysis
- Stack
- Time-migration with smoothed velocity function

Geometry Processing

For the compilation of the geometry, a set of equidistant stations was defined along a 2D-line. Because of the time-triggered shots and the irregular speed of the vessel, the distance of each shot to the next station was calculated. In combination with the fixed acquisition geometry (Fig. 2.4), each trace could be assigned to its appropriate CMP.

Editing

In this step, bad traces were deleted from the dataset. Whereas the data of the cruise M44/3 had a good quality and only few traces had to be deleted, the dataset of M52/3 implicated some more problems. All channels were affected by randomly occurring spikes. Not all of them could be detected by removal tools; this could be seen by some 'migration smiles in the final sections.

Bandpass Filtering

A causal Butterworth Filter was used for the filtering of the data with a high pass threshold of 20 Hz and low pass threshold of 350 Hz. Three iterations correspond to a filter-slope of 18 dB per octave. The high pass threshold of 20 Hz should eliminate the low frequency noise that was caused by e.g. the ships propeller and the sea state. The low pass threshold reduced electronic noise from the vessel's net and the recording unit.

Predictive Deconvolution

For the reduction of reverberations and multiple energy a predictive deconvolution increased the quality of the CMP gathers. A design window that was fitted to the seafloor, was used for the derivation of the deconvolution operator. The prediction lag was determined by the second zero crossing of the autocorrelation of each trace.

CMP Sorting

The CMP distance is defined by the geometry processing. The theoretical spacing between the CMP, using rays, is half the channel distance, for geometrical reasons. As the vessel speed is not constant and the acquisition setup is also moving in the sea state, the CMP could not be defined as a discrete point, but as a plane. Rays that reflect from this plane were assigned to the CMP. The maximum size of this plane is described by the first Fresnel zone, because the air-guns don't produce a spike signal, but a signal with a considerable time-duration. The first Fresnel zone is dependent from the signal frequency and water depth. Because of the size of the first Fresnel zone, it was possible to double the initial CMP spacing and thus to increase the fold and the signal/noise relation of each CMP. The NMO-corrected CMP gathers were stacked to achieve a zero offset section.

Velocity Analysis

The velocity analysis was carried out by correlation of a hyperbola to the hyperbolic moveout of the reflections. This was supported by velocity spectra. Because of the small streamer offset and the considerable water depth, the moveout difference between the distinct reflections was too small to discriminate them. Only high velocity gradients were detected. In order to consider the increasing seismic velocities with depth, a smooth velocity gradient to the end of the recording time of each trace was inserted.

Residual Static Correction by Cross-Correlation with a Pilot Trace

The high resolution frequency bandwidth up to 350 Hz led to the consequence that residual static correction must be calculated. A signal with 350 Hz has got a wavelength $\lambda = 4.3 \text{ m}$ with a sound velocity of $v_w = 1500 \text{ m}^{-1}$ for sea water. Thus, streamer undulations of ca. 2 m would result destructive stacking results. To prevent this, the CMP gather were NMO corrected using the first velocity analysis, and a pilot trace was produced out of three CMPs. To calculate the

residual static, the single traces were cross-correlated with the pilot trace within a time window that was fitted to the seafloor reflection (50 ms above and 300 ms below). Figure 2.5 illustrates the result of the static correction by a NMO-corrected CMP of the Line G_99_077. The application of the residual static correction to marine seismic data is justifiable because of the small streamer offset and the assumption that the seismic velocity of the sea water is known. After the static correction a second velocity analysis was accomplished.

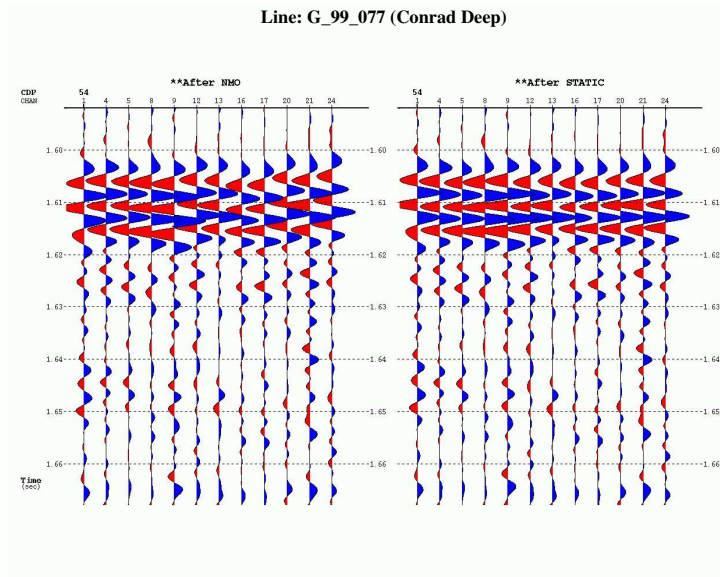


Fig. 2.5: Showcase of a NMO-corrected CMP before and after the static correction. After the application of the static the lateral coherency is amplified.

Stack and Migration

The NMO-corrected CMP gathers were stacked to achieve a zero offset section. The correct positional arrangement of the registered samples is not given by stacked sections, thus, a time migration was conducted. In order to consider lateral velocity variations, a ω -x FD migration yielded the best results. As the migration result is dependent on the quality of the provided velocity function, the results were also a validation of the velocity function derived from the stacking velocities. In order to reduce the spatial aliasing at high structural dips, a 300 Hz low-pass filter was applied before the migration operation. However, although this was not always achieved, the aliasing artifacts were not dominant, where the structural dip exceeds the calculated dip threshold.

3 Evaporites in the Red Sea Rift

This chapter gives a brief overview regarding the abundance of evaporites in the Red Sea Rift area (including the Gulf of Aqaba), as the evaporites are special in terms of their sedimentation, their thickness and their physical properties. These sediments play a key role in the development of surficial sediment structures, e.g. basins, because they represent a ductile interface between the basement and the overburden. In the Miocene large quantities of evaporites were deposited in the Red Sea main trough (e.g. Guennoc et al., 1988). Massive salt depositions are also reported from the Dead Sea Rift, e.g. in the Dead Sea area (Al-Zoubi and ten Brink, 2001).

3.1 Deposition of Evaporites

Evaporites are chemically precipitated sediments out of saturated surface or near-surface brines (after Warren, 1999). Some of the major evaporite minerals are anhydrite ($CaSO_4$), Calcite ($CaCO_3$), Gypsum ($CaSO_4 \cdot 2H_2O$), and halite ($NaCl$). Marine brines will develop, if sea water evaporates. Normal sea water has a density $\rho_w = 1.03 \text{ gcm}^{-3}$ and a salinity of 35 ‰. With ongoing evaporation, the salinity increases and the first minerals to precipitate are Calcium Carbonates at mesohaline waters ($\rho_{mh} = 1.10 \text{ gcm}^{-3}$ and 40–60 ‰). At five times the concentration of sea water, the status is penesaline ($\rho_w = 1.13 \text{ gcm}^{-3}$, 130 ‰) and gypsum and anhydrite precipitate. Precipitation of halite starts after 10 to 12 times the salinity of sea water ($\rho_w = 1.3 \text{ gcm}^{-3}$ and 340–360 ‰). The precipitated minerals will be deposited in that typical series for one cyclus of evaporation and re-flooding (see Fig. 3.1).

3.2 Stratigraphic Evolution of Evaporite Basins

The evaporites within the Red Sea were most probably deposited in a *shallow water deep basin* environment, like the Messinian Evaporites (Warren, 1999). A basin, like the Red Sea trough became isolated from sea water influx (the Street of Bab el Mandeb at the southern extension is only ca. 100 m deep). The residual water in the basin evaporates and higher and higher salinities cause the precipitation of a series of evaporites. Occasional flooding renewed the brine water. In this manner up to 7 km of evaporites were deposited (precipitated) in the Red Sea trough in the Miocene (Searle and Ross, 1975). Figure 3.2 illustrates with a sketch the model of the shallow water deep basin brines.

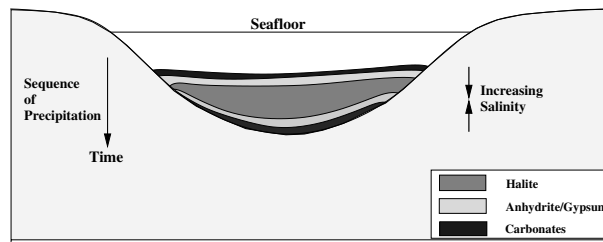


Fig. 3.1: The precipitated minerals form a series on the seafloor that reflects the salinity during one cyclus of evaporation and re-flooding.

3.3 Physical Properties of Salt Systems and its Structural Implications

Precipitated salt sediments have a lot of different physical properties in relation to usual marin sediments. After about 50 m to 100 m burial, salt has lost its porosity and is near incompressible to depths of 6 to 8 km (Warren, 1999). Its density $\rho_{salt} = 2.2 \text{ gcm}^{-3}$ is near constant which leads to positive buoyancy effects after a depth of burial of about 1 km. The depth where the density of the salt equals the density of the overburden is called Level Of Neutral Buoyancy (LONB). Another important difference is the viscosity η that is lower than that of clays or sand by 4 to 5 orders of magnitude (depending on temperature and moisture). This fact is, among others, responsible for the ascent of salt diapirs. In thick salt layers, these special properties can cause thermal convection, as the thermal expansion of the material is higher than the compression because of the depth of burial. Assuming a thermal gradient of 30 K/km and a depth of burial of 5 km, halite contracts only by 0.5% but expands by 2 %. E.g. Talbot (1978) assumed thermal convection in the Danakil Depression (Eritrea).

The weakness of the salt to geologic strain rates means also that the salt cannot easily drag or stretch the overburden. It rather acts as lubricant that decouples the sediments from the basement and makes it difficult for basement faults to

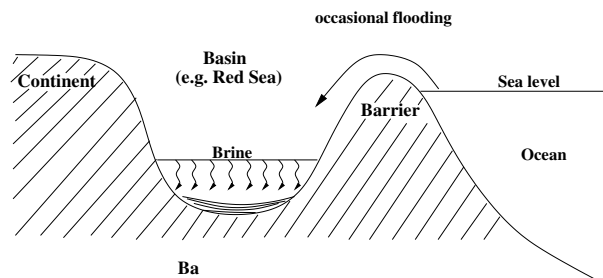


Fig. 3.2: Model of the shallow water deep basin brine (after Warren, 1999). Occasional flooding renewed the salt content within the basin and enabled the huge amount of evaporites within the Red Sea.

	Halite	Anhydrite	Claystone	Carb. oozes
p-wave vel.	4.2 kms^{-1}	4.9 kms^{-1}	$2.6 - 3.3 \text{ kms}^{-1}$	$1.6 - 2.1 \text{ kms}^{-1}$

Table 3.1: P-Wave velocities in the central Red Sea (after Whitmarsh et al., 1974)

affect the deformation of the overburden sediments (after Warren, 1999). On the other hand, structures in the overburden sediments must not reflect the morphology of the basement (Fig. 3.3). The processes of gravity gliding or raft tectonics represent thin-skinned tectonics that happen over a décollement layer like salt (Warren, 1999; Jackson and Talbot, 1999).

3.4 Physical Properties of Rock Salt and its Implications to Seismic Measurements

The special physical properties of rock salt do influence seismic measurements severely. The seismic p-wave velocity in salt is between $4.0 - 5.5 \text{ ms}^{-1}$ (Kertz, 1992), and causes, thus, a high velocity contrast to the overlying sediments. The p-wave velocities at the DSDP sites around the Atlantis II Deep (central Red Sea) are listed in Table 3.1 (Whitmarsh et al., 1974).

Sediment densities are reported to increase slightly from 1.4 gcm^{-3} to 1.9 gcm^{-3} and reach at the transition to the evaporites expected values of 2.14 gcm^{-3} for halite and 2.83 gcm^{-3} for anhydrite. This causes a high acoustic impedance contrast and a high reflection coefficient. The reflection coefficient for oozes and halite is calculated for a normal incident ray to be as high as $R_{pp} = 0.4$. Even for clay and halite the coefficient is appreciable high ($R_{pp} = 0.22$). This has important implications on the reflection seismic measurements. Because of this high reflection coefficient, the top of the evaporites yields a prominent reflection. In the case of the Red Sea, this reflection was recognized all over the Red Sea basin. On the other hand, the high reflection coefficient means a low transmission coefficient. Thus, the evaporites limit the seismic signal penetration noticeably. In the case of the Red Sea, the reduction of the signal penetration is very high, because the top of the evaporites seem so be very rough and has intercalated beds of clays and anhydrite (see Whitmarsh et al., 1974).

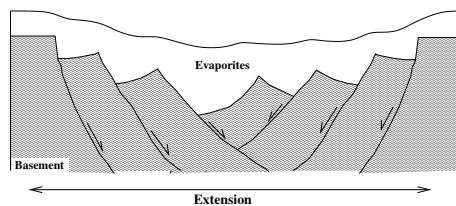


Fig. 3.3: Sketch of a rift system that is covered by evaporites that compensate the block faulting by lateral salt flowage.

4 Seismic Study of Pull–Apart induced Sedimentation and Deformation in the northern Gulf of Aqaba (Elat)

by Axel Ehrhardt, Christian Hübscher, Zvi Ben-Avraham and Dirk Gajewski

in Press, *Tectonophysics*, 2005

4.1 Abstract

New multichannel seismic and bathymetric data are presented which clarify the Plio-Quaternary evolution of the northern Gulf of Aqaba (Elat) and the Dead Sea Transform (DST). The seismic data reveal two main seismic sequences, a lower (pre-tectonic) unit and an upper (syntectonic) unit, separated by a prominent unconformity. These units are each linked to a distinct tectonic phase in the history of the DST. Parallel horizons and an undisturbed internal structure point to a tectonic quiet time or pure strike-slip without extension or compression during the first (pre-tectonic) phase. The second (syntectonic) phase that begins in the early Pliocene, is characterized by a major change in the activity of the DST. The pre-tectonic sedimentary unit subsided and, consequently, dips southward with a supplementary inclination to the east. The coeval sedimentation of the syntectonic unit is recorded by the divergent reflection pattern and onlap terminations on the unconformity. The apparent fault system seems to be rearranged in the second phase. The stepover of the main strand of the DST from the eastern side of the Elat Deep to the western side of the northern Gulf of Aqaba was mapped in detail for the first time. The very smooth shape of the stepover and the apparent lack of extensional tectonics do not fit with the classical pull-apart basin model for the Elat Deep and point to a decoupling of the crystalline basement from the sedimentary overburden. Comparisons of the new geophysical findings with analog models support this assertion.

4.2 Introduction

The Dead Sea Transform (DST), also called the Dead Sea Rift, is one of the main tectonic features in the Middle East, as part of the Red Sea Rift system. It is a continental plate boundary separating the Arabian Plate from the Sinai Sub-Plate (Fig. 4.1A), originating at the Red Sea Rift in the south and terminating after approximately 1200 km to the north at the continental collision zone of the Taurus Zagros orogenic belt. About 105 km of left lateral displacement is documented along the DST (e.g. Quennell, 1959; Freund et al., 1968; Bartov et al., 1980; Garfunkel, 1981).

Transform zones are often accompanied by pull-apart basins that have developed because of geometrical or mechanical irregularities at the transform fault (Ben-Avraham and Garfunkel, 1986). The DST is an ideal location to study the consequences of transform faulting, because it is a young and recently active structure. Left lateral strike-slip motion started only about 20–15 Ma ago (Garfunkel, 1981; Courtillot et al., 1987; Joffe and Garfunkel, 1987). Thus, the fault structure related to strike-slip faulting and basin formation is relatively young and only slightly overprinted by erosional and tectonic processes. Therefore the DST represents a world class site for studying transform faults and related processes.

The Gulf of Aqaba is a key area for studying continental transform faults and pull-apart basins by marine geophysical methods. In order to investigate the southernmost segment of the DST, a multinational approach started in 1999 when the research vessel R/V Meteor (cruise M44/3) surveyed the Gulf of Aqaba and the northern Red Sea. For the first time, it was possible to collect a dense grid of digital reflection seismic and swath sounder data in an area that covers the territorial waters of Egypt, Israel and Jordan. The main purpose was to study the consequences of the left lateral displacement in terms of basin evolution and crustal architecture along the DST fault stepover zones.

In this paper, we present a new and detailed map of the sedimentary fault system that reflects DST related tectonic activity. The results will be discussed in the context of the structural model for the northern Gulf of Aqaba of Ben-Avraham and Tibor (1993), seismological data of the most recent earthquakes (e.g. Klinger et al., 1999; Hofstetter, 2003) and recent results of analog sandbox

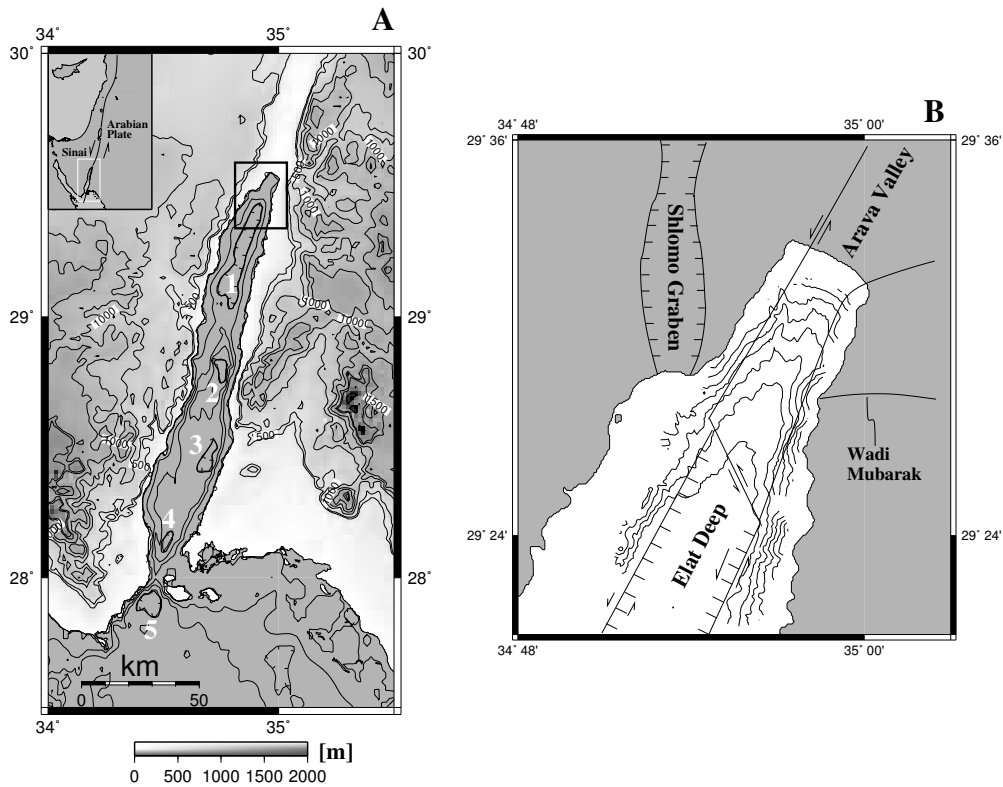


Fig. 4.1: A: The Gulf of Aqaba (Elat) and the Dead Sea Transform (DST): The opening of the Red Sea is accommodated by left lateral displacement along the DST between the Sinai Sub Plate and the Arabian Plate. The topography was extracted from the GEBCO dataset [*GEBCO Digital Atlas*, 2003], all levels > 0 m are grey-scale coded. The five main pull-apart basins are indicated by the numbers 1 to 5. 1: Elat Deep; 2: Aragonese Deep; 3: Dakar Deep; 4: Tiran Deep; 5: Hume Deep. B: Northern Gulf of Aqaba, the Gulf's Head. Fault structure after Ben-Avraham and Tibor (1993). Whereas the main strike-slip motion is accommodated along the eastern boundary fault, the western fault is predominantly normal. The transverse fault is located in the prolongation of the Shlomo Graben.

experiments on pull-apart basin development of Sims et al. (1999).

4.3 Geological Setting

The Gulf of Aqaba (Elat) is situated at the southern extent of the DST (Fig. 4.1A). It comprises four main sedimentary basins, the Dakar, Tiran, Aragonese and Elat Deeps, and slightly beyond the limits of the Gulf of Aqaba, the Hume Deep. These basins, distributed in an en-echelon pattern, have been considered to represent pull-apart basins (Ben-Avraham and Garfunkel, 1986; Ben-Avraham and Tibor, 1993). The evolution of the Gulf started with the initiation of the Red Sea Rift in the late Oligocene to early Miocene (Garfunkel and Ben-Avraham, 1996). The ongoing separation of the Arabian and African Plate was accommodated in the north by the Suez Rift and after about 15 Ma by the initiation of the Sinai triple junction and the formation of the DST between the Arabian and the Sinai Sub-Plate (Courtillot et al., 1987). The amount of displacement along the DST is determined by matching several structures and igneous bodies and is also inferred from regional plate kinematics. Left lateral displacement of 105 km (Quennell, 1959) along the transform fault probably occurred in two stages (Garfunkel, 1981). In the Miocene, the initial stage resulted in a 60 km offset, and a second more recent stage added another 40 km of sinistral offset. The duration of the break between the two stages is not clear (Girdler and Southren, 1987; Barjous and Mikbel, 1990). In contrast to the latter model, Joffe and Garfunkel (1987) suggest that the displacement along the DST was continuous since 20 – 17 Ma, with an increase in the component of transverse separation along the DST before 5 Ma, in order to explain the change in internal structures of the transform. In contrast to this model, the DST is also discussed to be a continuation of the Red Sea Rift that initiated in the Pliocene after the Suez Rift ceased. The Red Sea Rift changed its trend northward and caused an oblique opening (Mart and Hall, 1984; Pircard, 1987; Horowitz, 1989).

The northern Gulf of Aqaba is surrounded by metamorphic-plutonic rocks (Ben-Avraham et al., 1979) which are elevated to levels of more than 1000 m close to the Gulf. In general, the areas bordering the DST to the east and to the west were uplifted up to 4 km in the area of the Gulf of Aqaba (Ben-Avraham et al., 1979), whereas the Arabian Plate experienced an explicit larger amount of

uplift (Barjous and Mikbel, 1990; Khalek et al., 1993; Wdowinski et al., 1996). The region east of the northern Gulf is characterized by a platform area covered with alluvial sediments in front of a mountain range pediment composed of Precambrian basement. The western side of the northern Gulf is dominated by the presence of the N–S trending Shlomo Graben (Fig. 4.1B), a Miocene structure that was probably formed during the early phase of displacement along the DST (Garfunkel, 1981; Ben–Avraham and Tibor, 1993). Although the graben is presently inactive, Ben–Avraham and Tibor (1993) suggested that the Shlomo Graben lineament continues into the Gulf of Aqaba and controls the location of transverse faults in the Gulf. On both sides of the Gulf, outcropping basement is transected by a variety of faults (e.g. Eyal et al., 1981). The strike of these faults roughly corresponds to the trend of the DST and associated subordinate strike-slip faults, such as Riedel shears, conjugate Riedel shears and P-shear faults (Christie–Blick and Biddle, 1985).

The Elat Deep is the northernmost basin in the marine part of the DST (Fig. 4.1B). It is approximately 50 km long, up to 25 km wide and is bounded by faults at its longitudinal margins and shows faulting at its northern and southern extensions (Reches et al., 1987; Ben–Avraham and Tibor, 1993). The transition from the Elat Deep to the Arava Valley, the adjacent onland sedimentary basin (Ben–Avraham et al., 1979), takes place at the top end of the Gulf, the Gulf's Head, where the Gulf narrows considerably (Fig. 4.1B). In this area a left stepover related to the pull-apart basin formation of the Elat Deep is expected. The morphology of the Elat Deep is characterized by an almost flat seafloor of approximately 900 m water depth and steep scarps, bounding the Deep along the western and eastern flanks (Fig. 4.2A). The boundary faults separate the coarsely stratified sediments on the slopes from regularly bedded infill of the deep basins (Ben–Avraham, 1985). The sedimentation rate in the northern part of the Gulf is fast enough to level out large scale tectonically induced irregularities (after Reches et al., 1987; Ben–Avraham and Tibor, 1993), resulting in a flat-like seafloor.

4.4 Previous Work

The Gulf of Aqaba, and especially its northern part plays a key role in the understanding of the mechanics of the DST and the related development of

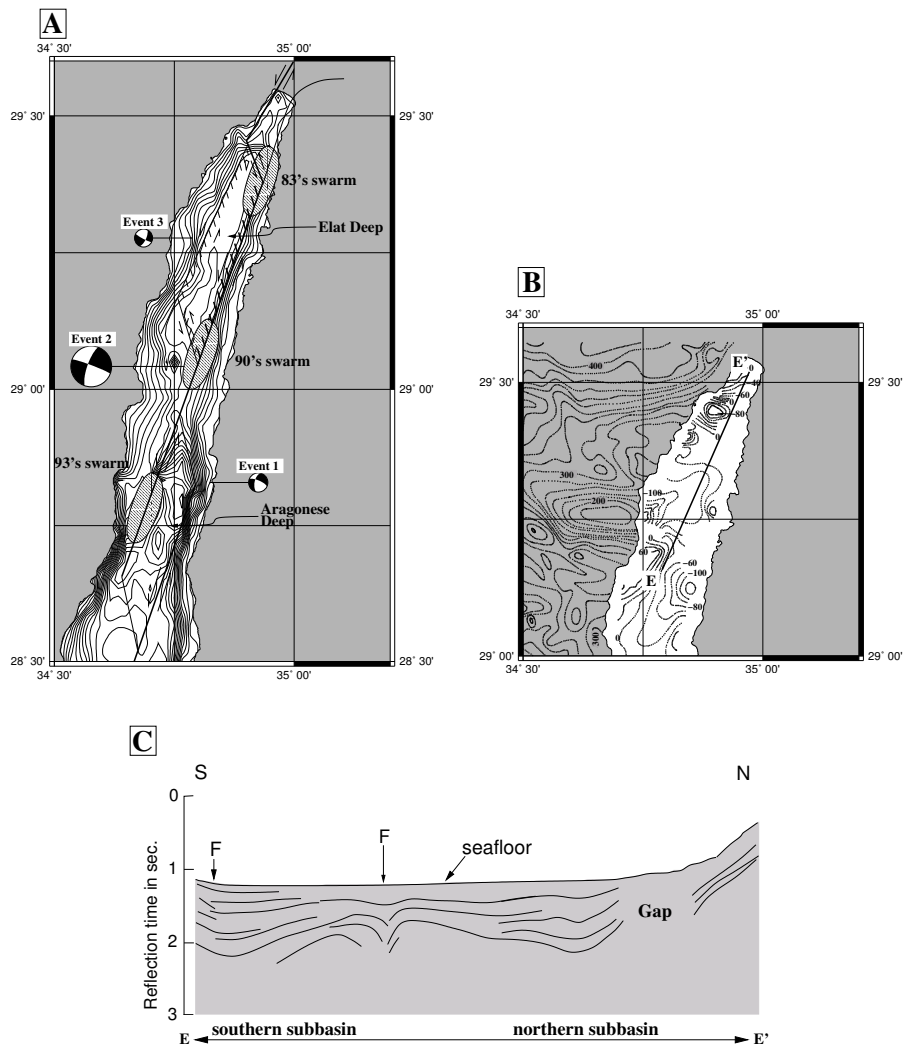


Fig. 4.2: A: Northern Gulf of Aqaba, including the Aragonese Deep and Elat Deep. Fault structure after Ben-Avraham (1985) and Ben-Avraham and Tibor (1993). Superposed are the location of the earthquake swarms of '83, '90 and '93 as well as the focal solutions of the three subevents of the $M_w = 7.3$ earthquake of 1995 (Klinger et al., 1999) (please note that the symbol size of Event 2 and 3 is enlarged by a constant). B: Magnetic anomaly map of the northern Gulf and Sinai (contour interval: 20nT) [after Ben-Avraham, 1985]. Magnetic anomalies seem to continue undisturbed from Sinai to the Gulf. C: Line drawing of the reflection seismic profiles 37_{II} and 38_{II} of Ben-Avraham (1985). See Fig 4.2B for the location (E–E'). The Elat Deep seems to be a sequence of two separate Deeps. The gap in the northern part of the section is caused by the poor quality of the seismic image.

Latitude (degree)	Longitude (degree)	Strike (degree)	Dip (degree)	Rake (degree)	Depth (km) _{1/2}
28.829	34.825	191.6	58.6	-21.2	18.8 / 14.0
29.042	34.777	199.6	74.3	-5.0	18.65 / 14.0
29.277	34.786	24.7	67.2	-8.5	5.15 / 1.0

Table 4.1: Source parameters of the 3 subevents of the 1995 earthquake, after 1: Klinger et al. (1999) and 2: Klinger et al. (2000).

pull-apart basins. Therefore this area was previously the subject of several geophysical and geological expeditions and other investigations. Single-channel seismic data acquisition, sediment echo sounder and bathymetric measurements were conducted to derive a model that fits surficial fault structures and sedimentary patterns (Ben-Avraham et al., 1979; Ben-Avraham, 1985; Reches et al., 1987; Ben-Avraham and Tibor, 1993). Marine geomagnetic and aeromagnetic data, as well as gravimetric data acquisition completed the dataset to derive a model for the Gulf of Aqaba (Fig. 4.2B) (e.g. Ben-Avraham, 1985; Alamri et al., 1991). Geological sampling by gravity cores was conducted by Arz et al. (2003).

Alamri et al. (1991) combined seismological data of 1985 to 1989 with aeromagnetic measurements of the Mydian region, east of the Gulf. The earthquake swarms of 1983, 1990, 1993 and the $M_w = 7.3$ earthquake of 1995 were the subject of several publications (e.g. El-Isa et al., 1984; Karaki et al., 1993; Pinar and Türkelli, 1997; Klinger et al., 1999; Hofstetter, 2003). The epicentral distribution and focal solutions give insight into the fault dynamics of crustal or intra-sedimentary processes that could not be resolved within the limits of active seismic measurements. Figure 4.2 gives an overview of the relevant data in the area of the northern Gulf, including the Aragonese Deep and the Elat Deep. Klinger et al. (1999) performed body wave inversion of the 1995 $M_w = 7.3$ earthquake in order to propose a model for the rupture process. Three subevents were modeled to find a good fit between the synthetic and observed data. Those subevents are shown in Table 4.1 and (Figure 4.2A).

The seismological data indicate that the main part of the left lateral displacement is accommodated at the through going strike-slip fault between the Aragonese Deep and the Elat Deep. This is in agreement with the latest fault model of the northern Gulf from Ben-Avraham and Tibor (1993), who interpreted the

eastern boundary fault of the Elat Deep as the main strike-slip fault and the western boundary fault as a predominantly normal fault with minor strike-slip motion (Fig. 4.1B). This interpretation is further consistent with the magnetic anomalies that continue undisturbed from the Sinai Peninsula to the western side of the Gulf (Fig. 4.2B) and the asymmetric sedimentation patterns within the Gulf. In the area of the northernmost Gulf of Aqaba, the Gulf's Head, the strike-slip motion must step over to the western side of the Gulf's Head. The Elat Fault (Reches et al., 1987; Ben-Avraham and Tibor, 1993) accommodates left lateral displacement on the western side of the Gulf's Head. This fault can be defined on land, in the Arava Valley, where it is known as Evrona Fault. Thus, the Elat Deep is interpreted as a complex sediment filled basin that has developed as a pull-apart basin. The appropriate stepovers are located at its southern and northern extensions. A longitudinal reflection seismic line that images the Elat Deep over the survey area of the actual dataset, is presented as linedrawing in Fig. 4.2B and C. Although the seafloor is flat and continuous, the subsurface structure reveals that the Elat Deep is a composition of two elongated basins (Ben-Avraham, 1985).

4.5 Geophysical Data

During the Meteor Cruise M44/3 in 1999 a dense multichannel seismic dataset was simultaneously acquired with swath sounder data (Fig. 4.3). In order to enable three dimensional interpretations, the lateral offset between the profiles is not larger than 2.4 km.

4.5.1 Bathymetric Data

Swath sounder data were continuously recorded by means of an ATLAS HYDROSWEEP system. A swath width of twice the water depth enabled complete coverage of the seafloor topography. Due to uncertainties in the velocity-depth function of the sea water and the compensation of the sea state, the vertical error is in the order of 1% – 3% of the water depth, i.e. small-scale features are not resolved.

The resulting bathymetric chart reveals a complete coverage of the seafloor of the northern Gulf of Aqaba (Fig. 4.4). The observed features split the survey area

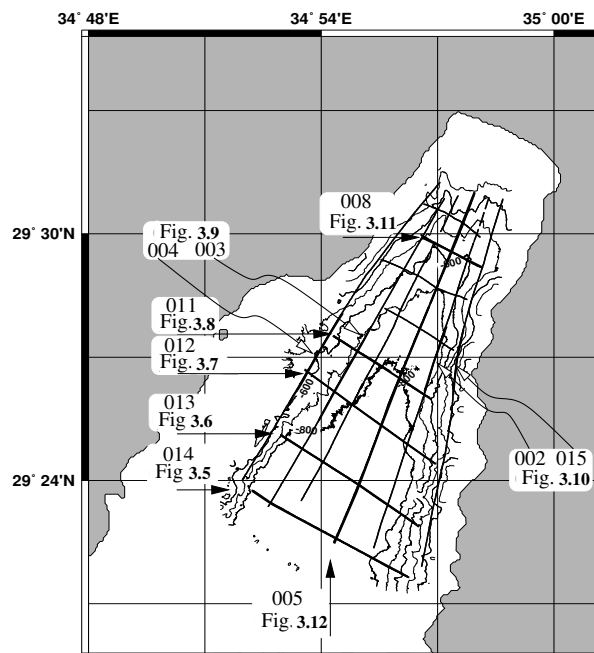


Fig. 4.3: Base map of the seismic survey of cruise M44/3. Overall six longitudinal and eight transverse profiles with a total length of 143 km were measured. The profiles that are discussed in the text are marked with heavy lines (figure numbers in brackets). Figures 4.9 and 4.10 show parts of longitudinal profiles that are marked with heavy lines and open arrows.

into three sectors. The southern sector (Elat Deep, Sector I) is characterized by steep slopes. These scarp-like features bound the almost flat basin floor. The western slope has a slope angle of 17.5° and is steeper than the eastern slope with a slope angle of 14.0° . In the central sector (Transition Zone, Sector II) the western slope changes its slope angle abruptly and is inclined much more gently ($5.7^\circ - 6.4^\circ$). Linear graben-like features trend nearly perpendicular to the slope in the seaward continuation of the Shlomo Graben. The eastern slope is dominated by two conspicuous features: a linear ridge-like structure trends subparallel to the strike of the Gulf, and further north a cone is well expressed by the bathymetric data. The limits of the central sector can be correlated with the continuation of the Shlomo Graben. The northern sector (Northern Edge, Sector III) shows a steepening of the slope on its western side to about 16° . This is not observed on the eastern side of this sector, but the considerable water depth of 500 m close to the coastline points to a steep scarp-like slope a short distance east of the survey area. The Gulf's Head exhibits two northward

Source-Parameters	
Source	1 GI-Gun
Volume	2 x 0.4 l
Mode	True GI Mode
Dominant Frequency Bandwidth	20 Hz – 350 Hz
Time Shot Interval	10 s
Spatial Shot Interval	approx. 25 m (Ship velocity 4.9 knots)
Receiver-Parameters	
Streamer	SYNTRON
No. of Channels	24
Active Length	300 m
Group Interval	12.5 m
Geometry and Processing	
CDP Interval	12.5 m
Average Fold	12
Static corrections for streamer undulations	
Stack	
f-x Migration	Smoothed velocity function ¹

Table 4.2: MCS acquisition and processing parameters

trending channels (Channel A and B in Figure 4.4). Channel A seems to connect to the Elat Fault, whereas Channel B is not continuous to the northern limit of the survey area.

4.5.2 Reflection Seismic Data

The multichannel seismic data acquisition was adjusted to achieve high structural resolution. Therefore a volume reduced GI-Gun was used as signal source. Reflections from these source signals could be correlated within a bandwidth of up to 350 Hz. Because of the very narrow shape of the Gulf of Aqaba only 300 m of active streamer length were used. Table 4.2 shows the basic acquisition and processing parameters. 15 profiles with a total length of 143 km were collected: seven longitudinal lines parallel to the strike of the Gulf, and eight transversal lines, perpendicular to the strike (Fig. 4.3).

¹derived from stacking velocity analysis

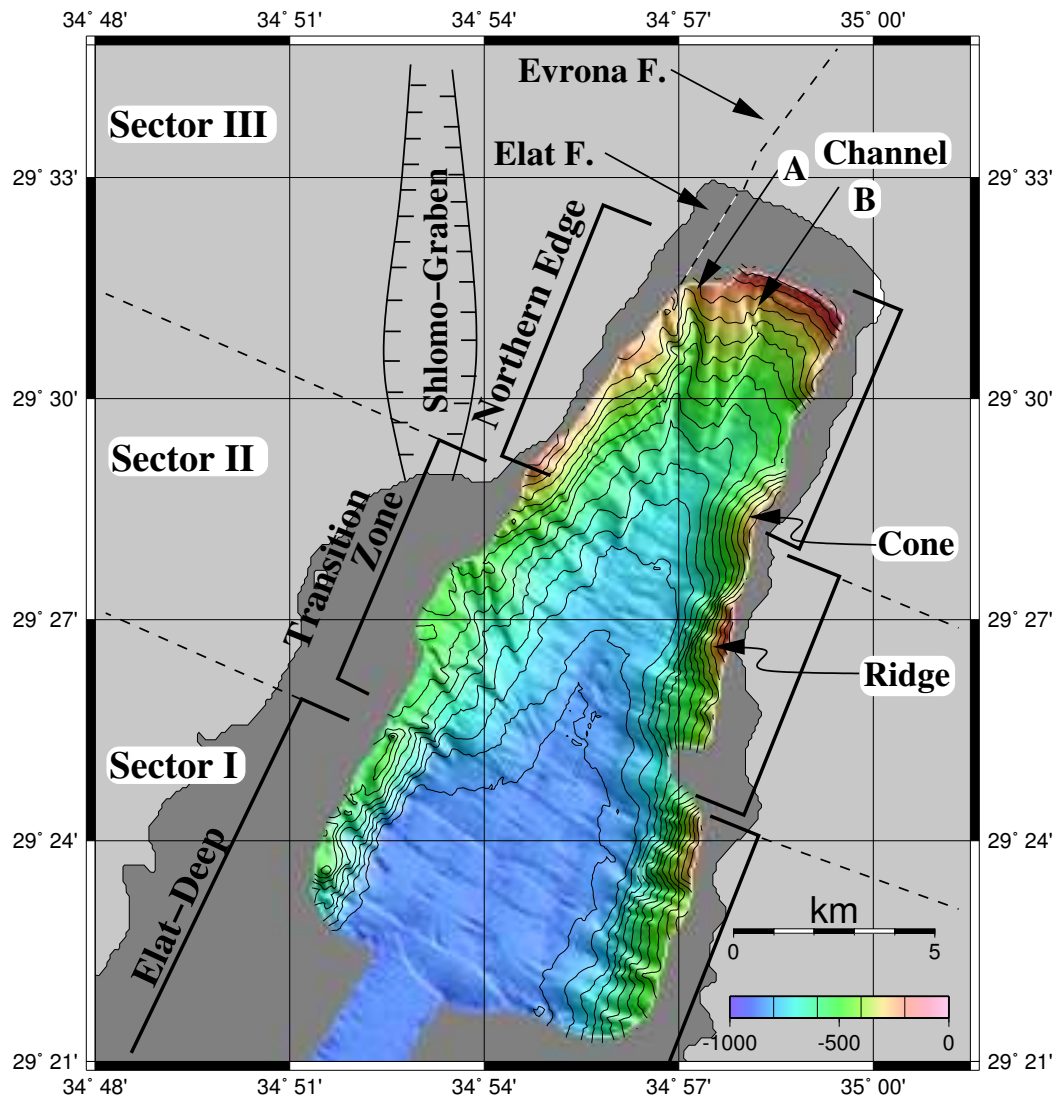


Fig. 4.4: Bathymetric map of the Northern Gulf of Aqaba from the multibeam data of Cruise M44/3 (illuminated and color-coded, isobath interval: 100 m). The area is subdivided into three sectors, the Northern Edge, the Transition Zone and the Elat Deep sectors. Bathymetric features are explained in the text. The transition zone is located in the seaward prolongation of the Shlomo Graben. Location of Elat and Evrona Faults after Ben-Avraham and Tibor (1993).

The seismic data were processed with respect to the high frequency bandwidth. Static corrections were calculated and applied to increase the quality of the stacking result and therefore the lateral coherence of events. The seismic sections presented in this paper are processed including time migration, using a smoothed velocity function, derived from a velocity-analysis with super-gathers.

To discuss the subsurface structure of the northern Gulf of Aqaba, six selected seismic profiles are presented here. The locations of these profiles are shown in Fig. 4.3. We present seismic data of each bathymetric sector and a longitudinal profile, crossing all sectors. Additionally, seismic images of prominent structures in the survey area are included.

Elat Deep Sector: Profile 014 (Fig. 4.5) is the southernmost line and crosses the Elat Deep. As already observed in the bathymetry, the almost flat-like seafloor in the Deep is bounded by a steep slope in the west and a less steep slope in the east. A prominent eastward dipping unconformity, the Horizon he1 (west 1.6 s TWT to east 2.0 s TWT) separates two major sedimentary sequences. The sediments are bounded by faults on the eastern and western slope. Both faults show normal displacement caused by the subsidence of the basin. The eastern fault was already known and according to Ben-Avraham and Tibor (1993) and Klinger et al. (1999) this fault also accommodates the main part of the left lateral motion along the DST. Thus, we name the western fault fn1 (fault normal 1) and the eastern fault fsn1 (fault strike-slip normal 1). The upper sedimentary unit is characterized by well stratified and eastward divergent reflections which onlap he1. The lower sedimentary unit shows parallel to subparallel reflection patterns with a constant dip angle of about 3° .

2.4 km further north and parallel to 014, profile 013 (Fig. 4.6)) represents a cross-section of the northern end of the Elat Deep. Whereas the sub-bottom structure has changed, the seafloor topography is very similar to profile 014 (Fig. 4.5). On the eastern slope, fault fsn1 is continuous from profile 014 to 013. In contrast to profile 014 no normal fault can be observed on the western slope. The upper sedimentary unit still onlaps the unconformity he1, but unlike profile 014 the lower sedimentary unit dips with a steeper angle (7.5°) to the east and also reveals no sign of faulting on the west. Thus, the fault fn1 terminates between the profiles 014 and 013.

Transition Zone: The profiles 012 and 011 (Fig. 4.7 and 4.8) are located in the transition zone. In contrast to the seafloor in the south, a depression is

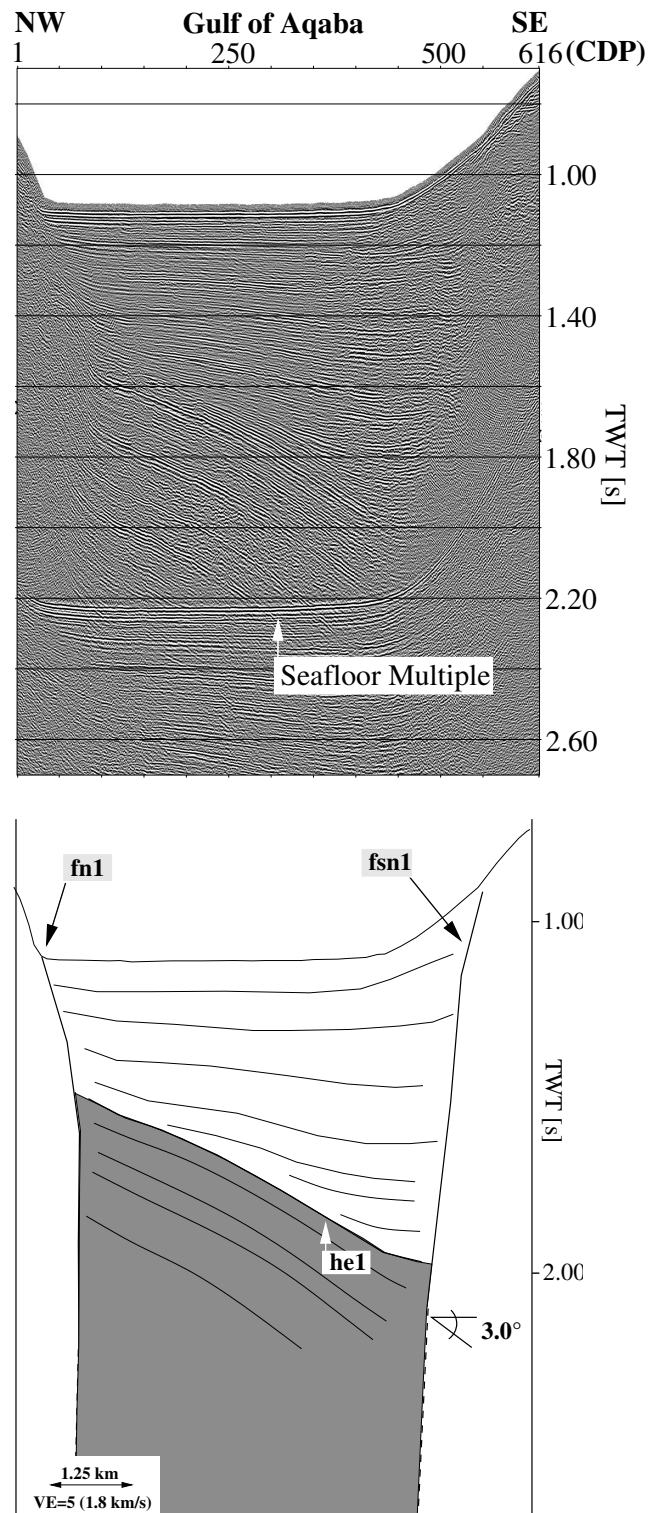


Fig. 4.5: Profile 014; time-migrated section of Cruise M44/3. For recording and processing parameters refer to Table 4.2. The scale of the profiles 014 to 008 (Fig. 4.5 to Fig. 4.8) is constant. Profile 014 is the southernmost transversal profile of the survey. It crosses the Elat Deep. The eastern side is bounded by the fault fsn1 that resembles strike-slip (Ben-Avraham and Tibor, 1993; Klinger et al., 1999) and normal displacement, whereas the western side exhibits a normal fault (fn1). The prominent unconformity he1 separates two sedimentary units.

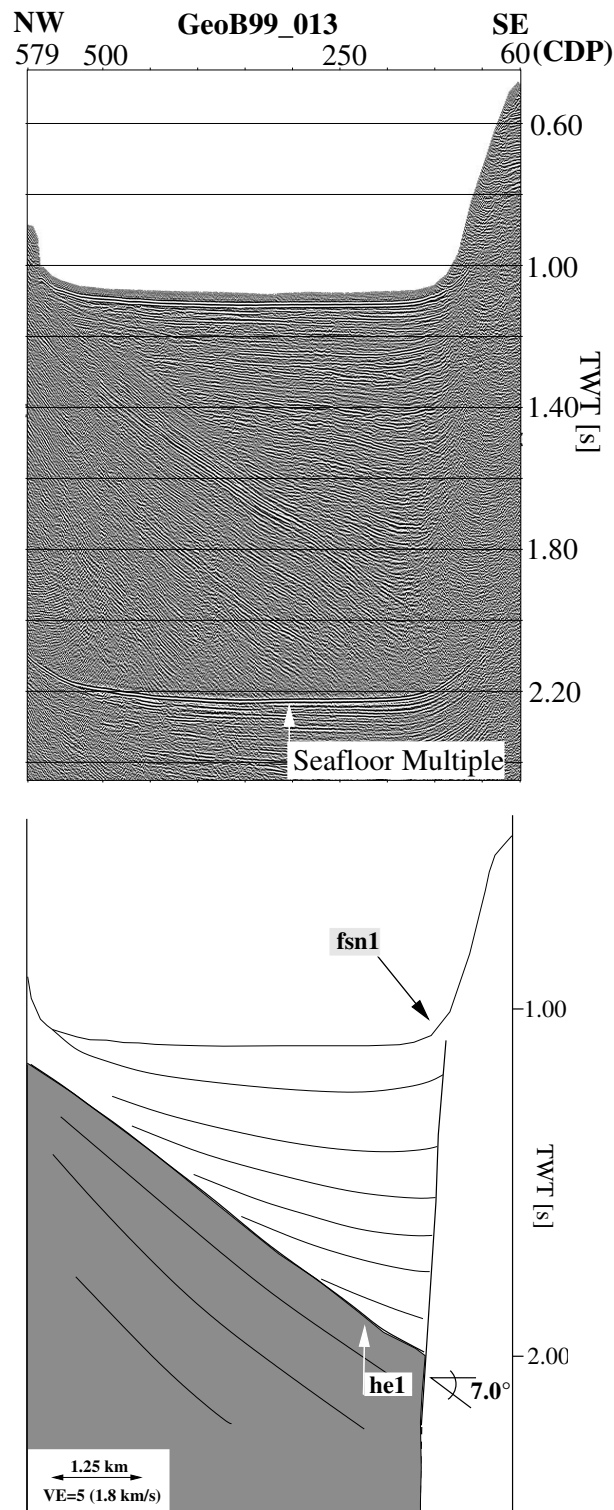


Fig. 4.6: Profile 013, 2.4 km north of 014 (Fig. 4.3). The fault fsn1 is continuous between both lines. The western normal fault fn1 does not continue and the dip of the lower sedimentary unit has steepened. The upper unit reveals onlap structures on the unconformity he1.

formed in this zone. As in the Elat Deep sector, the prominent unconformity he1 intersects the sedimentary infill and divides the two sedimentary units. The upper unit onlaps the unconformity he1. The lower unit dips with a constant angle of 7° to the east. The depth of the unconformity he1 gradually decreases, thus indicating a supplementary dip to the south. Both profiles show no faulting on the western slope of the Gulf, although they cross the potential linear prolongation of fault fn1. The eastern boundary of the Elat Deep in the transition zone is characterized by the bifurcation of the fault fsn1. Between the profiles 012 and 011 the fault fsn1 splits into two branches. The eastern slope of the Gulf is bounded by the fault fsn2. This fault has an appearance similar to fault fsn1 on lines 014 and 013 (Fig. 4.5 and 4.6). The central fault (fc1) on profile 011 (Fig. 4.8) separates the eastward dipping horizons from almost horizontal layered horizons. West and southward of fault fc1, the lower unit exhibits an eastward dip, whereas east of fault fc1 an almost horizontal and concordant stratigraphic architecture is observed.

The NW–SE trending graben-like structures, detected in the bathymetry on the western slope, can be correlated with faults that are located in the seaward continuation of the Shlomo Graben (Fig. 4.9). The faults SG1, SG2 and SG3 are parallel with the graben-like features from the bathymetric map. These linear features, which are almost perpendicular to the strike of the Gulf, support the statement that fn1 is a normal fault without a strike-slip component that terminates between profiles 014 and 013. The linear ridge-like feature on the eastern slope is caused by thrust faulting that can be identified on the marginal longitudinal profiles (see Fig. 4.10) and gives evidence for the strike-slip component of the fault fsn2.

Northern Edge: Profile 008 (Fig. 4.11) is a representative section of the northern sector. A strike-slip normal fault is well expressed on the western slope. It correlates with the location of the Elat Fault (Reches et al., 1987; Ben-Avraham and Tibor, 1993). A boundary fault on the eastern slope cannot be observed in the survey area. The depth of the lower unit has further decreased, as well as the thickness of the upper unit. Channel A and Channel B, identified in the bathymetry (Fig. 4.4), are well expressed in the seismic data. Channel A is close to the Elat Fault. Channel B is not affected by any faulting. Like in profile 011 (Fig. 4.8), east of the strike-slip normal fault, the upper sedimentary unit shows horizontal reflections without onlap structures on he1.

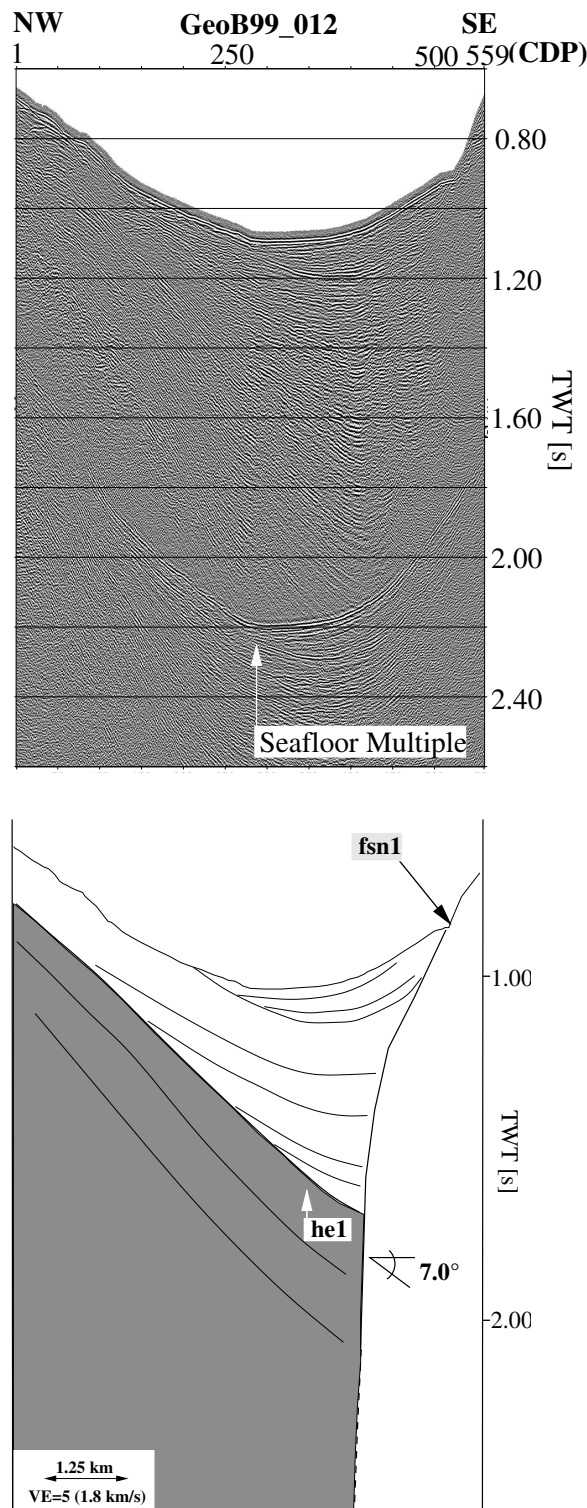


Fig. 4.7: Profile 012 in the southern part of the transition zone. In comparison to profile 013, this line extends further to the western coast. The eastern slope reveals the presence of the fault fsn1. Similar to profile 013 the western slope is not affected by faulting.

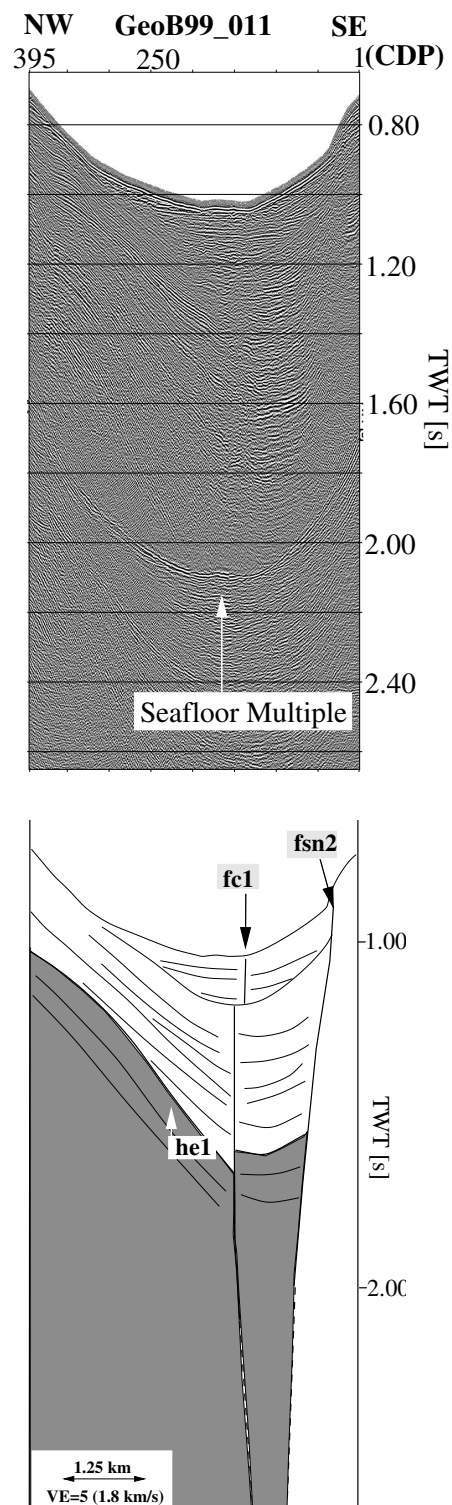


Fig. 4.8: Profile 011 is located in the transition zone. The dip of the lower sedimentary unit is still very steep. The fault fsn1 is partitioned into two branches. The fault fc1 is trending oblique to the strike of the Gulf and forms a connection with the western side. The fault fsn2 is now bounding the Gulf in the east.

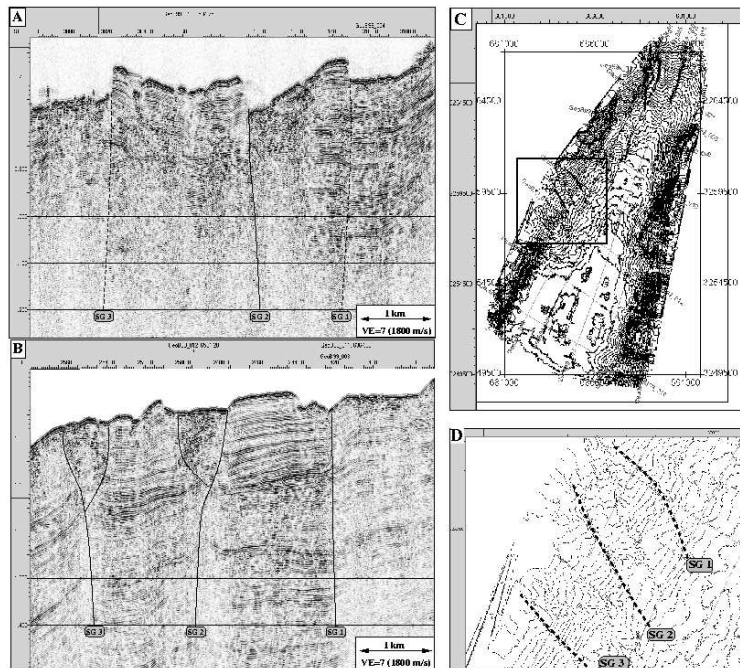


Fig. 4.9: Bathymetric map and seismic cross-sections of the seaward prolongation of the Shlomo Graben. A: Part of profile 004, for the location refer to Fig. 4.3 and 4.9 C, D. Bathymetric channels are related to NW–SE trending faults (SG1, SG2, SG3). B: Part of profile 003. This section is transected by faults that can be linked with faults SG1, SG2 and SG3 of profile 004. C: Bathymetric map of the survey area, the box marks the location of the enlargement displayed in Fig. 4.9D. D: Enlargement of the bathymetric map. The traces of the faults SG1, SG2 and SG3 are superimposed.

North–South Transect: Profile 005 (Fig. 4.12) crosses all sectors and trends parallel to the strike of the Gulf. It shows the already assumed southward dip of he1 and the strata beneath. The overburden parallels he1 in the northern part but onlaps on he1 in the south. The fault structure on this line exhibits two faulting areas, the southern faults can be correlated with the central fault (fc1) of line 011 (Fig. 4.7), the northern fault (fn2) cannot be discerned on the transversal profiles. Fault fn2 seems to be predominantly normal and exhibits a vertical offset of 120 ms that corresponds to 108 m, assuming a medium sound velocity of 1800 m/s for the upper sedimentary layer (derived from CDP velocity analysis). Clear faulting can be observed throughout the lower sedimentary unit. The upper unit is affected by gravity sliding, so that an explicit fault trace is not present. The faults fc1 and fn2 cause slides and splay in the unconsolidated sediments of the upper unit into several branches in order to accommodate the

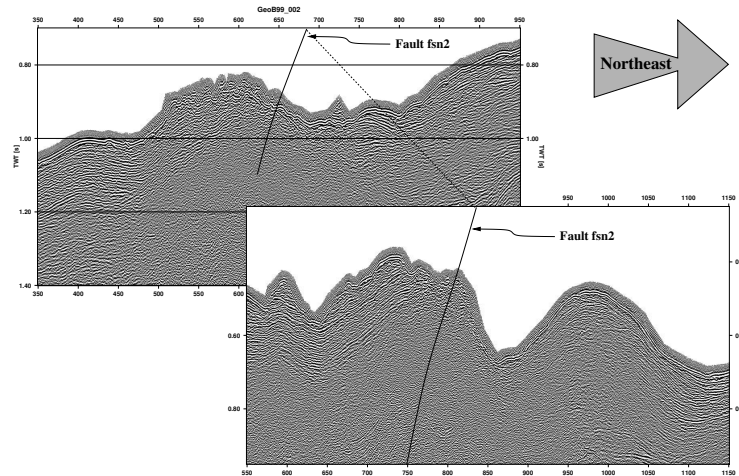


Fig. 4.10: Thrust faulting on profiles 002 and 015 (Fig. 4.3). The right bending of the fault fsn2 causes a compressional regime. The result is thrust faulting that seems to be recently active and gives evidence for the strike-slip component of fault fsn2. The fault fsn2 forms the ridge that is shown on the bathymetric map (Fig. 4.4)

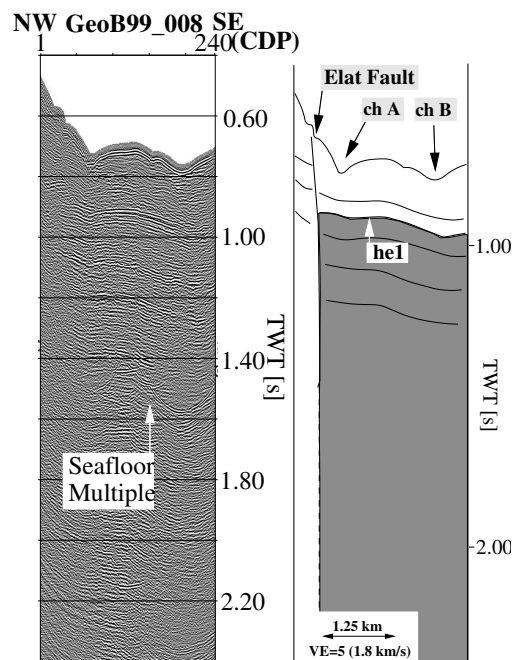


Fig. 4.11: Profile 008: The Northern Edge of the Gulf is bounded in the west by a strike-slip normal fault. This fault is known as the Elat Fault (Reches et al., 1987). The two sedimentary units are characterized by almost horizontal reflections.

displacement. The lower sedimentary unit is almost continuous over the entire profile, only the two faulting areas affect the unit causing subsidence and a slight amount of extension.

4.6 Fault System and Seismic Stratigraphy

In order to unravel tectonic processes in the northern Gulf of Aqaba we identified faults and sedimentary sequences in all seismic lines except the marginal longitudinal lines. A compiled map of correlated faults and bathymetry data is presented in Fig. 4.13. The spatial geometry of key features is elucidated by a three dimensional view into the survey area with the mapped faults superimposed on it (Fig. 4.14). The volume is cut along profile 005 in order to provide insight into the narrow part of the northern Gulf and to show the sub-bottom structure of the volume.

In the northern part of the Elat Deep (sector I), the main strand of the DST correlates with the eastern boundary fault *fsn1* in agreement with the latest model of Ben-Avraham and Tibor (1993) and focal solutions of Klinger et al. (1999) (Fig. 4.1, 4.2). This fault accommodates the left lateral strike-slip motion in the area of the Elat Deep and shows additionally a significant normal component. In contrast to the latest model, the western boundary fault *fn1* terminates between the profiles 014 and 013 (Fig. 4.5, 4.6). The next line further north (profile 012, Fig. 4.7) extends close to the western coast of the Gulf and reveals no evidence of strike-slip faulting. Because of these findings, a significant strike-slip motion along *fn1* is unlikely.

The main strand of the DST continues into sector II (Transition Zone) where the left stepover occurs. Similar to previous models the stepover is located in the southern prolongation of the Shlomo Graben. However, the fault runs smoother than previously proposed and it does not strike in an apparent continuation of the Shlomo Graben (Ben-Avraham and Tibor, 1993). The seaward continuation of Shlomo Graben correlates with some linear, southeast-northwest trending faults within the sediments (Fig.4.4, 4.9 and 4.13). These features are probably a result of the junction between the Shlomo-Graben and the Gulf of Aqaba. Their presence confirm the previous interpretation of fault *fn1* as normal fault, as they show no sign of displacement related to strike-slip faulting parallel to the strike of the DST.

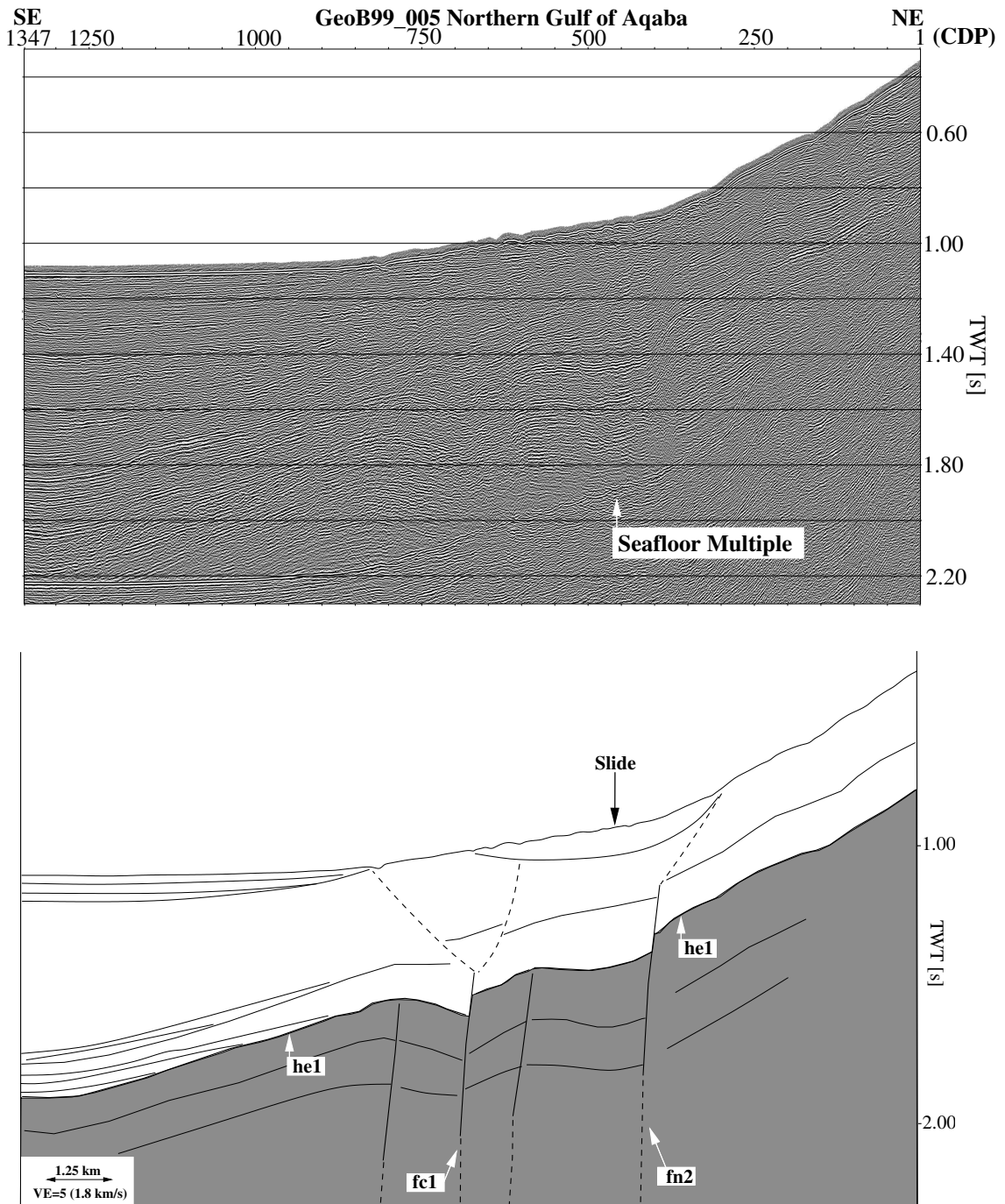


Fig. 4.12: Profile 005 is crossing all sectors. The unconformity he1 dips under the Elat Deep. Two fault systems cut through the lower sedimentary unit. Fault fc1 is probably splayed into several branches. The fault trace of faults fc1 and fn2 is diffuse in the upper sedimentary unit. Instabilities in the faulting zone have caused gravitational sliding of the sediments with the unconformity he1 as sliding surface. A vertical offset of about 110 m is observed at fault fn2.

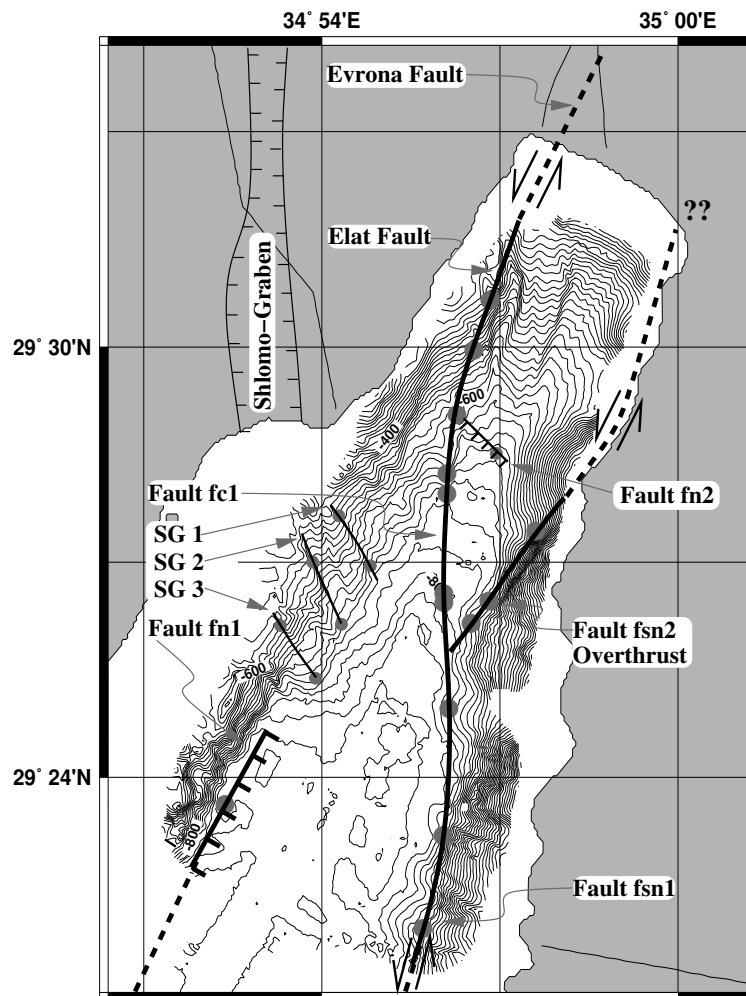


Fig. 4.13: Fault map deduced from the reflection seismic data. The map is superposed on the new bathymetric data of Cruise M44/3. The solid lines mark the observed fault system; the dashed heavy lines indicate the possible continuations of the faults. The grey dots represent the locations, where the faults are observed in the seismic data. The main strand of the DST which bounds the Elat Deep on its eastern side, splits into two branches. One is connecting the Elat Fault on the western side, the other is right bending, thus causing overthrusting. Fault fn1 can be correlated in the south with data of Ben-Avraham and Tibor (1993). The faults SG1, SG2 and SG3 are running almost perpendicular to the strike of the DST. The normal fault fn2 accommodates partly the general difference in altitude between the Arava Valley and the Elat Deep.

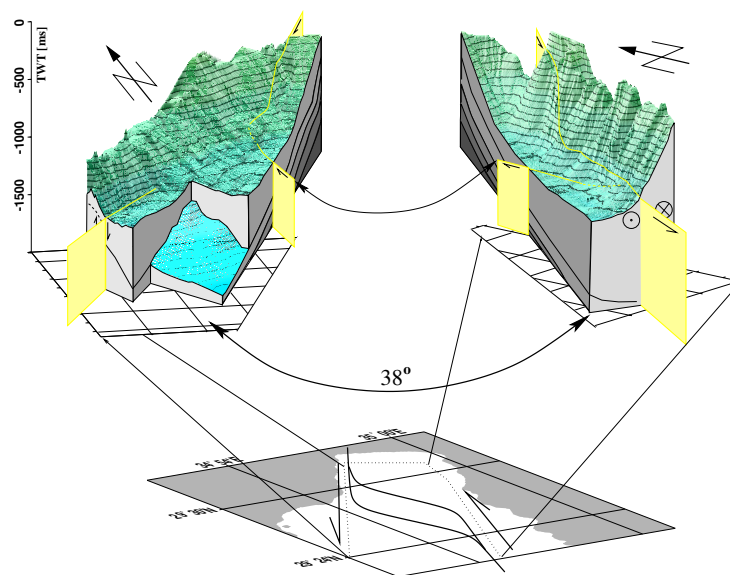


Fig. 4.14: Three dimensional image of the pre- and syntectonic units in combination with the fault system. The volume is cut along profile 005 (Fig. 4.9) to provide insight into the western and eastern slope of the Gulf. Along the intersection the pre-tectonic unit is indicated in dark grey colors, the syntectonic unit in light grey colors. The expected stepover in the basement is indicated in the lower part. Note the difference in the topography of the lower and upper sedimentary units ($VE=5$ ($v=1500\text{m/s}$)).

Close to the inflection point the bifurcation of the main strand of the DST into the faults *fc1* and *fsn2* can be observed (Fig. 4.8, 4.10, 4.13). Fault *fsn2* splits from *fsn1* and bends right. The resulting transpressional setting contains the observed thrust fault segment of *fsn2* and indicates recent strike-slip tectonic activity along this fault (Fig. 4.10). The NE continuation of *fsn2* is not resolved, it might continue parallel to the Jordan coastline and delimit the steep escarpment. The cone shortly northward is interpreted as a sedimentary fan of the Wadi Mubarak (Fig. 4.1 and 4.13). Fault *fc1* strikes toward the western side of the northern edge of the Gulf (sector III) where it correlates with the previously identified Elat Fault and its onshore continuation in the Arava Valley, the Evrona Fault (Reches et al., 1987; Ben-Avraham and Tibor, 1993). We conclude that fault *fc1* also exhibits stratigraphic displacement because it links fault *fsn1* and the Elat Fault.

The resolved sedimentary sequences can be subdivided into three main sequences: the slope sequence comprises the coarsely stratified and irregular bedded sediments east of fault *fsn1* and *fsn2*, and the sediments west of fault *fn1*

and the Elat Fault (e.g. Fig. 4.5, 4.8, 4.11). The strata between the bounding faults are subdivided by the prominent unconformity he1 into a lower and an upper sequence. The lower sequence is characterized by an almost continuous and parallel reflection pattern. It dips generally to the south under the Elat Deep, but shows also a very steep eastward inclination south of fault fc1 (Fig. 4.14). Normal faulting with a throw of about 110 m can be observed on fault fn2 on profile 005 (see Fig. 4.12). This fault accommodates parts of the differential uplift between the Arava Valley and the Elat Deep. The bathymetric expression of the vertical offset is obliterated by the gravity slide (Fig. 4.12). The lower sequence was identified in previously published single channel seismic lines south of the survey area (Ben-Avraham et al., 1979; Ben-Avraham, 1985; Ben-Avraham and Tibor, 1993). After the correlation of our data with the single channel data from the central and southern Elat Deep, we suggest that the lower sequence is continuous beneath the entire Elat Deep, separated by a fault zone in the center of the Elat Deep (Fig. 4.2C). Since the top of this sequence (he1) represents an onlap surface for the upper sequence, we conclude that the unconformity he1 subdivides the resolved strata in a pre-tectonic- and a syntectonic unit concerning the latest development of the Elat Deep. The pre-tectonic sequence was deposited before onset of the latest phase of the Elat Deep formation. In order to reconstruct the development of the uniformly layered pre-tectonic sediments, a relatively shallow marine basin must have existed in the first phase of the deposition of the Elat Deep sediments. The undisturbed internal structure of the pre-tectonic sequence suggests that either it was deposited during a break in the displacement history of the DST, or the DST, during that time, was characterized by pure strike-slip motion. A break during displacement of the 105 km left lateral offset (e.g. Quennell, 1959) is reported by Girdler and Southren (1987) and Barjous and Mikbel (1990) before about 5 Ma. The prominent unconformity he1 represents a major change in the development of the Elat Deep. The pre-tectonic unit is tilted to the south accounting for the general difference in altitude between the Arava Valley and the Gulf of Aqaba. South of the fault fc1, this dip is modified by an additional dip component towards the east. This additional eastward inclination could be explained by an increase in separation along the DST before 4.5 Ma (proposed by Joffe and Garfunkel, 1987). As this theory is associated with a continuous displacement along the DST, pure strike-slip must have been present during the first phase

of sediment deposition (pre-tectonic phase). The second phase is temporally linked with the initiation of the stepover that is mapped in the sediments, the south and eastward inclination of the pre-tectonic unit and the coeval deposition of the syntectonic sediments with their typically divergent reflection pattern caused by progressive subsidence of the Elat Deep. The estimation of the age of the major unconformity is not straight forward, as the sedimentation rates are not well known for the Gulf of Aqaba. The results of the Meteor Cruise M44/3 (Abu-Ouf et al., 2000) show a strong variation in time and space, as the average sedimentation rate for the northernmost Gulf of Aqaba is about 33cm/1000a and for the central part of the Elat Deep it is about 5cm/1000a (Arz, pers. comm., 2004), for the last 8000 years. The sedimentation rate is also affected by the climatic conditions, as Arz et al. (2003) calculated higher values for cold/wet periods and lower values for hot/dry periods. This periodic scheme is also known for the Dead Sea area Horowitz (1987, 1989), where sedimentation rates were determined up to the Miocene. The maximum observed thickness of the syntectonic unit is 900 ms TWT. This is equivalent to 855 m assuming an average sound velocity of 1900 m/s for the sedimentary column (derived from CDP velocity analysis). In order to correlate the unconformity he1 with the results of Girdler and Southren (1987) and Joffe and Garfunkel (1987) who both described a change in the tectonic history of the DST in the early Pliocene, although for different reasons, a sedimentation rate of 19cm/1000a is necessary. Even though this value is just a rough estimation that is within the minimum and maximum sedimentation rates of the Holocene (Arz, pers. comm, 2004), it points to the correlation of the unconformity he1 with the proposed change in the tectonic regime.

4.7 Discussion

The presented fault map and bathymetry (Fig. 4.13, 4.14) show some major features which have been identified by other authors (e.g. Ben-Avraham, 1985; Ben-Avraham and Tibor, 1993, Fig. 4.1, 4.2). In particular the fault map confirms basically the presence of the main faults of previous models, like the western boundary fault, the eastern boundary fault and the Elat Fault. The progression of the main strand within the northern Gulf of Aqaba is now located more precisely. The discovery of the bifurcation at the inflection point explains

morphological features on the Jordan side of the Gulf's Head. However, some of the interpretations presented here contradict published observations. The main results presented here that can not be correlated with previously published models include the type of the western boundary fault, the shape of the stepover and the overall sedimentary pattern.

4.7.1 Comparison to Previous Results

The western boundary fault of the Elat Deep, termed fn1 (Fig. 4.5) was interpreted by Ben-Avraham and Tibor (1993) as predominantly normal with minor strike-slip motion. This interpretation was supported by the body wave inversion of the 1995 $M_w = 7.3$ earthquake in the Gulf of Aqaba by Klinger et al. (1999). They modeled three successive subevents for the main shock, with the third subevent, left lateral strike-slip with normal component, located at the western boundary fault of the southern part of the Elat Deep (see Fig. 4.2A). In contrast to these observations, we do not observe strike-slip motion along the fault fn1. It cannot be resolved north of profile 014 and additionally, no left lateral offset can be observed along the slope (see submarine grabens in Fig. 4.11). In order to explain the inconsistency with the subevent of the 1995 $M_w = 7.3$ earthquake, it should be noted that this particular subevent took place in the southern part of the Elat Deep. But the Elat Deep is a composition out of two subbasins (see Fig. 4.2C) (Ben-Avraham, 1985). The calculated strike-slip motion could be accommodated by the western boundary fault of the southern subbasin. Moreover, the depth of the subevent was determined between 1.0 and 5.0 km, respectively, after Klinger et al. (1999, 2000), so the hypocenter is more likely located in the sedimentary overburden and the event might be a subprocess of the main shock. Thus, we differentiate between the southern part of the Elat Deep and its northern part to explain the results of the body wave inversion of Klinger et al. (1999).

The left stepover of the main strand of the DST was suggested by various authors in the area south of the Shlomo Graben (Fig. 4.1, 4.2) and the transverse fault between the eastern and western part of the DST was interpreted as normal fault with strike-slip component. The new geophysical dataset enabled us to compile a detailed fault map and to trace the stepover between the Elat Deep and the northernmost Gulf (Fig. 4.13). The shape of this fault structure is much smoother than previously suggested and fault fc1 that forms the stepover

shows strike-slip motion with a minor normal component. The combination of the faults fsn1, fc1 and the Elat Fault is more likely a single through going strike-slip fault than a sharp stepover as previously suggested.

The pull-apart basin related model for the Elat Deep (Fig. 4.1, 4.2) implies that substantial amounts of extension and subsidence have affected a pre-tectonic sedimentary unit. The new seismic data resolve two main sedimentary sequences, and the lower unit was deposited before onset of the latest phase of the basin formation. This unit is dipping almost continuous below the Elat Deep. The fault fn2 (Fig. 4.12) is accommodating the general difference in altitude between the Arava Valley and the Elat Deep, and the subsidence because of the eastward inclination of the pre-tectonic unit in the Elat Deep area. In analogy to the mapped fault system (Fig. 4.13), the pre-tectonic unit was mainly affected by subsidence and strike-slip faulting in the area of the stepover and only a little by extension. The difference in altitude between the Arabian and the Sinai-Sub Plate is pointed out at the left stepping DST, because both, the differential uplift and the lateral displacement, are compensated in this key area of the Gulf of Aqaba. As a result of this constellation, the deeper situated Gulf strikes out at the stepover against the higher situated Arava Valley.

4.7.2 Comparison to Analog Models

The lack of significant vertical tectonism and extension in the northern Gulf as well as the smooth stepover suggests that the northern margin of the Elat Deep does not represent a rift shoulder of a pull-apart basin. The crystalline basement is not resolved in available seismic data. However, a synthesis of all available information including recently published results of analog modeling points towards a new model for the evolution of the northern Gulf of Aqaba. Sims et al. (1999) performed analog modeling of pull-apart basin formation. In order to model the observed basin asymmetry of e.g. the Gulf of Aqaba, sandbox experiments were conducted with a special ductile décollement layer between the moving plates and the sedimentary overburden. This was then compared to a model with a rigid décollement layer. Whereas the experiment with a rigid décollement layer provides results similar to the classical theory of pull-apart basin development, the experiments with a ductile décollement layer show elongated asymmetric subbasins, like in the Gulf of Aqaba (see Fig. 4.15). Sims et al. (1999) demonstrated that the shape of the sedimentary basins and

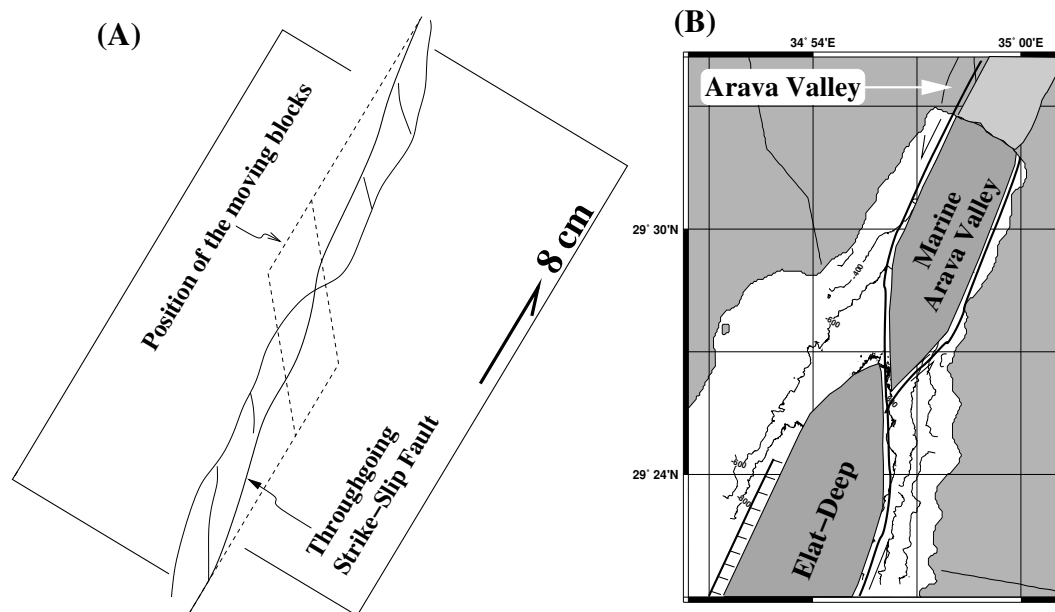


Fig. 4.15: A: Sketch of the observed fault system in an analog model (after Sims et al., 1999). Elongated basins occur symmetrically to a through going strike-slip fault. B: Fault map of the Northern Gulf of Aqaba. The fault system is similar to that observed in analog models.

its fault system does not necessarily reflect the shape of the underlying pull-apart area in the crystalline basement, as far as a ductile décollement layer is involved. Salt layers within the sediments could act as ductile décollement layer. Evaporites are widespread in the Middle East Region. Although evaporites were not recovered in the Northern Gulf of Aqaba and Arava Valley region yet, we assume that salt layers could be present within the sediments, similar to the Miocene evaporite occurrence of the Red Sea (Searle and Ross, 1975), or the Pliocene evaporite deposition of the Dead Sea area (Al-Zoubi and ten Brink, 2001). The mapped fault system between the Elat Deep and the Arava Valley is similar to analog modeling results from Sims et al. (1999). This approach explains some of the conspicuous features of the northern Gulf that could not be explained by the classical pull-apart model. Like in the analog model, elongated sedimentary basins are arranged along a through going strike-slip fault; the opposite bounding fault is predominantly normal.

The sedimentary pattern, as it is observed in the northern Gulf, could have developed if a ductile décollement layer is present below the pre-tectonic sedimentary unit that decouples the basement from the sedimentary overburden.

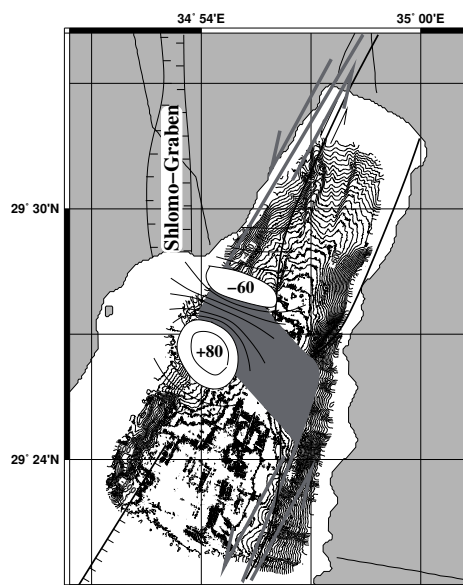


Fig. 4.16: Fault system of the Northern Gulf of Aqaba. The heavy grey lines indicate the assumed stepover in the basement. Superposed is the dipole type magnetic anomaly after Ben-Avraham and Tibor (1993) which may represent magmatic additions in the extended basement in the stepover zone (Magnetic field in nT).

Following this approach, the stepover of the DST in the basement is located beneath the transition zone where the through going strike-slip fault changes from one side of the basin to the other. A strong dipole type magnetic anomaly (Fig. 4.2B) is reported in this region by Ben-Avraham and Tibor (1993), probably caused by a magmatic intrusion. The location of this anomaly and thus the magmatic body could be controlled by the stepover, because of the stretched and weakened basement in this particular area. The decoupling of basement and overlying sediments was already suggested by Garfunkel and Ben-Avraham (1996) for the Dead Sea basin.

The discussion is summarized in a model for the northern Gulf of Aqaba (Fig. 4.16). It explains the surficial fault pattern and the combined conclusions for the basement fault structure in this area. It should be noted that the survey area covers only about 1/4 of the entire basin and that the necessary décollement layer was not observed owing to the limited penetration of the seismic signal. However, the new model presented here is consistent with the geophysical evidences from this region.

4.8 Conclusion

A dense grid of multichannel seismic and bathymetric data from the northern extension of the Gulf of Aqaba reveals a complex fault system and sedimentation pattern. Two main sedimentary sequences units separated by a prominent unconformity were identified and interpreted as pre-tectonic (lower unit) and syntectonic (upper unit) sequences, respectively. Two tectonic phases can be linked to the deposition of the sediments and the development of the recent fault system:

During phase one, the pre-tectonic unit (probably deposited in a relatively shallow basin in the Miocene and early Pliocene) is characterized by a parallel reflection pattern and an undisturbed internal structure. No evidence was found for stepover related tectonism during this phase. The undisturbed layering of the sediments points to tectonic quiescence or pure strike-slip motion, without extension or compression. The upper boundary of this sequence forms the unconformity which marks a major change in the tectonic activity of the DST and the transition from phase one to phase two.

During phase two, increased subsidence of the Elat Deep caused southward tilting of the pre-tectonic unit. The (re-) initiation of strike-slip motion and the stepover from the eastern side of the Elat Deep to the western side of the Gulf's Head occurs. This caused the additional eastward tilting of the pre-tectonic unit and increased the subsidence on the eastern flank of the Elat Deep. The typical divergent reflection pattern and onlap structures on the unconformity reveals coeval sedimentation of the syntectonic unit. The thickness of the synsedimentary unit indicates that the latest phase of the formation of the Elat Deep began in the early Pliocene. This corresponds to the findings of Girdler and Southren (1987) and Joffe and Garfunkel (1987) who suggested a major change in the tectonic history of the DST at almost the same time.

Close to the stepover, the strike-slip fault bifurcates and a newly discovered right bending branch runs northeastward toward the Jordan coast where thrust faulting is shown in the seismic data. This recently active transpressional deformation indicates that strike-slip motion is partly accommodated along the eastern slope of the northern Gulf. The previously proposed stepover of the main branch of the DST along the western side of the Gulf's Head is mapped for the first time in detail. The stepover is much smoother than previously suggested

and it does not follow the steepest slope gradient of the Elat Deep.

The lack of significant extension within the pre-tectonic sequence as well as the smooth stepover of the DST are in contrast to recent geodynamic models in which the entire Elat Deep represents a rhomb shaped pull-apart basin. A synthesis of our new findings and other published information points towards a decoupling between the left stepover in the deeper basement and the tectonic response of the shallower sedimentary sequences.

4.9 Acknowledgments

We would like to thank Jürgen Pätzold (University of Bremen) for providing the bathymetric data. Thanks also go to Volkard Spiess (University of Bremen) for providing the seismic acquisition equipment and Mohammed Salem (University of Bremen) for editing of the bathymetric data. We are grateful to the crew of the R/V Meteor for the technical assistance provided during cruise M44/3. Further we would like to thank Isabelle Manighetti and Amotz Agnon for their helpful suggestions. The interpretation was supported by the KingdomSuite – software. All maps were produced with GMT. This work was funded by the German Research Foundation (DFG) grant HU698/4.

5 Conrad Ocean Deep, Northern Red Sea: Transtension Basin within the Axial Depression

by Axel Ehrhardt, Christian Hübscher and Dirk Gajewski
submitted to *Tectonophysics*, 04/2004

5.1 Abstract

The northern Red Sea represents a continental rift in the late stage of rifting and close to the following stage of seafloor spreading. Ocean deeps within the Red Sea seem to accompany this process and are thought to be surface expression of first seafloor spreading cells. The Conrad Deep is one of the northernmost Red Sea deeps. It is in an early stage of its development. In 1999 during R/V Meteor cruise M44/3 a dense multichannel seismic and hydroacoustic survey was conducted in order to investigate the initial formation process of a northern Red Sea deep. Three seismic units were differentiated in the uppermost part of the Miocene evaporites and the Plio-Quaternary sediments. The fault system and the orientation of salt walls and rises point to a tectonic induced formation mechanism for the Conrad Deep. A weakness zone within the evaporites oblique to the main extension direction of the Red Sea led to a transtension process that opened the Deep. Its formation is directly associated with the emplacement of magmatic bodies in its vicinity and the focusing of the Red Sea extension to the axial depression. The Conrad Deep is an intra-evaporite basin that cannot be regarded as surficial expression of a basement structure, but its position and shape in combination with the accompanying geophysical anomalies point to a transition from Red Sea extension to Dead Sea Transform strike-slip displacement.

5.2 Introduction

Ocean deeps are widespread features within the Red Sea; their formation is thought to be a first sign documenting the transition from continental rifting to seafloor spreading (Bonatti, 1985; Martinez and Cochran, 1988; Cochran and Martinez, 1988). The Red Sea Rift makes, as part of the African–Arabian rift system (Fig. 5.1), a good location to study the evolution from continental rifting to seafloor spreading. Whereas the southern part of the Red Sea exhibits already organized seafloor spreading since 5 Ma (e.g. Röser, 1975), the northern part is thought to be in the late stage of continental rifting (Martinez and Cochran, 1988). The central part is in an intermediate stage (Searle and Ross, 1975) (Fig. 5.2).

The Conrad Deep is one of the northernmost Red Sea Ocean deeps. It is located in the axial depression of the northern Red Sea at $27.05^{\circ}\text{N}/34.75^{\circ}\text{E}$ slightly shifted in the south-westward prolongation of the Gulf of Aqaba, about 100 km

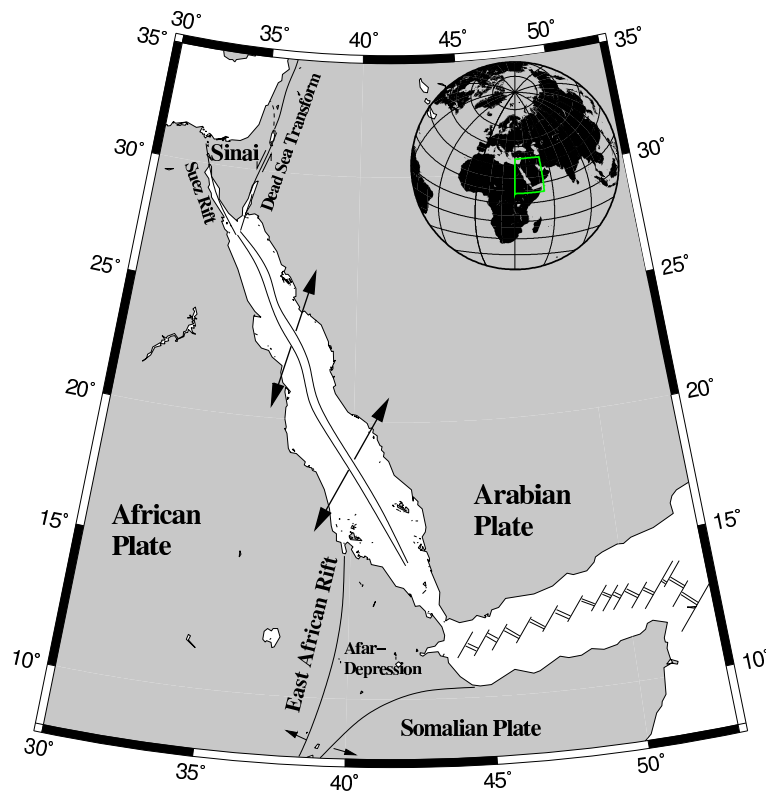


Fig. 5.1: Overview of the Red Sea Rift system (after Joffe and Garfunkel (1987)). It comprises the East African Rift, the Red Sea Rift and the Dead Sea Transform.

south of Ras Muhammad (Sinai) and 110 km north of the next prominent deep, the Shaban Deep (see Fig. 5.3). Because huge amounts of evaporites were deposited in the main trough of the Red Sea in the Miocene, direct basement observations were prevented, and up to now the nature of the basement type of the northern Red Sea, and hence the status between rifting and drifting is still under debate. Thus, surficial structures like the Red Sea deeps probably give hints of deep processes like crustal extension, magmatic intrusions or seafloor spreading. As the northern Red Sea deeps are in an early stage of their formation, they are an ideal study object for the investigation of their initial development and the derivation of the driving forces that initiated the formation process. Up to now different reasons for the development of the northern Red Sea deeps have been published, the endmember models are collapse structures and pull-apart basins. However, these models were not verified by a detailed survey of a northern Red Sea deep.

In 1999, during the Cruise M44/3 of the R/V Meteor (Hübscher et al., 2000), a dense high resolution seismic and hydroacoustic survey was conducted in the area of the Conrad Deep in order to resolve the internal structure of the Plio-Quaternary sediments and the top of the Miocene evaporites.

The purpose of this paper is to reconstruct the structural evolution of the Conrad Deep. As a result of this study the different geologic and tectonic circumstances like magmatic intrusions, ductile properties of evaporites and extension stress will be brought into consideration for the evolution and the location of the Conrad Deep as a Red Sea Ocean deep. After a short review of the geological background of the working area and the previous research, we present the new seismic and hydroacoustic data. Based on the dense coverage of 2-D multichannel seismic lines a three-dimensional mapping of the main sedimentary units above the Miocene evaporites and the associated fault system was performed. This information led to a model for the development of the Conrad Deep that will be discussed with respect to the regional geological and tectonical settings.

5.3 Geological Setting

The Red Sea Rift forms an elongated, northwest striking depression with a length of approximately 2000 km. It separates the African Plate from the Arabian Plate as part of the entire rift system that includes the Gulf of Aden, the

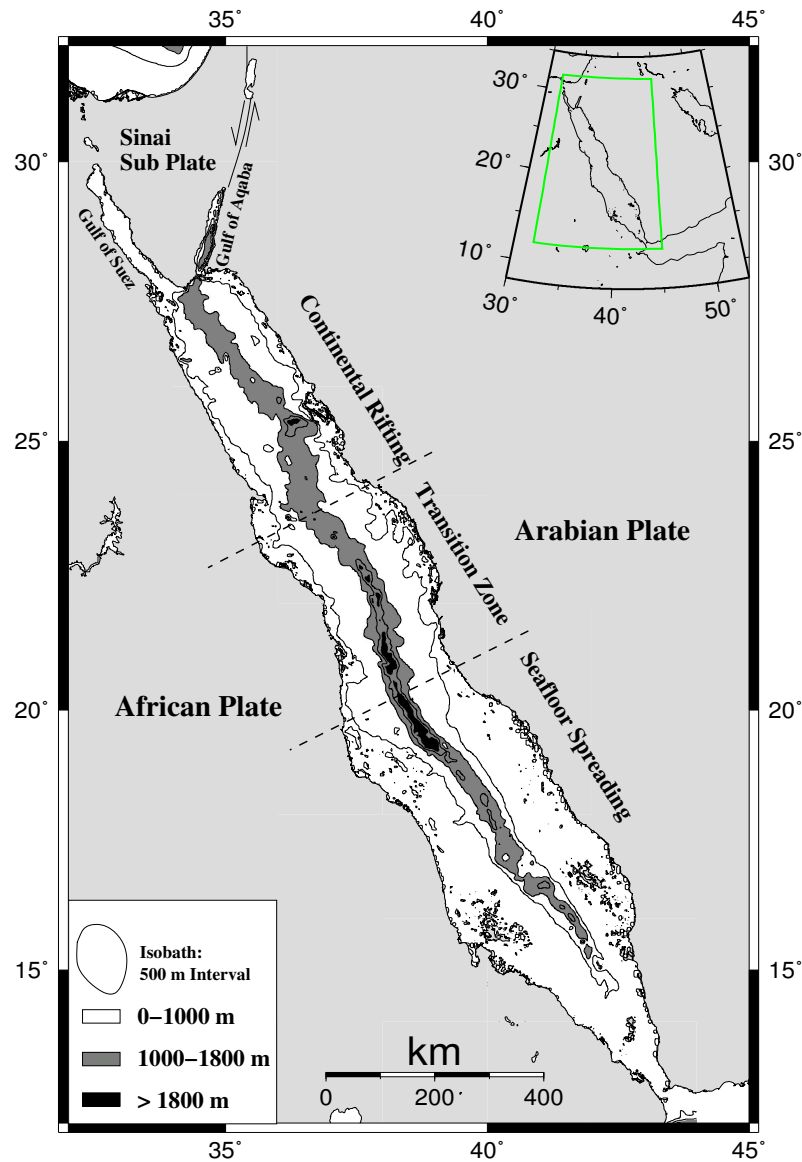


Fig. 5.2: The Red Sea can be separated into three parts along strike. The southern part is characterized by organized seafloor spreading. The central part is a transition zone between continental rifting and seafloor spreading. The northern part shows no sign of spreading. The grey shaded area comprises water depths of more than 1000 m and images the axial trough and axial depression, respectively (satellite altimetry from Sandwell and Smith (1999)).

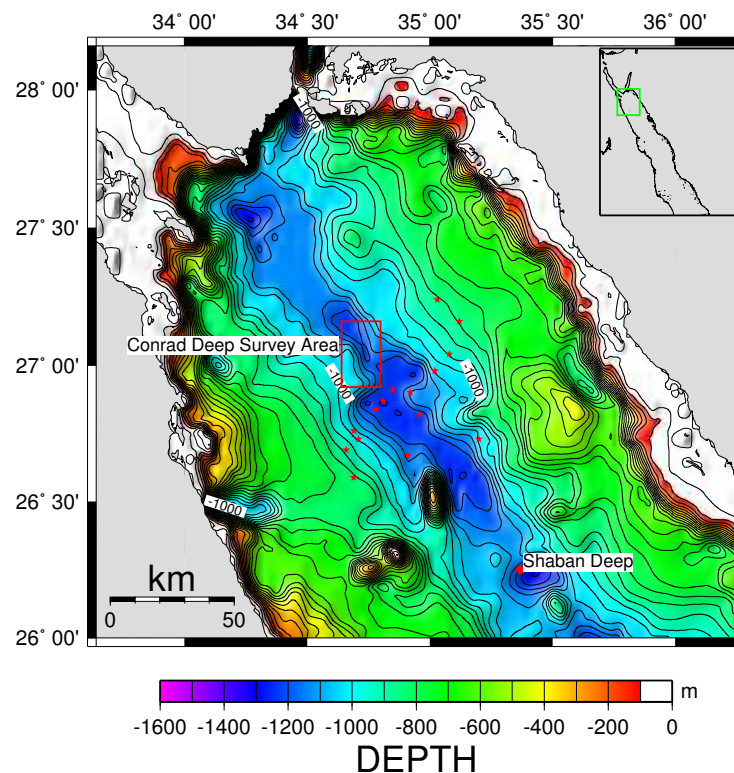


Fig. 5.3: Northern Red Sea: The red square indicates the survey area of the Cruise M44/3. Red stars mark the position of epicenters localized by the NEIC Earthquake Catalogue (2004). Note the apparent correlation of the alignment of the epicenters with the lateral offset of the axial depression. That points to a transform fault of the Red Sea Rift, 5 km south of the Conrad Deep.

East African Rift, the Gulf of Suez and the Gulf of Aqaba (see Fig. 5.1). With the initiation of this rift system in the Oligocene to Early Miocene, the former continuous Afro–Arabian shield was fragmented and split into the African and Arabian Plates (Martinez and Cochran, 1988). A major stage of the rifting process occurred in the Early to Middle Miocene, when the opening of the Red Sea was compensated in the north no longer by the Suez Rift but by the sinistral Dead Sea Transform. The onset of the transform motion started about 20 Ma ago (Girdler, 1985; Joffe and Garfunkel, 1987).

The formation of the Red Sea depression led to a typical symmetrical shape across the strike of the basin (Fig. 5.4). The coastal shelves are identified to depths of about 400 m. Between these shelves, a main trough exhibits depths up to 1000 m and is bisected by an axial trough and axial depression, respectively, with water depths exceeding 1000 m. Whereas in the southern and central parts

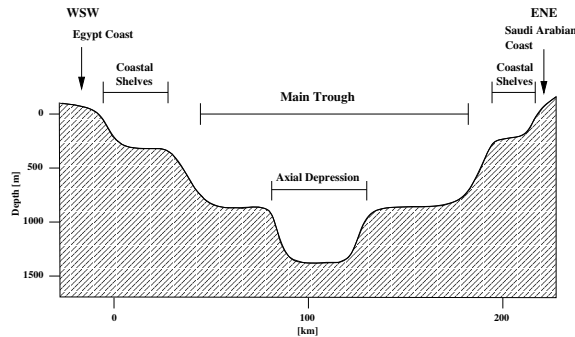


Fig. 5.4: Sketch of a cross section of the northern Red Sea. The Red Sea has an almost symmetric shape with marginal shelves (400 m), the main trough (1000 m) and the axial depression (1200 m) that bisects the main trough (after Guennoc et al., 1988).

of the Red Sea the axial trough shows maximum depths of more than 2000 m, in the northern part the average water depth in the axial depression is about 1200 m and more than 1500 m within the deeps.

Several kilometers of Miocene evaporites are found in and near the main trough (Lowell and Genik, 1972; Girdler and Styles, 1974; Searle and Ross, 1975). Isolated from continuous sea water influx, huge amounts of evaporites were deposited during the Miocene epoch. These evaporites are widespread in the Red Sea depression and mask the underlying basement. Thus, direct observations of the basement are very rare and the nature of the basement, especially in the northern Red Sea is still under debate. Because of the immense mass of evaporites, even their base was mapped only by a few surveys (e.g. Gaulier et al., 1988). In contrast, the top of the evaporites is well expressed in reflection seismic data. A high amplitude, low frequency reflection images the top of the evaporites that could be identified all over the Red Sea. This prominent reflector is named S-Reflector (Whitmarsh et al., 1974; Searle and Ross, 1975). The high amplitudes are caused by the strong impedance contrast between the overlying nanno oozes and the top evaporites (halite or anhydrite). The seismic velocity changes from about 2.3 km/s (ooze) to 4.2 km/s (halite) and 4.8 km/s (anhydrite) (see SITE 227, 228 of the DSDP Whitmarsh et al. (1974)). Thus, the high impedance contrast enables a pretty good identification of the Miocene evaporites, but also limits the seismic signal penetration considerably. The S-

Reflector is typically covered by an amount of Plio-Quaternary sediments that corresponds to 200 - 300 ms TWT.

Along strike of the Red Sea, it is possible to observe different stages of the development of the Red Sea Rift, from rifting to seafloor spreading. According to its tectonic evolution, the Red Sea can be separated into three parts (Cochran, 1983) (Fig. 5.2). The southern part of the Red Sea between 15°N and 20°N is characterized by a well developed axial trough. Within that trough seafloor spreading can be observed with a maximum age of 5 Ma (Röser, 1975). To the North, the oceanic basement becomes progressively younger (2–3 Ma) (Searle and Ross, 1975). The central part of the Red Sea is located between 20°N to 23.3°N. In this area, the axial trough becomes discontinuous and is intersected by intertrough zones (Searle and Ross, 1975). In between these intertrough zones, there are well developed deeps with water depths of about 2000 m; e.g. Atlantis II Deep, 14 km x 5 km and maximum depth of 2200 m (Warren, 1999). These deeps are partially floored by oceanic basement, but the spreading commenced not earlier than 1.7 Ma ago (Searle and Ross, 1975). Bonatti (1985) interpreted these deeps as initial spreading centers. Thus, the central part seems to be a transition zone between regular seafloor spreading and continental rifting. The northern part is dominated by an axial depression with a water depth of about 1200 m that is punctuated by several isolated deeps. Located in the axial depression, the northern Red Sea deeps, like the Conrad Deep or Shaban Deep (Fig. 5.3), are smaller and less developed as initial spreading centers in comparison with those of the central Red Sea.

Most of the Red Sea deeps are located in the axial trough and axial depression, respectively. In addition to the morphological anomaly, the Red Sea deeps are also associated with heat flow and magnetic anomalies. In general, the heat flow in the Red Sea is very high with values exceeding the world mean by the factor of 2 to 10 (Makris et al., 1991b). On a cross section of the Red Sea, the highest heat flow density correlates with the location of the axial depression and axial trough, respectively. In the vicinity of deeps, the heat flow density is even higher, reaching top values of up to 600 mWm^{-2} (see Cochran et al., 1986). Most of the deeps correlate also with magnetic anomalies (e.g. Cochran et al., 1986; Martinez and Cochran, 1988; Guennoc et al., 1988). Whereas the central Red Sea deeps display already linearly aligned magnetic anomalies, indicating the recently commenced of seafloor spreading, the northern Red Sea deeps are

characterized by dipole type anomalies, caused by single intrusions. Many of the Red Sea deeps are associated hypersaline brine bodies that are caused by increased salinities. Leaching of the underlying evaporites may have enriched the salinity in the deeps and caused thus a density contrast in the water column (e.g. Manheim, 1974; Hartmann et al., 1998; Winckler et al., 2001). This density contrast is imaged by reflection seismic methods by a clear horizontally reflection within the water column, the brine reflector.

5.4 Previous Work in the Northern Red Sea

The Red Sea and especially the northern Red Sea experienced in the 1980's and early 1990's a phase of intensive investigations (Pautot et al., 1984; Mart and Hall, 1984; Bonatti, 1985; Cochran et al., 1986; Guennoc et al., 1988; Martinez and Cochran, 1988; Cochran and Martinez, 1988; Gaulier et al., 1988; Rihm, 1989; Coutelle et al., 1991; Makris and Rihm, 1991a; Makris et al., 1991b; Cochran et al., 1991; Makris and Henke, 1992). In this time several Red Sea deeps were discovered: e.g. the Shaban Deep (alias Jean Charcot Deep) in 1983 (Pautot et al., 1984), the Conrad Deep in 1984 (Cochran et al., 1986) and several unnamed deeps (Martinez and Cochran, 1988). Many authors explained the presence of the deeps in the context with the opening of the Red Sea. Because of the more or less equidistant spacing between the deeps of 60 km (Martinez and Cochran, 1988), the magnetic anomalies that are accompanying most of the deeps, the regional stress field and the processes of the rift development were used for the explanation of the location of the deeps and for the presence of the deeps itself. Two major models were published to explain the location and presence of the deeps. Bonatti (1985) proposed a punctiform initiation of seafloor spreading in the Red Sea because of regularly spaced asthenospheric diapirs. These diapirs were initiated by possible density/viscosity inversions in the upper mantle that can be treated as Raleigh–Taylor instabilities. Martinez and Cochran (1988) concentrated their theory on the presence of bathymetric terraces that correlate with gravity anomalies (Cochran and Martinez, 1988). They introduced three major accommodation zones that cut the northern Red Sea into provinces perpendicular to its strike. Deepes are located midway, in between the accommodation zones that seem to control the emplacement of large magmatic intrusions and therefore the location of the deepes.

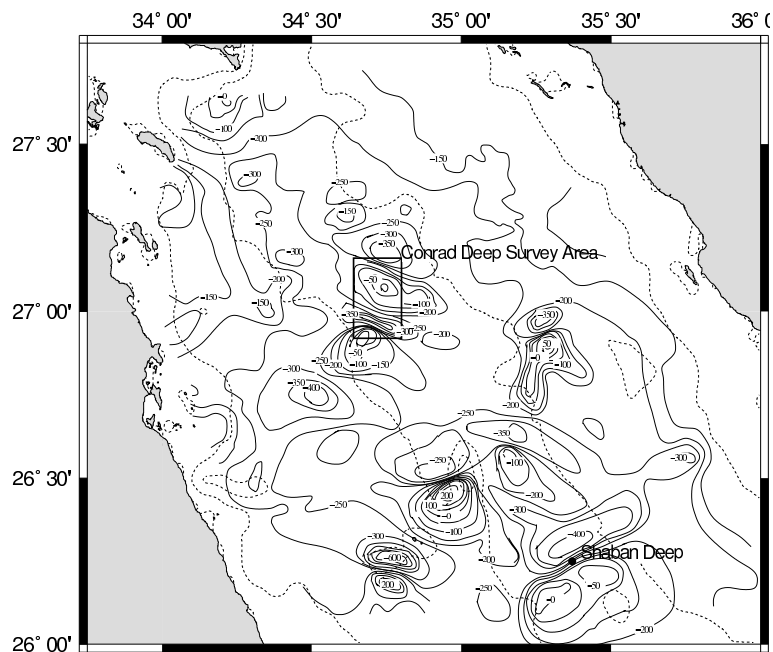


Fig. 5.5: Total intensity magnetic map (after Martinez and Cochran, 1988). Magnetic interval at 50 nT, the dotted lines represent isobaths at 500 m interval. The survey area is marked by the black box. On the northern and southern extensions of the Conrad Deep dipole type magnetic anomalies are found.

The Conrad Deep is located in the axial depression of the northern Red Sea ($27.05^{\circ}\text{N}/34.75^{\circ}\text{E}$) slightly offset in the southward prolongation of the Gulf of Aqaba (Elat) (see Fig. 5.3). During the cruise of the R/V Conrad in 1984 (Cochran et al., 1986), the Conrad Deep was detected during a concentrated geophysical survey. Additional to direct ship born measurements, satellite altimetry and seismological data are available in the world wide web (Sandwell and Smith, 1999; NEIC Earthquake Catalogue, 2004). Figure 5.3 shows satellite altimetry by Sandwell and Smith (1999) and epicenter distribution by NEIC Earthquake Catalogue (2004). With a grid spacing of 0.5 min, the satellite altimetry can not resolve small scale structures like the Conrad Deep, but the bathymetrical trend in the northern Red Sea is imaged correctly. About 5 km southeast of the survey area, the satellite altimetry reveals a lateral offset of the axial depression. It correlates with a conspicuous SW–NE alignment of seismological events. This offset is possibly the surface expression of a transform fault in the northern Red Sea Rift. Whereas the gravimetric data of the R/V Conrad Cruise (Cochran et al., 1986) do not resolve small scale features like the Conrad Deep, the magnetic survey revealed two major dipole–type magnetic anomalies

that are associated with the Deep, located at the southwestern and northeastern end, respectively (Fig.5.5). Cochran et al. (1986) modeled two intrusion bodies to explain the magnetic anomalies and dated the intrusion to have occurred very recently, only 40,000 years ago. As all magnetic anomalies in the northern Red Sea have a normal polarization, their maximum age of emplacement is 0.7 Ma (Guennoc et al., 1988).

5.5 Methods and Results

The area of the Conrad Deep was investigated in 1999, during the R/V Meteor Cruise M44/3. A dense grid of high resolution 2-D multichannel seismic lines was measured combined with Parasound (sediment echograph) and Hydrosweep (swath echosounder) measurements (see Fig. 5.6). Hydrosweep and Parasound measurements were conducted parallel to the seismic lines and midway, between the seismic lines (see dashed lines in Fig. 5.6).

5.5.1 Bathymetry

The bathymetry measurements were performed using an ATLAS HYDROSWEEP system. This multibeam echosounder had a swath width of twice the water depth. The dense line spacing led to a complete coverage of the seafloor topography. Due to uncertainties in the velocity-depth function of the sea water and the compensation of the sea state, the vertical error is in the order of 1% - 3% of the water depth. The general bathymetric trend is already visible in the satellite altimetry data (see Fig. 5.3). The new shipborn bathymetric data resolve the Conrad Deep in greater detail (Fig. 5.7). Whereas Figure 5.7 provides an illuminated DEM map for a better impression of the morphological structure, Figure 5.8 shows a contour line map, extended with information of the bathymetric survey by Cochran et al. (1986). The composition of both datasets clearly shows that northwest of the Conrad Deep a second, so far unknown, deep with at least the same water depth is present. Because of the apparent difference in the shape of the second deep, it will be regarded as an independent deep. In memoriam to our colleague Sonja Klauke, from R/V Meteor Cruise M52/3, we name this newly discovered deep 'Klauke Deep'.

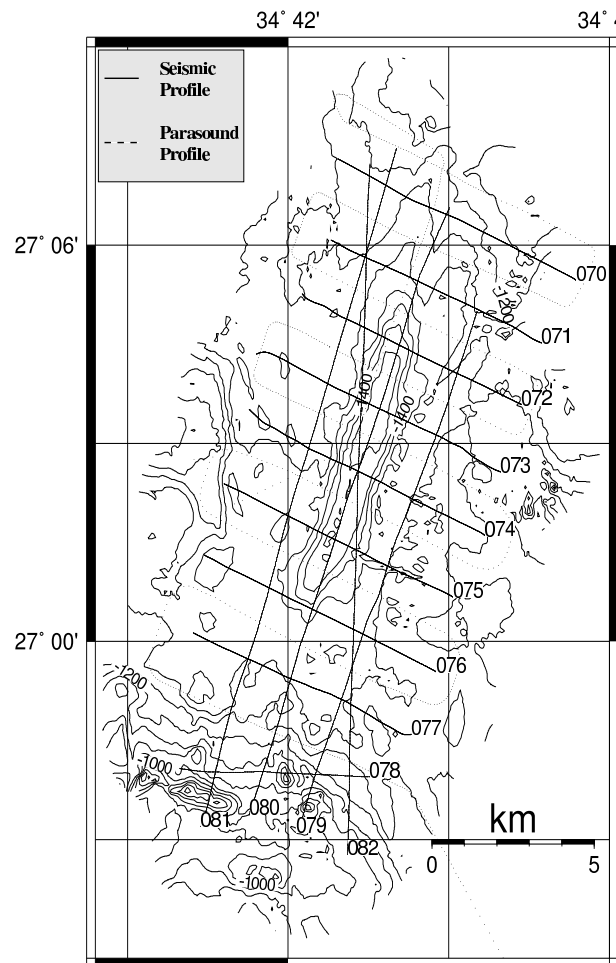


Fig. 5.6: Basemap of the reflection seismic data of the cruise M44/3. Solid lines mark reflection seismic lines, dotted lines represent the location of additional Parasound and Hydrosweep lines (after Hübscher et al., 2000).

5.5.2 Seismic Data

The high resolution seismic data acquisition was performed with a volume reduced GI-Gun. Thus, signal energy with frequencies up to 350 Hz contributed to the seismic imaging. A SYNTRON analogue streamer with 24 channels, distributed over 300 m active length, was used for the registration of the seismic energy. For seismic recording and processing parameters, please refer to Table 5.1. The processing was performed with special emphasis to the high frequency content of the signal. Because already small undulations of the streamer could lead to destructive interference along the hyperbolic moveout of an event in a CMP-gather, static corrections were calculated and applied to increase the

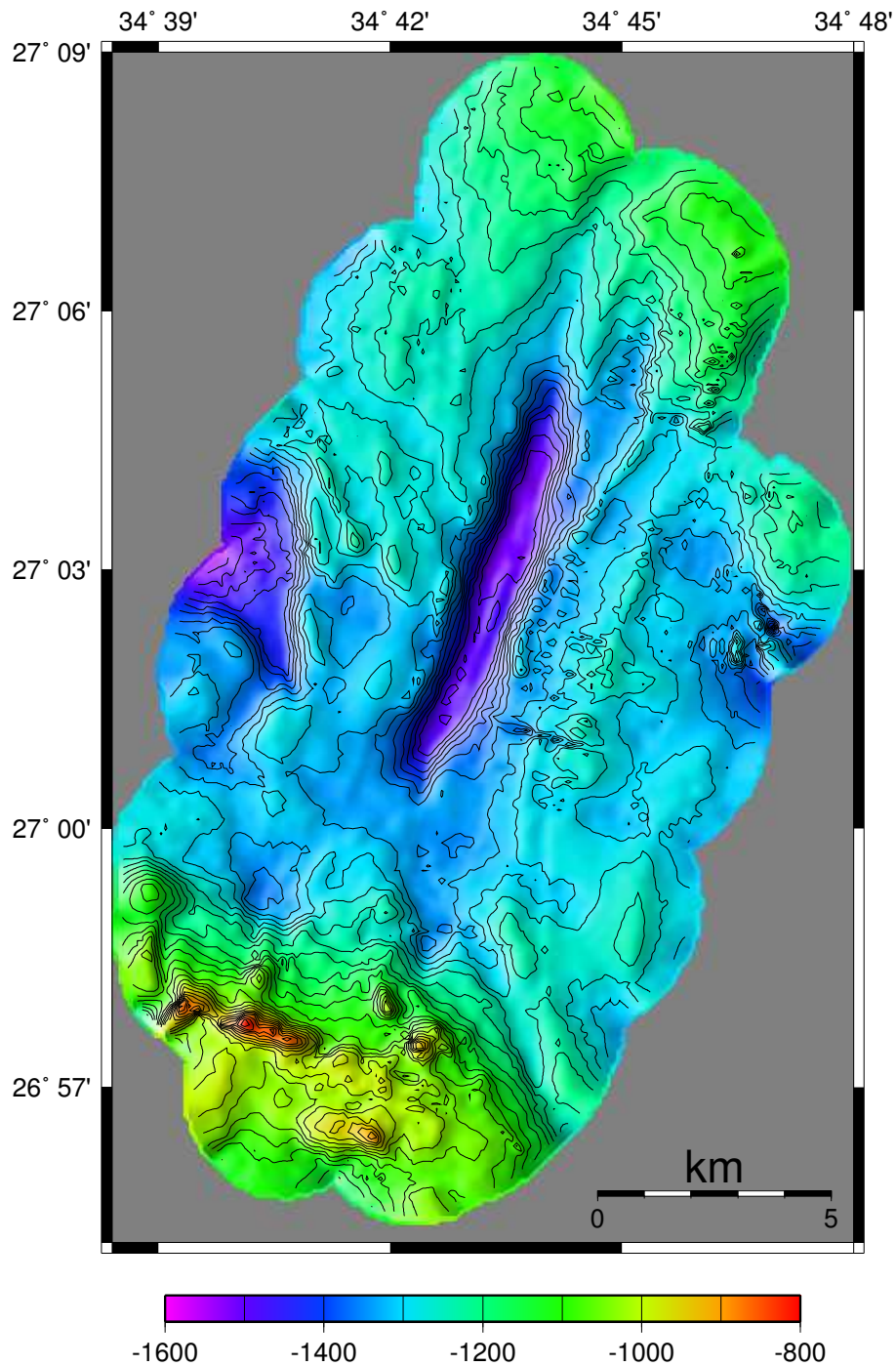


Fig. 5.7: Conrad Ocean Deep: The Deep forms an elongated rhomb-shaped basin, 10 km long and 2 km wide with a maximum water depth of 1500 m (ca. 250 m difference in depth to the axial depression) The Deep is orientated N20°E and strikes almost parallel to the Gulf of Aqaba (see Fig. 5.2).

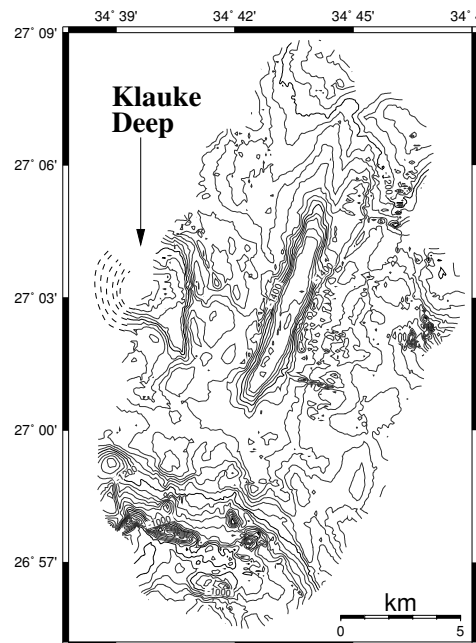


Fig. 5.8: The Klauke Deep: Adjacent to the Conrad Deep, a second Deep was discovered during the Cruise M44/3. The Deep is not fully covered by the Hydrosweep Multibeam data, but in combination with the data of Cochran et al. (1986) the shape of the Deep can be estimated. The dashed lines are indicating the data that is inserted in the bathymetric map.

quality of the stacking results and therefore the lateral coherency of events. All seismic lines were processed including time migration. A dense grid of profiles with a total length of 135 km, including nine lines crossing the Conrad Deep perpendicular to the strike, three lines parallel to the strike of the Deep and one line oblique to the strike of the Deep, enabled the interpolation of the fault system and sedimentary units between the 2-D lines (maximum distance between the lines is 2.1 km) (see Fig. 5.6).

In order to explain the subsurface structure of the Plio-Quaternary sediments and the top of the Miocene evaporites, the resolved sediments were distinguished into three seismic units concerning the formation history of the Conrad Deep. Line G_99_074 (Fig. 5.9) will be used as a showcase example, to introduce the seismic units. They can be described chronological as follows:

Source-Parameters	
Source	1 GI-Gun
Volume	2 x 0.4 l
Mode	True GI Mode
Dominant Frequency Bandwidth	20 Hz – 350 Hz
Time Shot Interval	10 s
Spatial Shot Interval	approx. 25 m (Ship velocity 4.9 knots)
Receiver-Parameters	
Streamer	SYNTRON
No. of Channels	24
Active Length	300 m
Group Interval	12.5 m
Geometry and Processing	
CMP Interval	12.5 m
Average Fold	12
Static corrections for streamer undulations	
Stack	
f-x Migration	Smoothed velocity function

Table 5.1: Acquisition and Processing Parameters

1. The Miocene evaporites: Huge amounts of evaporites were deposited in the Miocene in the area of the main trough. In the area of the Conrad Deep probably 3000 m thick evaporites were assumed (Cochran et al., 1991). The top of the evaporites is visible in the seismic data as high amplitude, low frequency reflection, in general 200 ms to 300 ms TWT below the seafloor. Depending on the material of the top of the Miocene evaporites (halite, anhydrite or gypsum) the internal reflectivity of the evaporite body alternates from seismic transparent to a layered pattern. The characteristic reflection at the top of the evaporites is known in the Red Sea area as S-Reflection (Searle and Ross, 1975). This term is also used in this work. The overlying Plio-Quaternary cover will be subdivided into pre- and synkinematic deposited sediments. The term kinematic is used in the context of the evolution of the Conrad Deep.

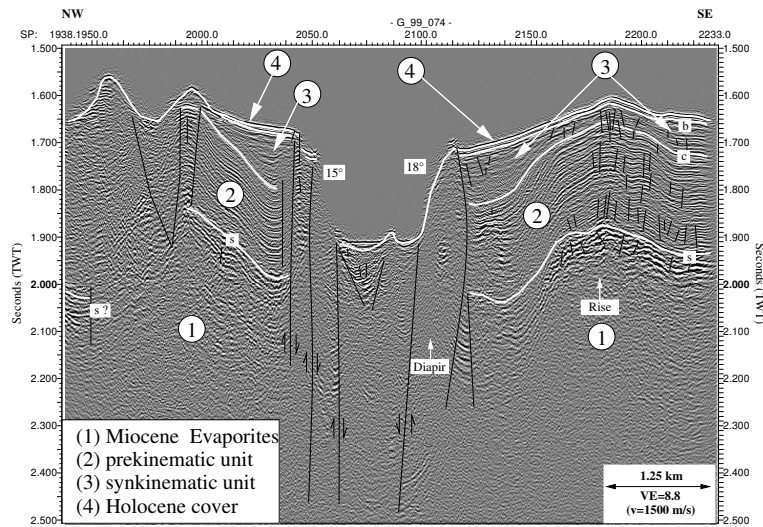


Fig. 5.9: Line G_99_074: Showcase example for the differentiation into distinct seismic units. Reflector S builds the top of the Miocene evaporites (1). Unit (2) is formed by prekinematic sediments that show concordant reflection patterns to the S-Reflector. The synkinematic unit (3) displays divergent features and growth faults (3). (4) depicts the uppermost continuous sediments, only disturbed by recently active faults.

2. Prekinematic unit: The S-Reflector is covered by a sequence of concordant layered sediments. This unit was deposited before the onset of the development of the Conrad Deep. The top of this prekinematic unit will be termed C-Reflector.

3. The synkinematic unit is characterized by lower amplitude reflections. In tectonically affected areas (e.g. at rises) the syn-unit shows divergent reflection patterns that onlap the C-Reflector. Growth faults are typical in this unit. The top of the synkinematic unit will be named B-Reflector. A high amplitude double reflection just underneath the seafloor covers most of the synkinematic sediments and the faults within the unit. However, some faults are cutting this unit as well, indicating recent tectonic activity.

5.5.3 Results

The Conrad Deep is situated within the axial depression of the northern Red Sea. It is about 10 km long, 2 km wide and has an overall strike of N20°E that is almost parallel to the Gulf of Aqaba, the main tectonic feature in the northern Red Sea area (Fig. 5.7). A more precise view to the bathymetric data reveal that the up to 19° steep slopes of the Conrad Deep are subdivided into en-echelon

distributed segments of $N25^{\circ}E \pm 2^{\circ}$ that are linked by N-S ($N1.6^{\circ}E \pm 1.0^{\circ}$) partitions, thus forming a zig-zag pattern (see Fig. 5.10). The Deep itself is a composition of at least two sub basins. The southwestern shallow basin is separated by a small rise from the deeper NE-basin (see Fig. 5.10). Diapirs or volcanic extrusions are located at the southern flank of the axial depression. These features are 150 m to 190 m higher than the surrounding seafloor of the main trough. The descent to the axial depression amounts ca. 200 m with gradients of $4^{\circ} - 6^{\circ}$. The seafloor of the axial valley is irregular and yields different orientations of surficial structures SE and NW of the Conrad Deep, respectively. The SE-shoulder reveals lineated structures that are orientated parallel and subparallel to the Deep, whereas mainly NW-SE trending structures are present on the shoulder of the Deep. On the northwestern most part a 2 km x 3 km patch of the NW-shoulder shows subsidence towards the Deep. Using the recent seismic grid, we investigated the subsurface effects of the bathymetrical structures.

The SE-shoulder is dominated by the two elongated parallel to subparallel anticlinal structures (see Fig. 5.11, 5.12, 5.13, 5.14). Line G_99_072 (Fig. 5.11) crosses the NE-part of the Deep, and the bathymetrical structures can be identified on the SE-shoulder. The parallel trending anticlinale is formed by a rise of the Miocene evaporites (SE-Rise). The prekinematic sedimentary unit overlies the uplifted evaporites concordantly and is affected by extensional faults. The synkinematic unit onlaps the top of the pre-unit (C-Reflector) and shows a divergent reflection pattern. The youngest sediments (visible as high amplitude double reflection) are undisturbed and reveal no growth pattern or faulting. This scenario is identical on the successive parallel cross sections G_99_73 (Fig. 5.12), G_99_074 (Fig. 5.13) and G_99_075 (Fig. 5.14). The subparallel bathymetric anticlinale feature trends $N34^{\circ}E$ and runs into the Deep, where it forms the SE-slope in the central part of the Deep (Fig. 5.12, 5.13). The seismic sections reveal, that this bathymetric anticline structure is caused by an elongated salt diapir (Salt Wall) that can be traced by the bathymetric and seismic data from the slope of the central part of the Deep (Fig. 5.10, 5.12, 5.13) into the SE-shoulder (Fig. 5.11). The vertical motion of the Salt Wall has affected all seismic units, including the uppermost and youngest sediments, indicating that the salt intrusion happens recently. The abrupt appearance of this structure is imaged clearly as well on the parasound sections. Sediment echographer data,

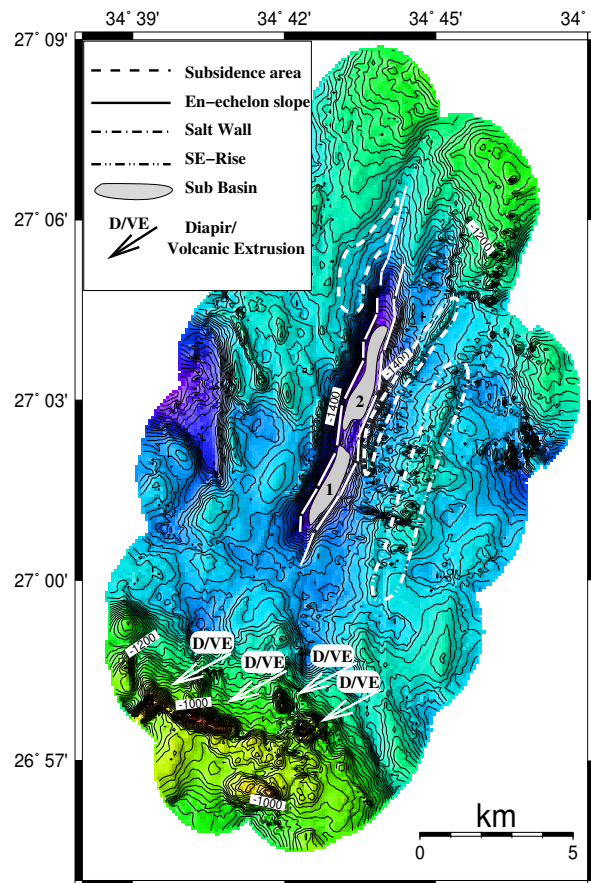


Fig. 5.10: Surficial structures in the Conrad Deep survey area. The SE-shoulder reveals NE-SW structures and the NW-shoulder NW-SE structures.

measured parallel to line G_99_072 and in the inter space to the adjacent lines G_99_071 and G_99_073 show the recent activity and its impact to the uppermost sedimentary layers (Fig. 5.15). Similar to the Salt Wall the Parasound data were used to identify the recent activity all over the survey area.

The SE-shoulder of line G_99_075 (Fig. 5.14) is not affected by the Salt Wall. A smaller and probably starved diapir has pierced the prekinematic unit but has not reached the seafloor. Without the Salt Wall that acts as backstop at the flank of the Deep (Fig. 5.11-5.13), the SE-slope became unstable, collapsed and caused mass wasting into the Deep. This is best seen NW of a small scarp (SP 2435, Fig. 5.14), where the flank slid along a rotational fault towards the Deep. As the uppermost sediments are cut by this event, it must have occurred recently, comparable to the activity of the Salt Wall. The longitudinal

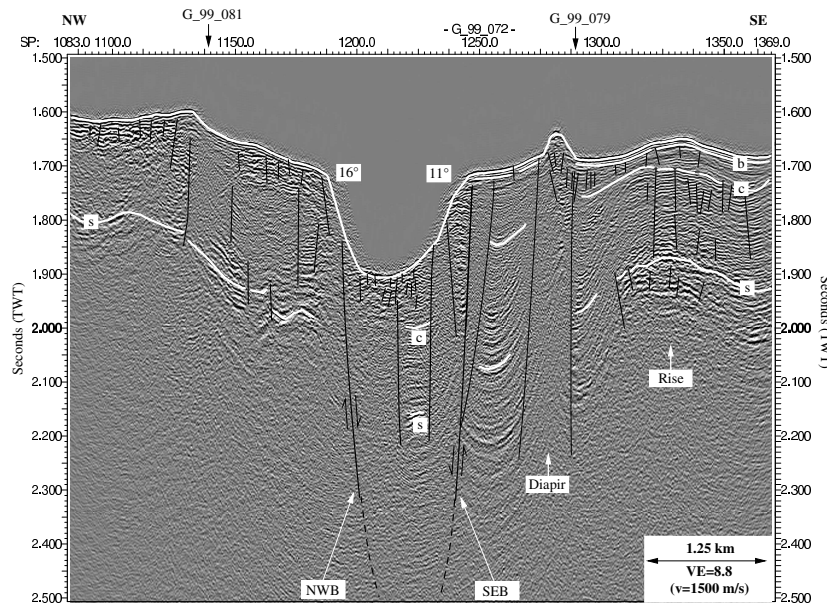


Fig. 5.11: Line G_99_072:

line G_99_079 (Fig. 5.16) depicts a cross section through the axial depression, parallel to the Conrad Deep. From SW to NE it runs from the main trough via a 150 m high extrusion into the axial depression on the deep-ward side of the SE-Rise. As already assumed from the cross sections the seismic units show a regular pattern parallel to the strike of the Deep. At SP 4410 (Fig. 5.16) line G_99_079 intersects the SE-Rise where it is affected by the small diapir (see Fig. 5.14). At this place the S-reflector exhibits a vertical offset of about 50 m.

The NW-shoulder of the Conrad Deep has a different appearance compared to the SE-shoulder (see G_99_081, Fig. 5.17). Similar to G_99_079 the longitudinal line parallel to the strike of the Deep, crosses an extrusion that is located at the southern flank of the axial depression. Within the depression four different sectors were identified. The line is dominated by a central located eroded diapir (sector III) and a patch of almost undisturbed sedimentation (sector II) that are enclosed by the outer sectors that are affected severely by mass wasting from the nearby slopes of the axial depression (Fig. 5.17). Indicated roll-back structures point to a rapid extension and subsidence at the SW-flank of the axial depression. The cross sections G_99_073 - 075 support the difference

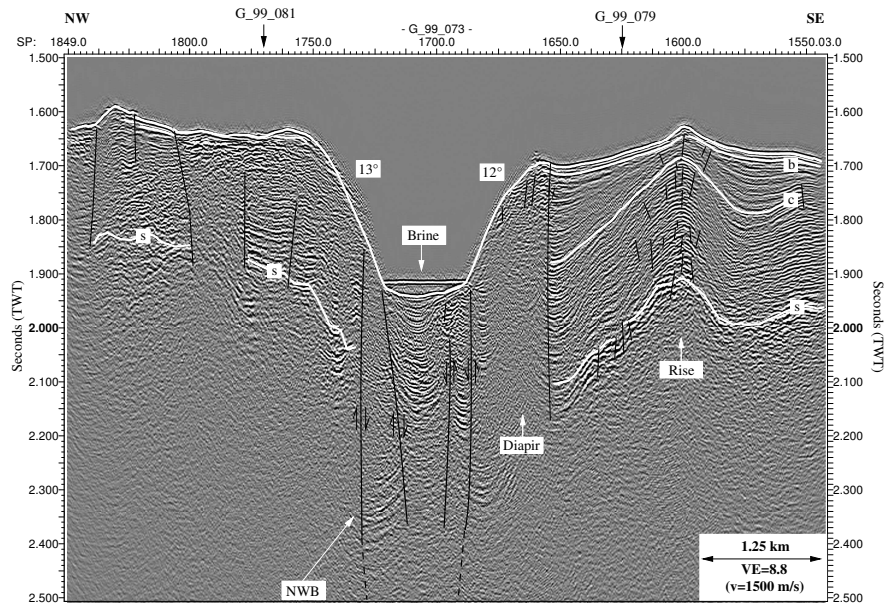


Fig. 5.12: Line G_99_073:

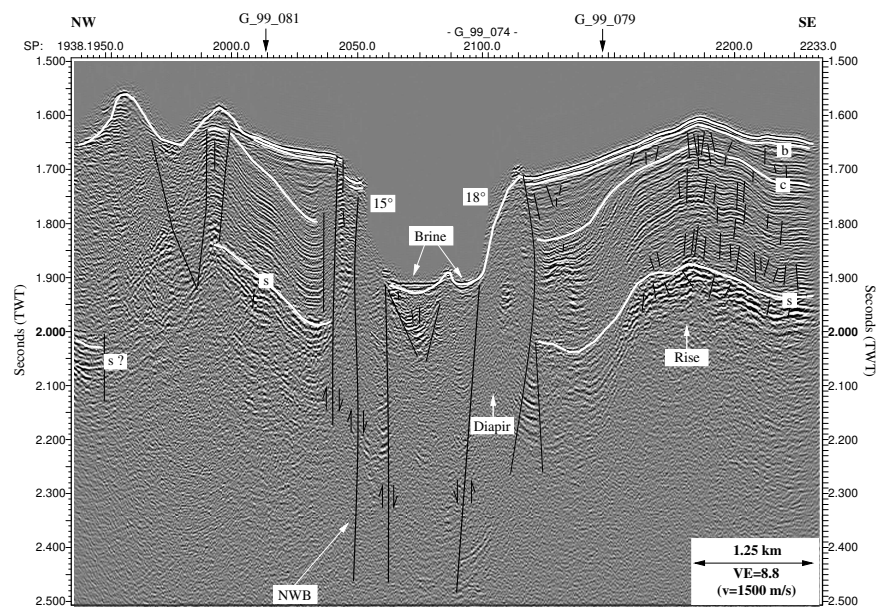


Fig. 5.13: Line G_99_074:

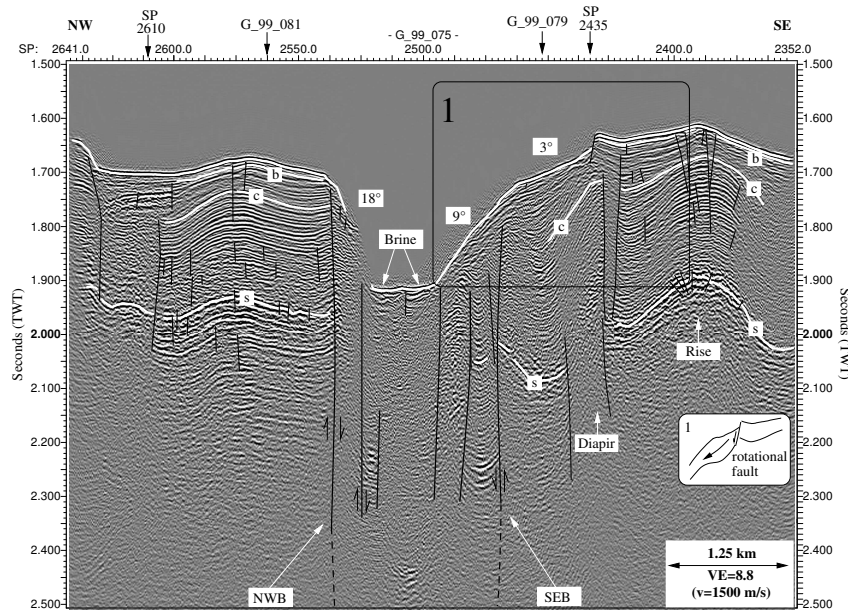


Fig. 5.14: Line G_99_075:

in the appearance. G_99_072 (Fig. 5.11) shows the subsidence of the NW-shoulder close to the Deep. Line G_99_073 (Fig. 5.12) crosses the caldera of the eroded diapir and reveals an increasing stratification of the Plio-Quaternary sediments towards the Deep. On line G_99_074 (Fig. 5.13) the Plio-Quaternary sediments are well stratified and uplifted possibly by vertical salt tectonics after the deposition of the prekinematic unit, probably related to the rise of the eroded diapir. The synkinematic unit shows the typical divergent pattern like on the SE-shoulder. Line G_99_075 (Fig. 5.14) exhibit the well layered sediments as already expected from the longitudinal line (Fig. 5.17). At SP 2610 (Fig. 5.14), the stratified sediments terminate against a transparent zone below a bright spot reflection, thus indicating vertical fluid or gas migration.

The Conrad Deep itself is characterized by steep slopes on both flanks (9 - 18°). By means of the bathymetric map (Fig. 5.10) the Conrad Deep has already been subdivided into two sub basins. This approach is manifested by the seismic appearance of the Deep. Line G_99_73 (Fig. 5.12) crosses the northern sub basin and exhibits layered sediments that are up bended on both slopes of the Deep, thus indicating continuous subsidence of this part of the Deep. Line G_99_74

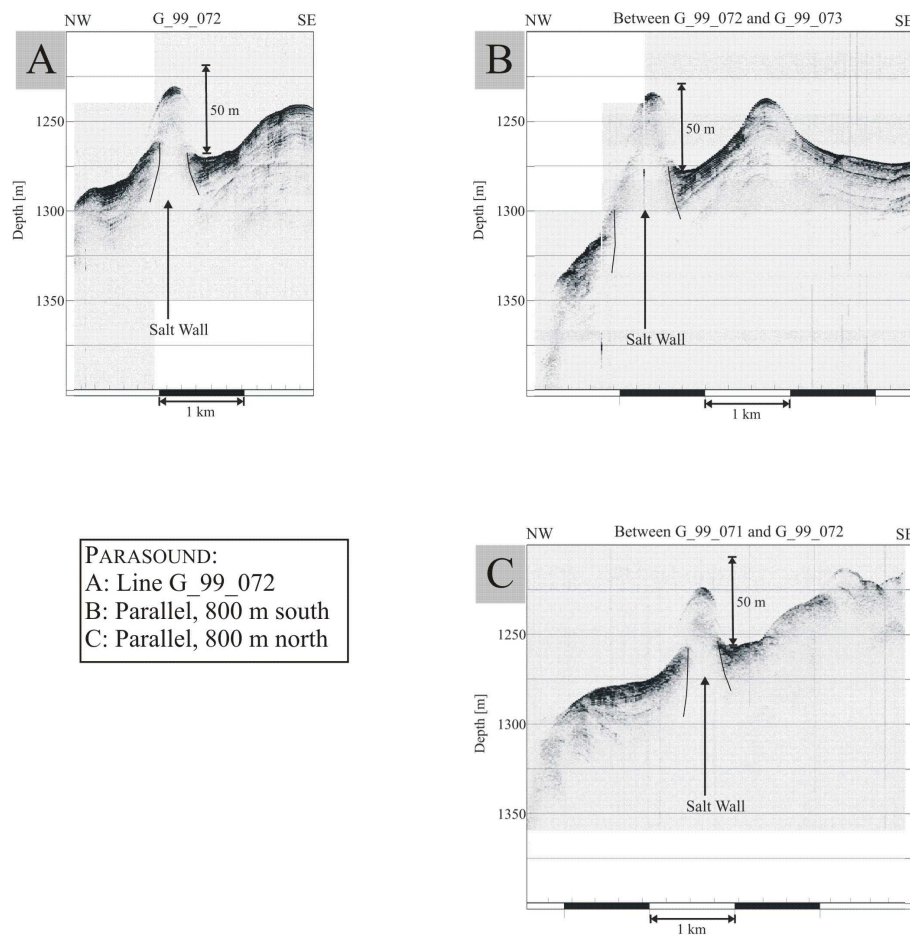


Fig. 5.15: Parasound section of the Salt Wall (SE-shoulder). The interval between the lines is ca. 800 m. Please refer to the Fig. 5.6 for the location of the Parasound lines. The elongated Salt Wall can be traced also on the bathymetric map (Fig. 5.7).

(Fig. 5.13) is located at the transition zone between both sub basins. The well stratified basin is fading out on the NW-slope of the Deep, on the SE-slope a more chaotic sedimentation pattern is observed. This trend is continuous to the southern sub basin (G-99-075, Fig. 5.14). The slopes of the Conrad Deep are associated with major normal faults. The scarp of the NW-slope is formed by the Northwest Boundary fault (NWB) but on the SE-slope the fault system is more complex and additionally obliterated by the salt tectonics. The Southeast Boundary fault (SEB) could be determined on the lines G_99_072 and G_99_075 (Fig. 5.11, 5.14). In between these lines the Salt Wall builds the slope of the basin. In the central part of the Deep, the Salt Wall acts as the SE-flank of

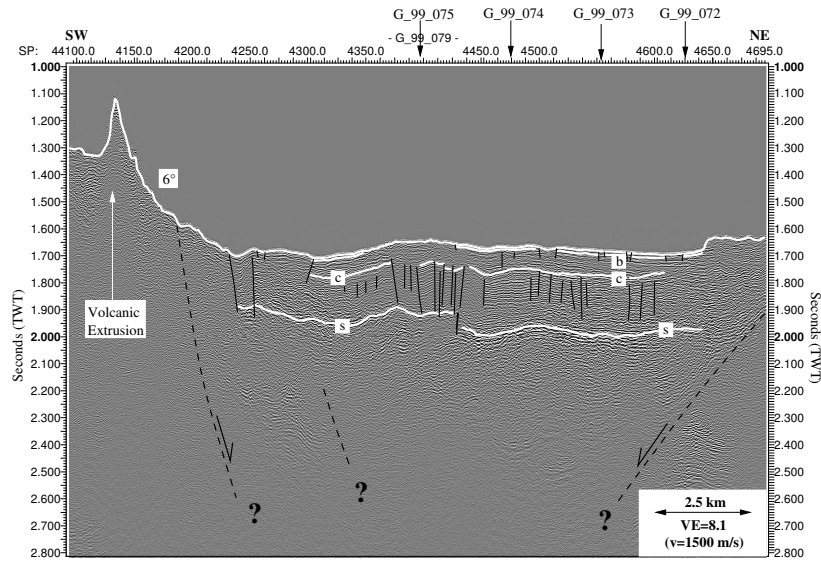


Fig. 5.16: Line G_99_079:

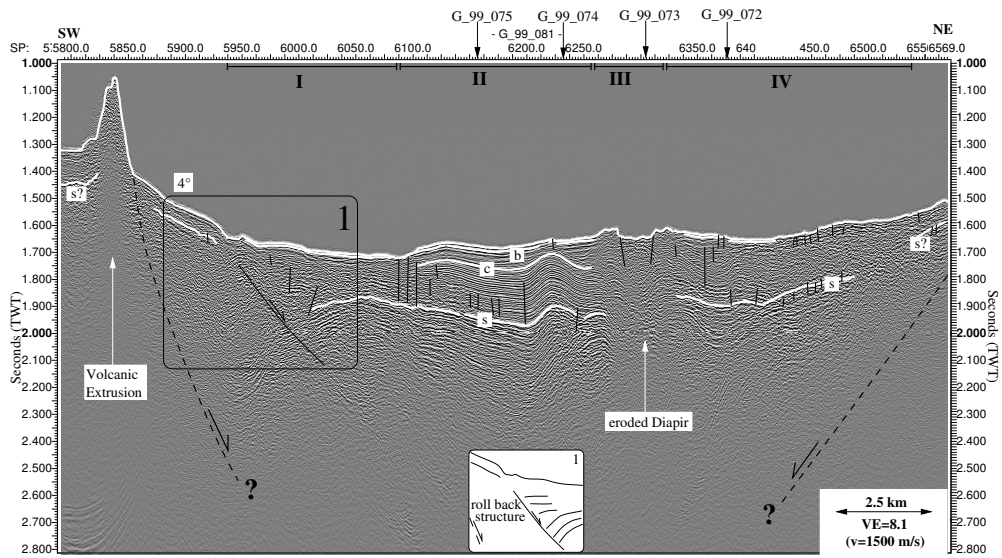


Fig. 5.17: Line G_99_081:

the Deep. Because the SE-shoulder was already destabilized by the SE-Rise the Salt Wall plays an important role as backstop for the Plio-Quaternary sediments. Without that backstop collapsing flanks may have filled the Deep, comparable to the process that is observed on line G_99_075 (Fig. 5.14).

5.6 Interpretation and Discussion

Using the seismic data it was possible to distinguish three main sedimentary units within the Miocene and Plio-Quaternary sequences. In addition vertical salt tectonics were determined. Thus, three main tectonic events could be distinguished in the area of the Conrad Deep that proceeded or were coeval with its formation.

SE-Rise: The first change in the sedimentation pattern could be observed along the elongated rise on the SE-shoulder (SE-Rise) that uplifted the S-Reflector and the prekinematic unit to an elongated rise that strikes parallel of the Deep (see Fig. 5.10, 5.11, 5.12, 5.13, and 5.14). On the cross sections G_99_072 to G_99_075 the sediments overlying the prekinematic unit are characterized by onlap patterns on the C-Reflector, the top of the pre-unit, suggesting a synkinematic deposition. The prekinematic unit overlies the Miocene evaporites concordantly. Both the top of the evaporites and the prekinematic unit reveal extensional faults due to the uplift of the SE-Rise. The linear morphology of the SE-Rise and its strike parallel to the Deep point to a formation along a pre-existing fault in the top of the evaporites. The uplift of the SE-Rise is probably related to the emplacement of one or both magmatic bodies at the flanks of the axial depression (Fig. 5.5).

A sub event that could be distinguished by seismic methods, is the formation of the central diapir on the NW-shoulder of the Conrad Deep (see Fig. 5.17). The synkinematic unit is partly concordant at the up bending pattern on the SW- and SE-flanks of the diapir (Fig. 5.13, 5.17). Thus, this event began after the start of the formation of the SE-Rise.

Salt Wall: This event is dominated by the development of the elongated diapir wall (Salt Wall), oblique to the strike of the Conrad Deep on its SE-shoulder (Fig. 5.10, 5.11, 5.12, 5.13, and 5.14). Like the formation of the SE-Rise, this diapir developed probably along a pre-existing fault zone. Thermal convection within the thick evaporite layer (about 3000 m after Cochran et al. (1991)) could

have triggered the diapir ascent, although the sedimentary cover is relatively thin (Talbot, 1978). Dissolution of the Salt Wall is probably slowed or prevented by a sedimentary cover. The interpretation of this structure as volcanic intrusion was ruled out, because it could not be correlated with a magnetic anomaly. Mud diapirism that forms similar structures is also unlikely as there are no evidences for overcompacted clays below the evaporites. The Salt Wall strikes N34°E and runs on its SW-extension into the Deep and acts partly as SE slope of the Deep. As the otherwise continuous uppermost sediments are cut by the diapir (Fig. 5.15), the rise occurred most recently and is still active.

Conrad Deep: In this event the main basin formation occurred. Because the Salt Wall is involved in the formation of the internal structure of the Conrad Deep, the formation of the Deep itself must have taken place after or coeval with the Salt Wall event. The Deep is segmented into a set of N25°E trending faults that are linked by N–S trending segments. The en-echelon distribution of the mapped N25°E segments point to a tectonic induced development of the Conrad Deep. Transtension or extension mechanisms are possible for the basin formation, in order to match the en-echelon, zig-zagging slopes of the Deep (Fig. 5.10). As the begin of the SE-Rise event is clearly marked by the C-Reflector unconformity, the onset of the tectonic activity could be estimated. At the NW-shoulder, southeast of the eroded diapir an undisturbed patch of sediments is an appropriate place to determine the thickness of the synkinematic unit (see Fig. 5.14, 5.17). Using an average seismic velocity of 1700 m/s for the synkinematic unit, the time interval of 87 ms TWT is equivalent to 74 m. Sedimentation rates are reported from Guennoc et al. (1988) to be as high as 1m/1000a, thus, the onset of the formation of the Conrad Deep began before ca. 74,000 years. This time interval is considered to be the main active period in the Conrad Deep area. This correlates roughly with the emplacement of the magmatic bodies that were dated by Cochran et al. (1986) very recently, only 40,000 years ago. As the Salt Wall has affected even the uppermost synkinematic sediments, its vertical motion is still active. This is valid also for the rotational fault of line G_99_075 (Fig. 5.14), indicating that the basin formation process is still active, too.

Mechanisms

The analysis of the seismic and hydroacoustic data led to the conclusion that the effective opening process for the Conrad Deep is either extension or transtension. The en-echelon shaped slopes of the Deep admit extension in N130°E direction, almost parallel to the Red Sea axial trend and perpendicular to the Deep, or transtension in N34°E direction, comparable to the strike of the slope and the Salt Wall (Fig. 5.18). Since the extension approach contradicts the regional tectonic stress field and does not explain the en-echelon pattern of the Conrad Deep slopes, the transtension is more likely. Beyond the good match of the slopes (Fig. 5.18), the transtension approach is in agreement with the orientation of faults, elongated diapirs (Salt Wall, SE-Rise) and the regional stress field. The transtension vector can be split into a strike-slip component that explains the en-echelon pattern at the slopes, and an extension component subparallel to the Conrad Deep and the SE-Rise.

The transtension opening mechanism has to be examined with respect to the geophysical and geological anomalies in the vicinity of the Deep. The combination of the results of the small scale seismic and hydroacoustic survey with the geophysical and geological anomalies provides additional information for the transtension model and the location of the Deep.

Framework

In order to derive a model for the development of the Conrad Deep, several aspects concerning the local and regional geological settings have to be considered:

(a) The extension and tectonic activity of the Red Sea, which had been previously distributed across the rift and became focused to the area of the axial depression (Cochran et al., 1986; Martinez and Cochran, 1988). Since that change, the ductile properties of the evaporites were probably not longer able to compensate the extension by lateral salt flow, thus forming the axial depression with its normal faulted flanks (Fig. 5.19a). The orientation of this highly stressed axial depression is nearly orthogonal to the Conrad Deep.

(b) The extension vector of the northern Red Sea is assumed to be orthogonal on the strike of the axial depression (N127°E). This leads to an orientation of the extension vector in the direction N37°E that is nearly parallel to the strike of the proposed transtension vector of N34°E. The trend of the extension vector is also supported by the linear distribution of seismological events that are located

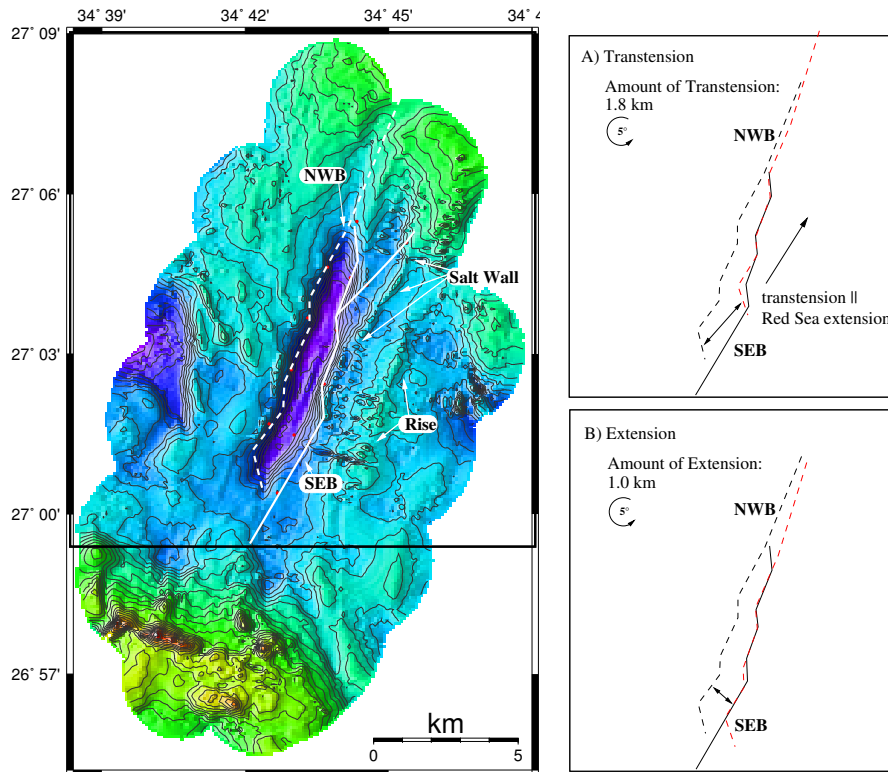


Fig. 5.18: Fault map: The main faults Northwest Boundary Fault (NWB) and Southeast Boundary Fault (SEB) are mapped and overlaid onto the bathymetric data. Red bullets mark the direct observations of the faults by seismic data. The interpolation of the faults was inferred by bathymetric evidences.

at a small lateral offset of the axial depression 5 km south of the Conrad Deep (Fig. 5.3), documenting a small transform fault.

(c) The dipole type magmatic anomalies are concentrated to the axial depression (Fig. 5.5). The corresponding magmatic intrusions are orientated normal to the global field, thus they are not older than 0.7 Ma (Guennoc et al., 1988) and could be as young as 40 ka (Cochran et al., 1986). Most of the magnetic anomalies correlate with the locations of the different Red Sea deeps. The Conrad Deep area is conspicuous, because it is accompanied by two anomalies, located at the slopes of the axial depression and in prolongation of the top ends of the Deep (see Fig. 5.5). The underlying magmatic intrusions seem to use the normal faulted slopes of the axial depression as zone of weakness for the ascend. Probably the diapir-like structures of the southern extension of the Deep are first witnesses of the magmatic activity (Fig. 5.10).

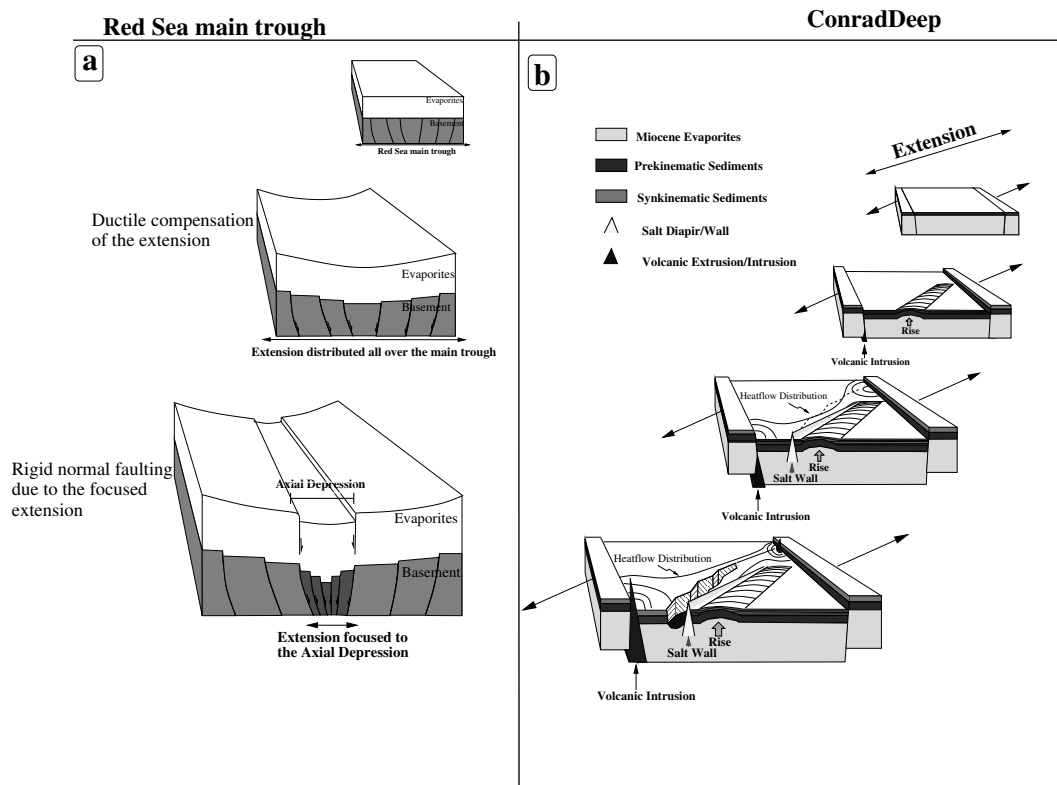


Fig. 5.19: The development of the axial depression and the Conrad Deep. The sketch on the left hand side (a) illustrates the development of the axial depression. The right hand side sketch (b) is a close up of the axial depression and illustrates the development process of the Conrad Deep.

(d) Associated with the concentration of the rifting to the axial depression and the magmatic activity, the heat flow in this area is anomalously high. Heat flow values of 250 mWm^{-1} to 350 mWm^{-1} (Cochran et al., 1986) were measured within the depression, i.e. 500% – 600% of the world mean. Thus, the enhanced heat transfer, especially between the two magmatic bodies, must have severely altered the viscosity of the Miocene evaporites (Fig. 5.20).

Evolution of the Conrad Deep

The points (a) to (d) provide the required conditions for the transtension model that was derived from the small scale seismic and hydroacoustic survey: The extension of the Red Sea Rift became focused to the axial depression (Fig 5.19a). The overlying Miocene evaporites were not longer able to compensate the enhanced extension by lateral salt flow and reacted with normal faulting. This marks the actual slopes of the axial depression. The highly stressed area is now affected by magmatic intrusions that use the normal faults along the slopes

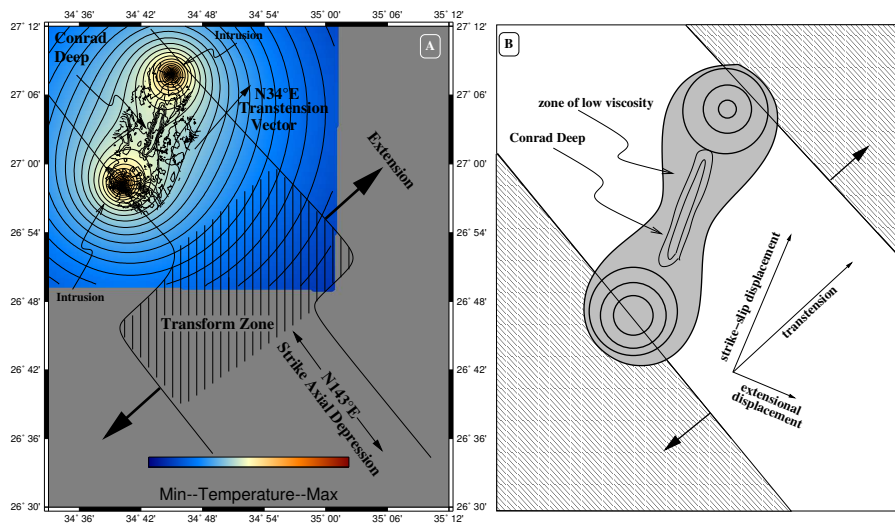


Fig. 5.20: A: Temperature radiation of the magmatic intrusions. The temperature distribution was calculated for a simple model without topography and multilayering. The amplitude decay proportional $-\ln(r)$ (r =distance to the intrusion). With increasing temperature the viscosity decreases. B: The low viscosity zone between the magmatic intrusions is oblique to the extension. This results in a transtension mechanism with a dominant strike-slip part and an extensional part.

of the axial depression for their ascent (Fig. 5.19b). Both magmatic intrusions make sure that the area between them is even more heated than the surrounding area (Fig. 5.20). Because of the increased heat transfer, the ductile properties of the evaporites are locally enhanced, i.e. the viscosity is lowered. This enables the evaporitic material in this small area to react faster to the extension, thus causing a deep in the axial depression. The Red Sea extension is acting oblique to the low viscosity zone between the two magmatic intrusions (Fig. 5.20). As the Plio-Quaternary sediments and most probably the top of the evaporites react brittle to the subsidence and extension, an en-echelon fault pattern was formed in these layers, integrating structural weakness zones, e.g. the flank of the salt wall. The conspicuous shape of the Conrad Deep was favored by the fact that two intrusions affected the area of the Deep. A single and central magmatic intrusion would have formed most likely a more or less circular deep.

Implications on deep basement processes

This model explains the observed features in the seismic data and fits the regional geological and geophysical framework, e.g. as the Red Sea extension and

the magnetic anomalies. No further assumptions regarding basement tectonics are necessary. As the main trough of the Red Sea in this area is assumed to be covered by up to 3000 m of Miocene evaporites (Cochran et al., 1991), and the evaporites tend to balance long term irregularities in the basement, we cannot emanate from the idea, that the Conrad Deep is a surface expression of a transtensional basin within the basement. However, it should be noted that the alignment of the intrusion bodies parallel to the strike of the Deep and to the strike of the Gulf of Aqaba point to a parallel weakness zone (fault) in the basement. This inferred fault or weakness zone in the basement correlates with the postulation of Makris et al. (1991c), who interpreted gravity anomalies as NE-SW orientated pull-apart basins within the basement.

5.7 Conclusions

The Conrad Deep is one of the northernmost Red Sea deeps. It is located in the axial depression and is conspicuous because of its elongated shape, striking in N20°E direction. In order to investigate the structure of the Plio-Quaternary sediments and the top of the Miocene evaporites, a dense seismic and hydroacoustic survey was conducted during the R/V Meteor Cruise M44/3. The sediments were distinguished into three temporary different units, corresponding to the evolution of the Conrad Deep. Salt tectonics and fault systems could be linked with the temporary series of events and this led to determine main events for the development of the Conrad Deep. These events happened during a main active period that started very recently (ca. 74,000 years ago) and is probably still active. The effective opening mechanism for the development of the Deep is transtension. The two magmatic intrusions/extrusions at the top ends of the Conrad Deep altered the viscosity of the evaporitic material and caused a higher mobility especially between both magmatic bodies. This low-viscosity zone is oblique to the extension direction of the Red Sea. The extension of the Red Sea Rift that is focused to the axial depression resulted in a transtension mechanism in the area of the Conrad Deep. Thus, the reason for the Deep's evolution is the focused extension that is forcing a region with locally reduced viscosity, due to the hot magmatic body of an intrusion/extrusion. The conspicuous shape of the Conrad Deep is caused by the superposition of the effects of two magmatic bodies at the flanks of the axial depression. The alignment of the two mag-

matic intrusions with the strike of the Gulf of Aqaba points to a weakness zones (faults) in the basement parallel to the Dead Sea Transform, the main tectonic structure in the Middle East. The magmatic activity was probably controlled by a fault structure in the basement that is parallel to the Dead Sea Transform. We have explained the initial development of the Conrad Deep. The validity of this model to other northern Red Sea deeps has to be examined. In general, this study leads to the conclusion that magmatic intrusions are the dominant causative processes for the development of a small and isolated deep. As the northern Red Sea deeps are within the massive evaporites, their ductile properties must be considered concerning the evolution and, of course, the life span of the deeps.

5.8 Acknowledgements

We would like to thank Jürgen Pätzold (University of Bremen) for providing the bathymetric data. We thank also Volkard Spiess (University of Bremen) for providing the seismic acquisition equipment and Mohammed Salem (University of Bremen) for editing of the bathymetric data. We would like to thank Klaus Reicherter and Martin Bak-Hansen for their valuable suggestions. We are grateful to the crew of the RV Meteor for the technical assistance provided during cruise M44/3. The interpretation was supported by the utilization of the KingdomSuite – software. All maps were produced with GMT. This work was founded by the German Research Foundation (DFG) grant HU698/4.

6 Development of the Conrad–, Shaban– and Kebrit Deep, northern Red Sea, based on Seismic and Hydroacoustic Data

by Axel Ehrhardt, Christian Hübscher and Dirk Gajewski

submitted to *Marine Geology*, 07/2004

6.1 Abstract

The development of the northern Red Sea Deep plays a key role in the evolutionary process of the Red Sea rift from continental rifting to seafloor spreading. Because of the abundance of evaporites within the Red Sea main trough, direct basement observations are prevented. Therefore, the evolutionary schemes of the Red Sea Deep can provide evidences for the basement dynamics. In order to derive evolutionary models for the Conrad–, Shaban– and Kebrit Deep, multichannel 2D seismic and hydroacoustic data were acquired during the cruises M44/3 and M52/3 of R/V Meteor. The seismic lines resolved the Plio-Quaternary sediments that cover the Miocene evaporites in the axial depression. The fault systems within the sediments and the stratigraphy were correlated with the existing results of magnetic and heatflow studies and models for the development of the distinct deeps were derived. Whereas the Kebrit Deep represents a collapse structure, because of hydrothermal circulation and dissolution of the Miocene evaporites, the Conrad– and Shaban Deep development is associated with the emplacement of magmatic intrusions or extrusions into the Miocene evaporites. The heat radiation from the hot intrusions lowered the viscosity of the evaporites locally. The translation of the Red Sea extension happened faster within the low-viscosity zones than in the vicinity and resulted in the amplified subsidence and thus the initiation of the development of the deeps. According to the development of the deeps, they could be classified roughly into two groups; intrusion related deeps and collapse structure deeps. The intrusion related deeps are settled in a NW–SE trending segment of the northern Red Sea (Conrad– and Shaban Deep) and the Kebrit Deep, as representative of the collapse structure deeps, is located in a N–S trending segment. The intrusion related deeps seem to be limited to the NW–SE segment, where the strike of the axial depression is normal to the Red Sea extension vector. The interpretation of bathymetric measurements during transits let assume that deeps in the Red Sea are more abundant than previously suggested.

6.2 Introduction

Ocean Deeps within the Red Sea are thought to be an accompanying phenomenon of the process between continental rifting and seafloor spreading (Bonatti, 1985; Martinez and Cochran, 1988; Cochran and Martinez, 1988). Thus, the meaning of the Ocean Deeps is a key question in order to understand the plate tectonic status of this region. The Red Sea rift that separates the African- and Arabian Plates is a unique place to study rift systems as it comprises all stages from organized seafloor spreading to continental rifting along its extension (Searle and Ross, 1975). Taking into account the thick sedimentary cover that generally characterizes the Red Sea basin and especially the massive Miocene evaporitic layers in the main trough (Cochran et al., 1991), the analysis of surficial structures, like the Red Sea Deeps, is one possible way to extract information about the rifting and the status and, thus, the nature of the covered and masked northern Red Sea basement.

This paper represents a geophysical analysis of the Conrad-, Shaban- and Kebrit Deeps, three distinct northern Red Sea Deeps, using a recently acquired set of multichannel seismic and hydroacoustic data. The purpose of this work is the interpretation of the detailed seismic and hydroacoustic data in order to derive development schemes for the distinct deeps and to enlarge the database of the Conrad-, Shaban- and Kebrit Deeps by a detailed geophysical survey, as several geological and geochemical investigations were already done, but a detailed small scale seismic and hydroacoustic survey is still missing.

6.3 Geological Setting

6.3.1 The Northern Red Sea

The Conrad-, Shaban- and Kebrit Deeps are situated in the northern Red Sea (see Fig. 6.1). The northern part of the Red Sea is thought to represent a rift in the late stage of continental rifting and close to the stage of seafloor spreading (Cochran, 1983). The entire Red Sea can be separated into three parts along its strike (Cochran, 1983; Cochran et al., 1986). In the southern part, seafloor spreading takes place since ca. 5 Ma (Röser, 1975). The spreading becomes progressively younger to the north and commenced not earlier than

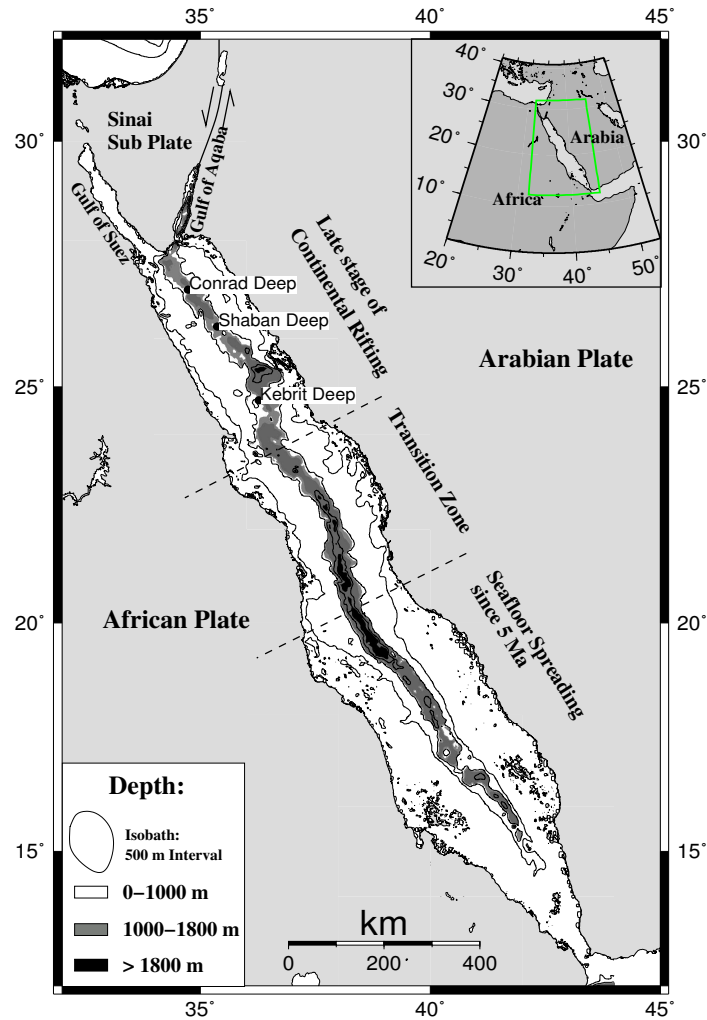


Fig. 6.1: The Red Sea can be separated along its strike into three provinces. The southern province provides already organized seafloor spreading, the central part is in a transition stage and the northern province of the Red Sea is most probably in the late stage of continental rifting (after Cochran, 1983).

1.7 Ma ago (Cochran et al., 1986) in the central part of the Red Sea where oceanized spreading cells are dominant that build well developed Ocean Deepes within the axial trough. In the northern part only isolated and less developed small deeps are distributed along the axial depression (Fig. 6.1). The axial depression is a characteristic feature of the northern Red Sea. It bisects the main trough and exhibits water depths of more than 1000 m (see Fig. 6.2).

The main trough is covered in most areas of the Red Sea with huge amounts of Miocene evaporites (McKenzie et al., 1970; Girdler and Styles, 1974; Searle and Ross, 1975; Michell et al., 1992) that cover the basement below. The top of the evaporites is seismically imaged as a prominent reflector that was named S-Reflector (Whitmarsh et al., 1974; Searle and Ross, 1975) and could be identified easily in most areas of the Red Sea.

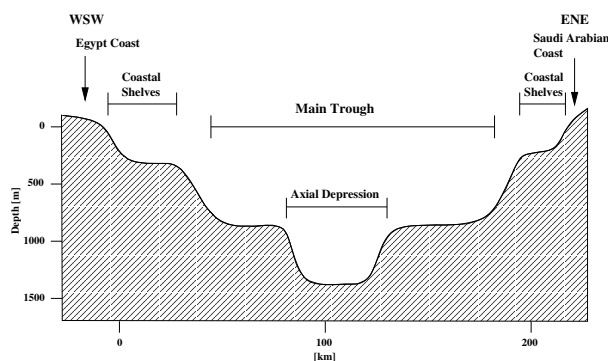


Fig. 6.2: Cross section through the Red Sea. The Red Sea is almost symmetrical with coastal shelves up to 400 m, a main trough with water depths to 1000 m and an axial depression that intersects the main trough and exceeds to water depths up to 1200 m (after Guennoc et al., 1988).

The extension of the Red Sea became focused to the axial depression that represents the tectonically most active part of the rift (Cochran et al., 1991). In the northern part of the Red Sea, the axial depression exhibits two main segments, a NW-SE segment from 25°N–28°N and a N-S trending segment from 24°N–25°N (Fig. 6.3). The N-S segments links the NW-SE segment in the north with a NW-SE segment in the south (Fig. 6.1). Many of the deeps that are located in the axial depression are associated with magnetic anomalies, like the Conrad- and Shaban Deeps, indicating magmatic intrusions and extrusions, respectively (Fig. 6.4). The Kebrit Deep is not correlated with magnetic anomalies and, consequently, not related with magmatic activity. It should be noted that the Kebrit Deep is located in the N-S orientated segment of the northern Red Sea (see Fig. 6.1). This segment represents a magnetic quiet zone (Fig. 6.4) in comparison to the northern part. The southern adjoining segment comprises deeps with pronounced rift structures and initial spreading activity, e.g. the Nereus Deep (Antonini et al., 1998).

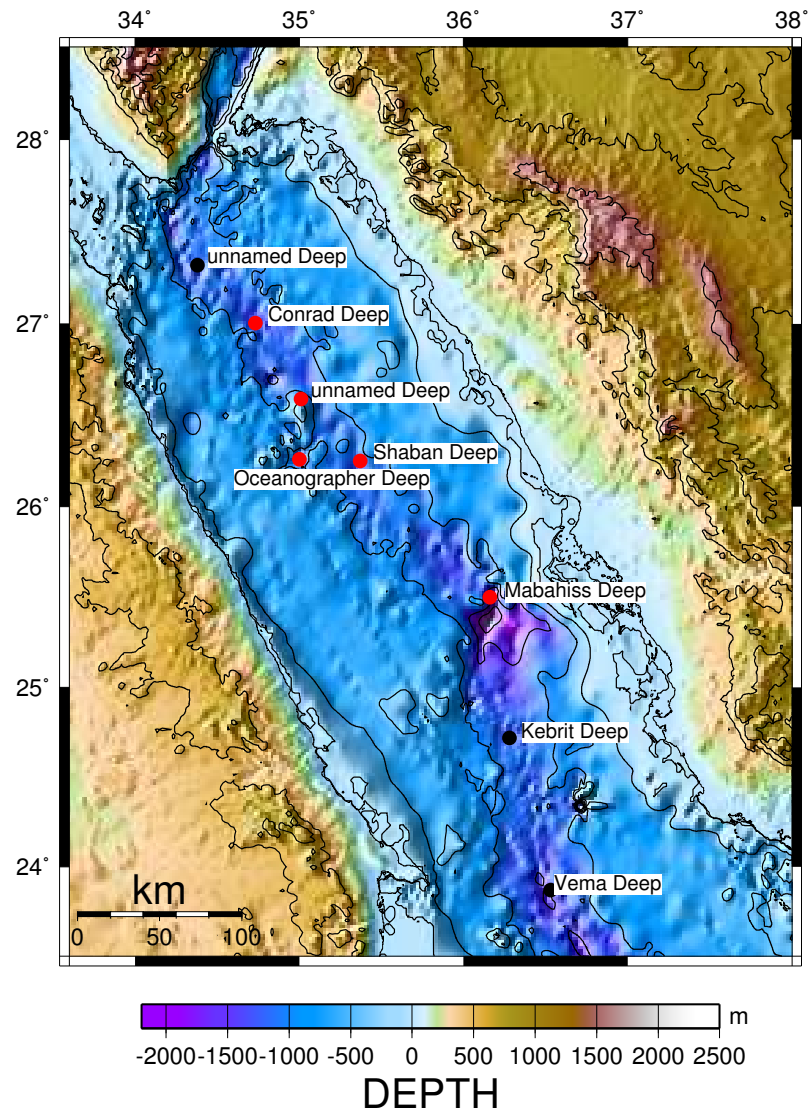


Fig. 6.3: Location of the Ocean Deeps in the northern Red Sea. Red bullets indicate Ocean Deeps associated with magnetic anomalies. The Deeps marked by black bullets show no magnetic anomaly after recent surveys. The topography is derived from the Gebco dataset (Gebco-Atlas, 2004)

As the northern part of the Red Sea rift is close to seafloor spreading stage and the extension already became focused to the axial depression, the heat flow is anomalously high. In general, values between 250 mW/m^2 – 350 mW/m^2 are measured over the axial depression (Martinez and Cochran, 1988), which is about 10 times higher than the world mean (Makris et al., 1991b). In the area of the Conrad Deep, the heat flow values change rapidly, indicating hydrothermal

circulation (Cochran et al., 1986; Martinez and Cochran, 1988). The widespread hydrothermal systems are the causative process of the abundant metalliferous sediments in and near the deeps and the hypersaline brine bodies within the deeps (e.g. Cocherie et al., 1994).

6.3.2 The Deeps

The Kebrit Deep was discovered already in 1974 (Bäcker et al., 1975), and was revisited several times, in order to provide long term datasets of the brine body (e.g. Blum and Puchelt, 1991; Hartmann et al., 1998; Winckler et al., 2001). Its name (Kebrit = arab. for sulphur) points to hydrothermal activity. Blum and Puchelt (1991) discovered black smokers at the flanks of the Deep and sampled them. Some of them consisted out of pure sulphur. The Kebrit Deep is oval shaped and includes a hypersaline brine body (e.g. Hartmann et al., 1998). Smooth slopes of the Deeps are intersected by graben or half graben like structures. The origin of the hypersaline brine body is still under debate, as Blum and Puchelt (1991) propose hydrothermal circulation, but Winckler et al. (2001) prefer lateral solution of the Miocene evaporites. This is important in order to find a model for the development of the Deeps.

The Shaban- and Conrad Deeps are located in the NW–SE trending segment of the northern Red Sea (Fig. 6.3) and were discovered as late as 1984 and 1986 (Pautot et al., 1984; Cochran et al., 1986), respectively.

The Shaban Deep (named after the arab. month of Shaban, also termed Jean Charcot Deep) is more or less rhombic in shape and associated with a dipole type magnetic anomaly that is caused by a magmatic extrusion (Pautot et al., 1984). This volcanic edifice forms an elongated NW–SE trending ridge in the center of the Deep. The Shaban Deep is separated into four sub basins that are filled with the hypersaline brine body. Geochemical analyses of the brine water and the surrounding sediments are contra dictionary, somehow. While Blum and Puchelt (1991) suggest hydrothermal circulation, Cocherie et al. (1994) analyzed REE signatures of the sediments and concluded that the Shaban Deep brine water is sea water dominated, thus it established by mainly lateral dissolution of the Miocene evaporites.

The Conrad Deep is one of the northernmost Red Sea Deeps. Only one Deep is reported at 27°19'N / 35°23'E, but without any significant magnetic anomaly (Guennoc et al., 1988). The Conrad Deep is conspicuous because of its elongated

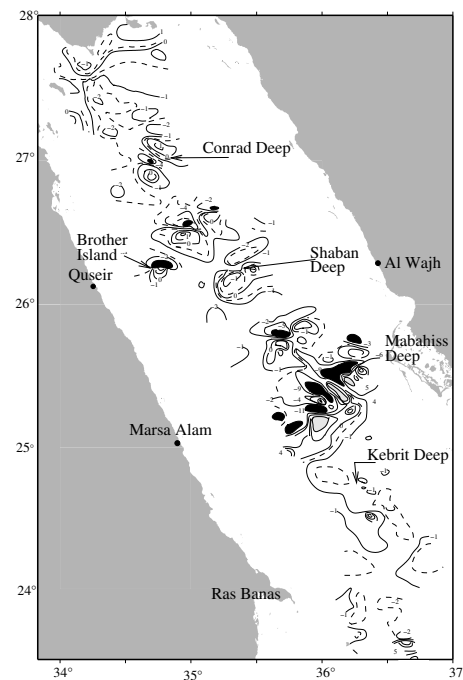


Fig. 6.4: Magnetic map of the northern Red Sea (after Coutelle et al., 1991). Isolated magnetic dipole anomalies point to intrusions into the basement. Anomalies are found at the Shaban- and Conrad Deeps.

N20°E trending shape and the fact that it is accompanied by two magnetic dipole type anomalies and thus most probably by two magmatic intrusions (Cochran et al., 1986). The strike of the Deep is almost parallel to the strike of the Gulf of Aqaba and the Dead Sea Transform. The location of the Deep is slightly shifted in the southward prolongation of the Gulf of Aqaba (Fig. 6.1, 6.3). So far, no geochemical and geological samples exist out of the Conrad Deep. Two major geophysical surveys were performed in the Conrad Deep area. The Conrad Deep was discovered during a multicomponent survey, including seismic, hydroacoustic, magnetic, gravity and heat flow measurements, of the R/V Conrad in 1984. In 1999, during the R/V Meteor cruise M44/3 (Hübscher et al., 2000), a dense multichannel seismic and hydroacoustic dataset was acquired in the Conrad Deep area. Ehrhardt et al. (submitted 2004) derived a model for the development of the Conrad Deep in a tectonic context and considered the impact of the magmatic intrusions into the Miocene evaporites. The data of the Conrad Deep and the model will be introduced and discussed later in this work.

6.4 Methods and Results

During the R/V Meteor cruises M44/3 and M52/3 in 1999 and 2002, respectively, three northern Red Sea Deeps, the Conrad-, Shaban- and Kebrit Deeps were investigated by multichannel seismic and hydroacoustic methods (swath echosounder and sediment echosounder) (Hübscher et al., 2000; Ehrhardt & Hübscher, 2003). It was intended to acquire a detailed dataset of the bathymetry and the subsurface structure of the Deeps. The close spacing of the seismic lines led to a complete coverage of the seafloor by the swath echosounder and enabled the interpolation between the 2D-seismic lines (Fig. 6.5).

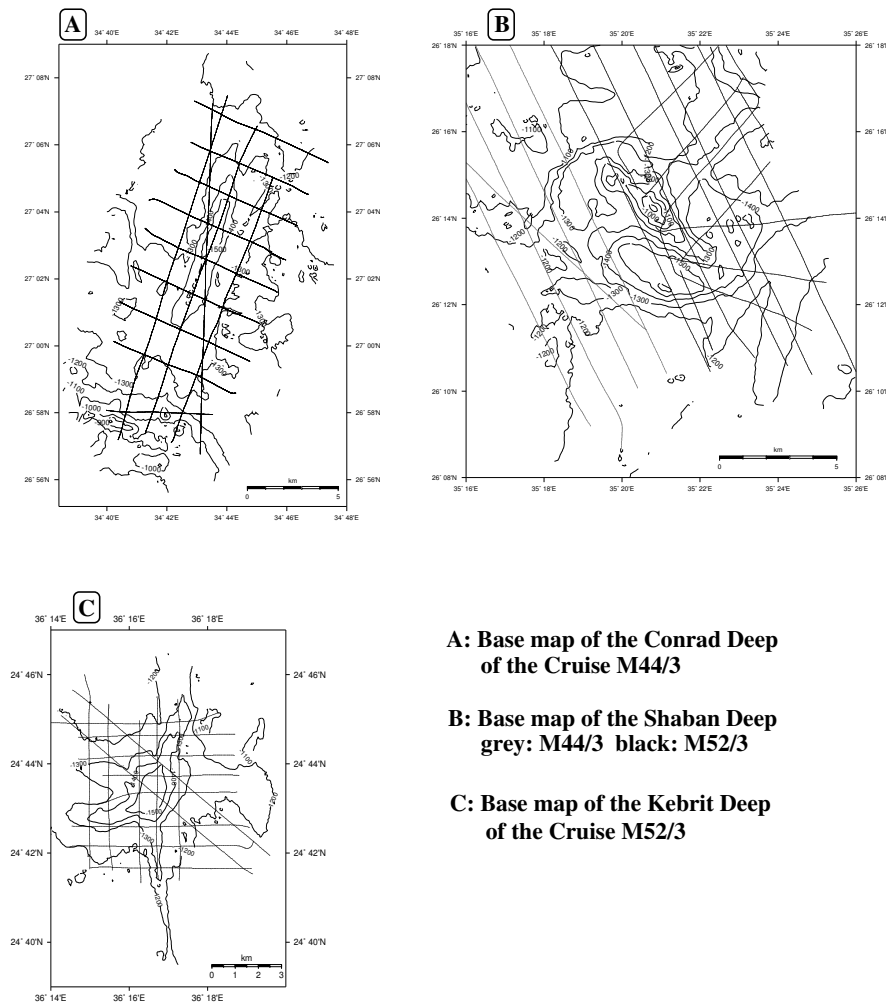


Fig. 6.5: Base maps of the multichannel seismic surveys in the areas of the Conrad-, Shaban- and Kebrit Deeps.

Swath echosounder (HYDROSWEEP) and sediment echograph (PARASOUND) devices were installed on board of the R/V Meteor, but the seismic equipment changed. Regarding the different seismic acquisition parameters and the subsequent data processing, please refer to Table 6.1 and Table 6.2.

The three northern Red Sea Deeps show major differences in size and shape and in the accompanying geophysical anomalies. The bathymetry of the independent deeps is displayed including the tracks of the seismic lines (Fig. 6.6, 6.7, 6.8). Selected 2D lines will illustrate the subsurface structure of the Deeps and their surroundings. The main parameters regarding the Deeps are listed in Table 6.3.

	M44/3	M52/3
Source	1 GI-Gun	2 GI-Guns
Streamer	analogue (Syntron)	analogue (Syntron)
active length	300 m	150 m
No. of channels / Group int.	24 / 12.5 m	24 / 6.25 m
Shot int. / Speed	10 s / 2.5 m/s	8 s / 2.5 m/s
Registration	0.5 ms	0.5 ms

Table 6.1: Acquisition Parameters of the cruises M44/3 and M52/3

6.4.1 Bathymetry

The Conrad Deep survey area (Fig. 6.6) images the SW-slope of the axial depression, the Conrad Deep and on its western side a second deep. At the slope of the axial depression several extrusive bodies are located. Their position correlates with the southern magnetic anomaly (Cochran et al., 1986) (Fig.6.4), thus they are most probably magmatic type extrusion bodies using the normal faulted slope of the axial depression for their ascent. The Conrad Deep itself has an elongated shape that is apparently parallel to the trend of the Gulf of Aqaba and thus the Dead Sea Transform (compare Fig. 6.3 and Fig. 6.6). It

CMP sorting (12.5 m / M44/3) (6.25 m / M52/3)
BP-Filtering
V-Analysis ¹
Static correction ²
Stack
$\omega - x$ Migration (smoothed V-function)

Table 6.2: Standard processing steps of multichannel seismic data.

	Conrad Deep	Shaban Deep	Kebrit Deep
Location	27°03'N/34°43'E	26°15'N/35°24'E	24°43'N/36°17'E
Size	10 km x 2 km	6 km x 5 km	4 km x 3 km
Volume ³	~ 1.5 km ³ (1340 m)	~ 6.2 km ³ (1250 m)	~ 2.5 km ³ (1240 m)
Brine Volume ⁴	~ 0.4 km ³ (1440 m)	~ 4.2 km ³ (1290 m)	~ 0.2 km ³ (1450 m)
Max. Brine height TWT	30 ms	250 ms	110 ms
Magn. anomaly	yes (2)	yes (1)	No

Table 6.3: Parameters of the Conrad–, Shaban– and Kebrit Deeps.

is composed out of two sub-basins that show a small left stepping offset. Its escarpment-like slopes are steep on the longitudinal sides and distributed in an en-echelon pattern. Several N34°E segments are linked with N–S segments (Fig. 6.6).

These facts point to a tectonic (strike–slip or transtension) related development process, as the Red Sea extension is slightly oblique to the strike of the Conrad Deep. The shoulders of the Conrad Deep are different in their morphology. The NW-shoulder is irregular and shows randomly distributed syn- and anticlinal structures. The deep depression west of the Conrad Deep belongs to a independent deep that was unrecognized so far and was named *Klauke Deep* (Ehrhardt et al., submitted 2004). The SE-shoulder is dominated by elongated anticlinals that are parallel and subparallel to the strike of the Conrad Deep.

The Shaban Deep (Fig. 6.7) is more circular in shape and is characterized by the high central ridge that is orientated parallel to the Red Sea trend. The ridge comprises a volcanic extrusion (Pautot et al., 1984) that is responsible for the magnetic dipole anomaly (Fig. 6.4). Perpendicular to this ridge a smaller ridge trends in SW–NE direction. Thus, the Shaban Deep is separated into four smaller sub-basins. The NNW- and SSW-slopes of the Shaban Deep are steep. Further north the shoulder has a regular surface. The southern shoulder, generally less high in comparison to the north, has a regular expression only on its western side, the eastern side is affected by two major graben striking

¹Crude V-analysis, because of the small moveout.

²Static corrections by correlation of the CMP-gather with pilot trace.

³The volume of each deep was calculated to the quoted depth.

⁴Top of the brine body was calculated from the seismic lines using constant velocity $v_w = 1.5 \text{ km s}^{-1}$

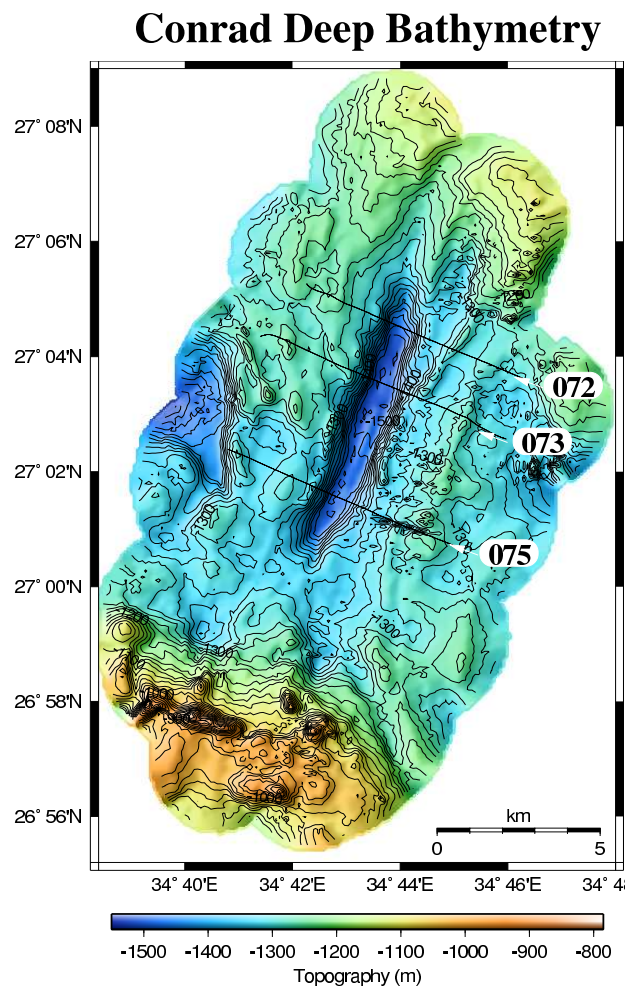


Fig. 6.6: Illuminated bathymetry of the Conrad Deep, cruise M44/3. The presented seismic lines are superimposed and annotated: G_99_072 (072, Fig. 6.9); G_99_073 (073, Fig. 6.10); G_99_075 (075, Fig. 6.11).

SW–NE. The WSW- and ENE-slopes are shallow and less steep. The difference in altitude between the NW-part of the Deep and its SE-part is reflected as well within the Deep; the northern (smaller) sub-basins are less deep than its southern counterparts. The bathymetry indicates a continuous WSW–ENE fault structure that is separated by the volcanic extrusion.

The Kebrit Deep (Fig. 6.8) has a more oval and asymmetric shape. It has smooth slopes that are intersected by two W–E trending graben and half graben, respectively, and a N–S trending graben that crosses the deep but is slightly offset to the east. It is reasonable that this is the expression of a troughgoing

Shaban Deep Bathymetry

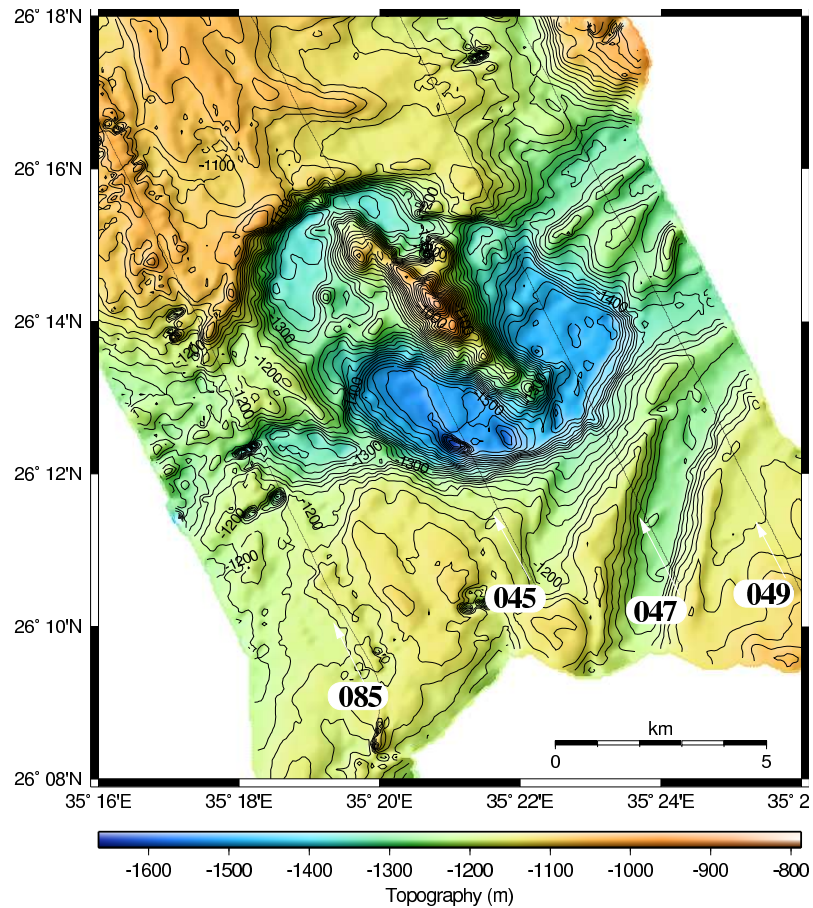


Fig. 6.7: Illuminated bathymetry of the Shaban Deep, cruises M44/3 and M52/3. The presented seismic lines are superimposed and annotated: G_99_085 (085, Fig. 6.12); HH02_045 (045, Fig. 6.13); HH02_047 (047, Fig. 6.14); HH02_049 (049, Fig. 6.15).

N–S trending fault. The morphology of the shoulders is regular and smooth west of the N–S trending graben but irregular and rough east of it.

6.4.2 Seismic Data

The internal structure of the Conrad Deep is best seen on the cross sections G_99_072, G_99_073 and G_99_075 (Fig. 6.9, 6.10, 6.11). The bathymetric map (Fig. 6.6) shows the location of the lines and the extension of the observed topography. Line G_99_072 (Fig. 6.9) is located at the NE-top end of the

Kebrit Deep Bathymetry

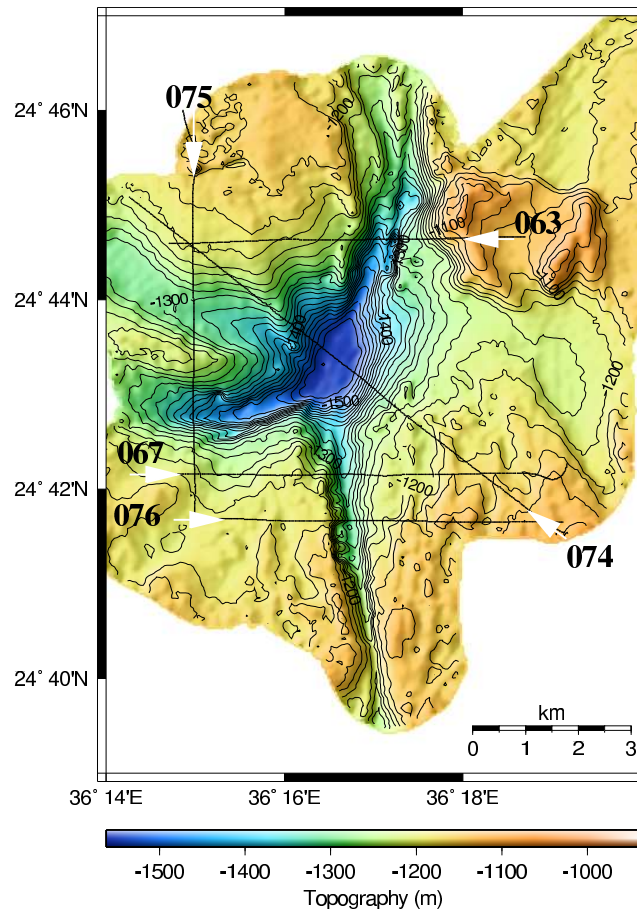


Fig. 6.8: Illuminated bathymetry of the Kebrit Deep, cruise M52/3. The presented seismic lines are superimposed and annotated: HH02_063 (063, Fig. 6.20); HH02_067 (067, Fig. 6.19); HH02_074 (074, Fig. 6.16); HH02_075 (075, Fig. 6.17); HH02_076 (076, Fig. 6.18).

Conrad Deep. The signal penetration resolved the Plio-Quaternary sediments and the uppermost Miocene evaporites. The S-Reflection that corresponds to the top of the evaporites is clearly visible across the profiles. Above the S-Reflector an amount of Plio-Quaternary sediments is deposited that are equal to 200 - 300 ms TWT which is typical for the Red Sea (Guennoc et al., 1988). The longitudinal margins of the Deep form steep slopes ($16^\circ / 11^\circ$) that are bounded by normal faults. The morphology of the S-Reflector is different on the individual shoulders of the Deep. On the NW-shoulder the top of the Miocene

evaporites bend smoothly down towards the Deep. The overlying sediments reveal a chaotic pattern. In contrast, on the SE-shoulder the S-Reflector is faulted and penetrated by a vertical salt wall. Two main salt tectonic structures were identified on the SE-shoulder. The up-doming of the evaporites has caused a rise of the S-Reflector, about 1200 m wide and 150 m high (see e.g. Fig. 6.9 and 6.10). A diapir like structure has pierced the Plio-Quaternary sediments, ca. 500 m wide and 500 m high (Fig. 6.9, 6.10). This structure is elongated (Fig. 6.6) and forms, thus, a salt wall. The sediments overlying the evaporites are stratified and two different units were determined within the Plio-Quaternary sequence. A prekinematic¹ unit overlies the evaporites which is characterized by concordant reflections and a synkinematic unit that shows divergent reflection patterns (e.g. west of the SE-Rise). The unconformity between the pre- and synkinematic unit represents the start of the development of the Deep. The salt tectonic structures (SE-Rise and Salt Wall) are elongated and strike parallel and subparallel towards the Deep (Fig. 6.6). Therefore, the subsequent cross sections (Fig. 6.6) have a similar appearance with the exception that the salt wall is heading to the Deep, building the SE-slope at line G_99_073 (Fig. 6.10). In this part, the Deep has reached its maximum depth and a thin brine body is indicated by the horizontal brine reflection. Underneath the brine well stratified sediments build the infill of the NE-subbasin of the Conrad Deep. Only minor stratification of the Plio-Quaternary sediments is seen at the NW-shoulder. The SE-shoulder is comparable to the line G_99_072 (Fig. 6.9). Pre- and synkinematic deposited sediments are covering the S-Reflector. The Salt Wall that is building the SE-slope of the Conrad Deep, acts as a backstop for the Plio-Quaternary sediments. Because the Salt Wall is exposed to the sea water, it must be covered by a thin sedimentary layer; e. g. carbonates that precipitate already in mesohaline waters (35 – 105 ‰ salinity) (Warren, 1999). The importance of the Salt Wall as backstop is shown in line G_99_075 (Fig. 6.11). Here, the SE-shoulder is not stabilized by the Salt Wall, which led to a the collapse of the shoulder and to mass wasting into the deep along a rotational fault. Line G_99_075 crosses the southern subbasin of the Conrad Deep that has a less stratified infill in contrast to the northeastern counterpart. The NW-shoulder reveals a patch of undisturbed sedimentation. This is an ideal location to measure the thickness of the synkinematic sedimentary unit and calculate the onset of the

¹The term kinematic is correlated to the start of the development of the Conrad Deep.

deposition. Assuming a sedimentation rate as high as 1m/1000a (Guennoc et al., 1988) and an average seismic p-wave velocity for the synkinematic unit of $v_p = 1700 \text{ ms}^{-1}$ the onset of the deposition and thus the development of the Conrad Deep started about 75000 years ago. Taking into consideration the uncertainties of the sedimentation rate and the average p-wave velocity, this is in the same order of magnitude with the time of the emplacement of the magmatic intrusions that was dated by Cochran et al. (1986) to have happened before 40000 years.

The structure of the Shaban Deep is shown on the NNW-SSE running lines HH99_085, HH02_045, HH02_047 and HH02_049 (Fig. 6.12, 6.13, 6.14, 6.15). The S-Reflector was identified on all lines as marker for the top of the Miocene evaporites. The typical amount of Plio-Quaternary sediments, equal to 200 - 300 ms TWT, is covering the evaporites, but in contrast to the Conrad Deep, no pre- and synkinematic units could be distinguished. The attributes of the S-Reflector correlate with the individual areas that were encompassed using the bathymetric survey (Fig. 6.7). The areas with regular bathymetry show a continuous and little folded S-Reflector that crops out at the slopes of the Shaban Deep (see HH99_085 and HH02_045, Fig. 6.12, 6.13). In general, similar to the bathymetry, the altitude of the S-Reflector is higher on the northern side of the Deep. West of the Deep (HH99_085, Fig. 6.12) block faulting could be identified within the SW-NE trending depression between the northern and southern part of the Deep as graben structure. Line HH02_045 (Fig. 6.13) crosses the central ridge at its northern extension.

The northernmost part of the ridge seems to be built out of an extrusion body with an adjacent patch of sediments. If we assume that the central and highest point is also built out of volcanic material, the ridge must be built out of several extrusions. The eastern part of the Deep, represented by the line HH02_047 and HH02_049 (Fig. 6.14, 6.15), reveals a different appearance concerning the S-Reflector and the bathymetry (Fig. 6.7). The southeastern part of the Shaban Deep is highly faulted, including S-Reflector and the Plio-Quaternary sediments. This caused the S-Reflector to dip below the Deep (Fig. 6.14). Similar to the western side, the easternmost line (Fig. 6.15) reveals a faulted graben as the corresponding counterpart to the western side (Fig. 6.12). The appearance of this SW-NE graben is similar to an extensional graben crossing the Deep, but in the meantime it is separated by the volcanic extrusion. Additional to the

extension structure, the SW-NE trending graben at the SE-edge of the survey area shows an affinity to a strike-slip fault with normal component (Fig. 6.15). It is apparent that this strike-slip affected part has a similar orientation as the Conrad Deep (Fig. 6.6).

The Kebrit Deep differs in many details from the previously described Deeps. Apart from size, shape and location, also the internal structure shows major discrepancies to the above mentioned Deeps. The cross section HH02_074 (Fig. 6.16) is heading from SE to NW (see Fig. 6.8). In the southeast, the seafloor topography is rough and irregular. The subsurface structure reveals a chaotic pattern above a high amplitude reflector. Below this reflector well stratified sediments were resolved that cover the S-Reflector. The level of the S-Reflector is rising to the southeast and the overlying stratified unit thins out towards the S-Reflector high. The rough surface above the high amplitude reflector was formed by a slump, most probably from the nearby slope of the axial depression. Towards the Deep, the S-Reflector dips down and is normal faulted, thus forming the depression. But the slopes of the Deep, although steep (12° and 17°), do

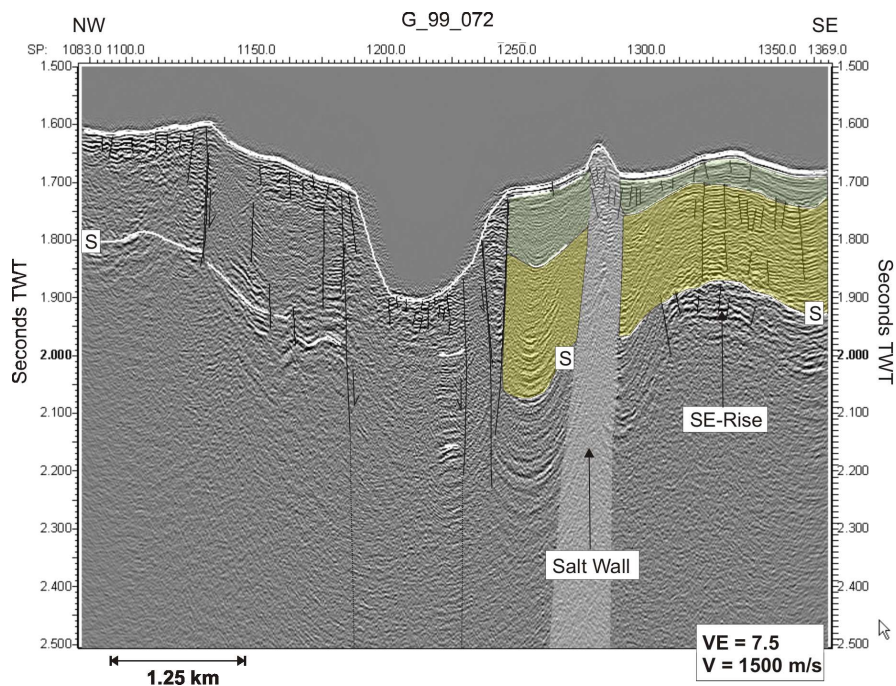


Fig. 6.9: G_99_072, NW-SE cross section (see Fig. 6.6): Prekinematic (yellow) and synkinematic (green) units were identified on the SE shoulder. The pre-unit reveals concordant reflection patterns; the syn-unit (green) is characterized by onlap structures and divergent reflection patterns. Both units are cut by the Salt Wall.

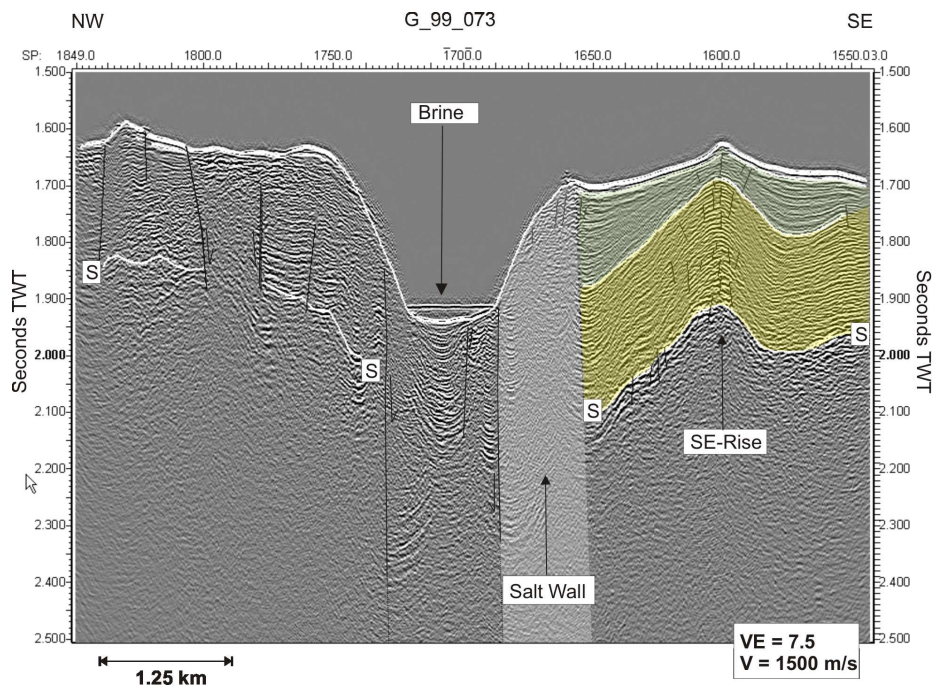


Fig. 6.10: G_99_073, NW–SE cross section (see Fig. 6.6): The Salt Wall runs into the deep and forms in this cross section the SE slope of the deep. It is also used as backstop for the Plio-Quaternary sediments.

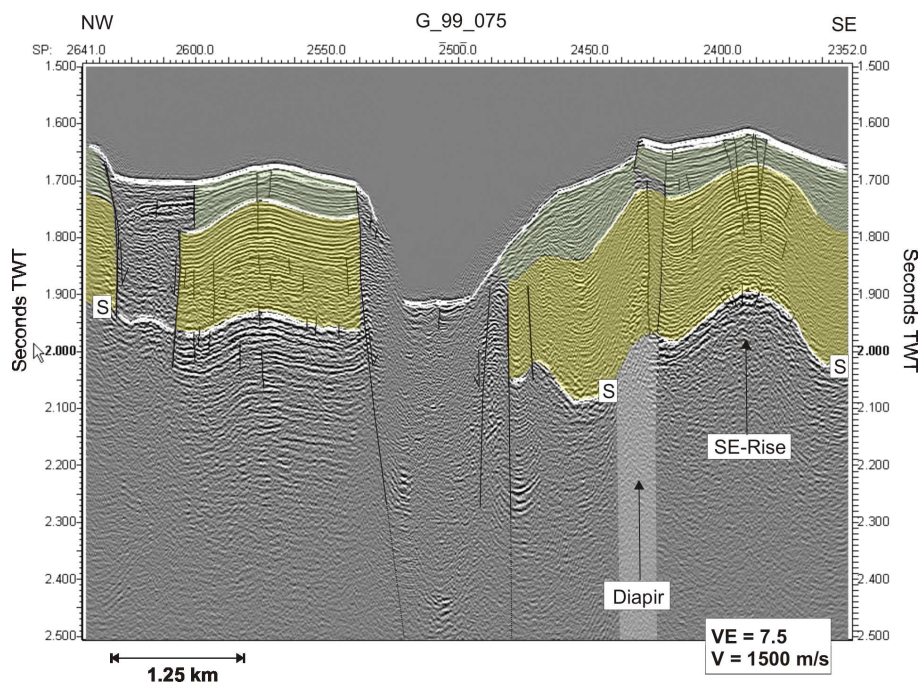


Fig. 6.11: G_99_075, NW–SE cross section (see Fig. 6.6): Pre- and synkinematic units were identified on both shoulders. Without the Salt Wall, acting as backstop (Fig. 6.10), the SE slope became unstable and collapsed.

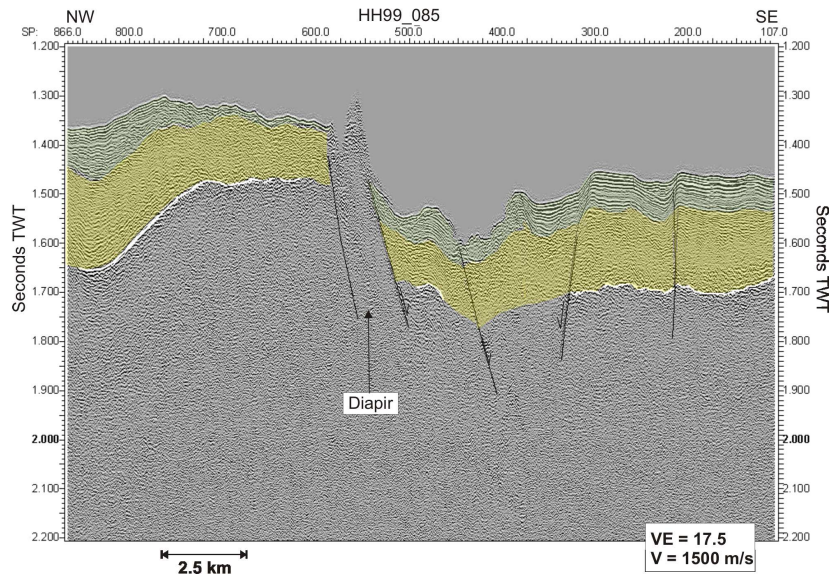


Fig. 6.12: HH99_085, NW-SE cross section (see Fig. 6.7): Two sedimentary units were identified. The NW and SE parts of the Shaban Deep are separated by extensional block faulting.

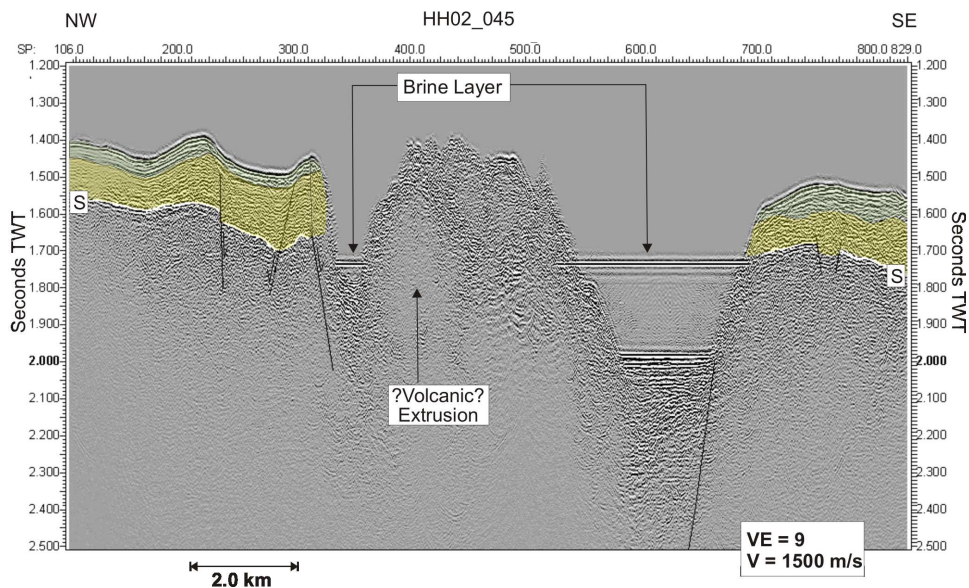


Fig. 6.13: HH99_045, NW-SE cross section (see Fig. 6.7): A volcanic ridge is located in the center of the Deep. The top of the Miocene evaporites (S-Reflector) terminates on both sides towards the deep.

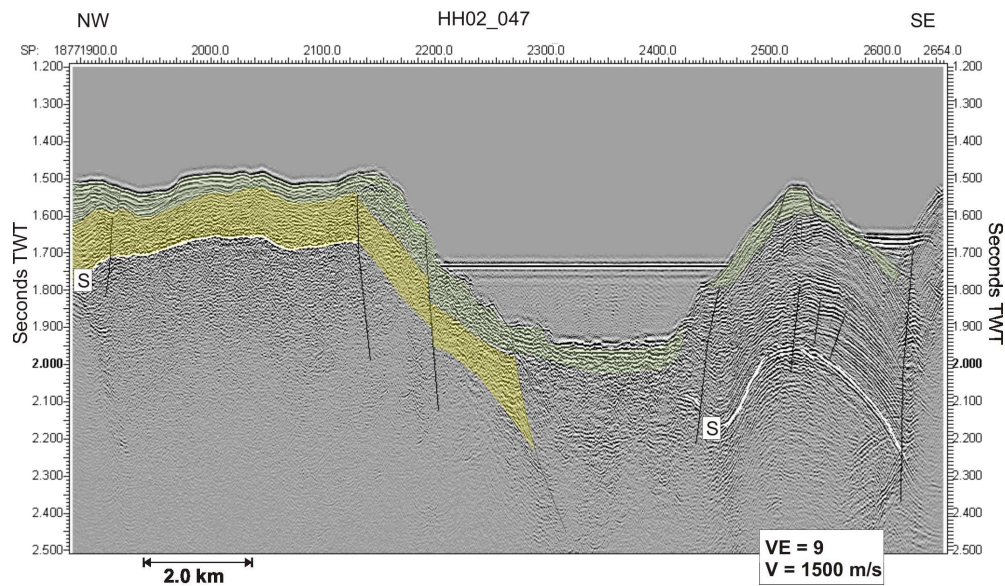


Fig. 6.14: HH99_047, NW–SE cross section (see Fig. 6.7): The eastern part of the Shaban Deep is more faulted. The evaporites tend to dip below the deep and the SW–NE trending graben (Fig. 6.7) affects severely the evaporites and Plio-Quaternary sediments.

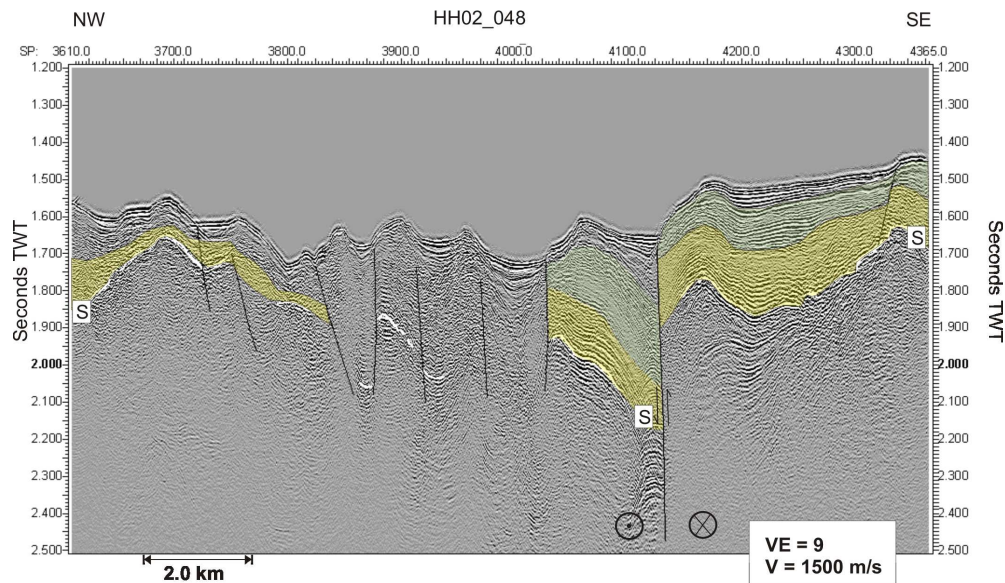


Fig. 6.15: HH99_049, NW–SE cross section (see Fig. 6.7): Similar to the western margin of the deep (Fig. 6.12), extensional faulting can be observed. The SW–NE trending graben tends to be formed by a strike-slip fault.

not form scarps. The subsidence of the entire sedimentary cover points to a subsidence process that forced the top of the evaporites and the Plio-Quaternary sequence to bend down. Within the Deep a clear brine reflection is visible. The appearance of the NW-slope of the Deep is different. The amount of sediments covering the S-Reflector is increasing (up to 600 ms, atypical for the Red Sea, see previously mentioned deeps). A divergent reflection pattern could be observed towards the Deep. The top of the Plio-Quaternary sequence is affected by slumps that dumped sediments into the Deep. The lateral N–S section HH02_075 (Fig. 6.17) shows similar structures. The northern part is well stratified with divergent reflection patterns towards the south. Two W–E trending graben and halfgraben were formed by normal faults that compensate the considerable subsidence in the center of the Deep. In the south, the S-Reflector forms a local high and the Plio-Quaternary sequence thins out towards this high. The difference of the SW- and SE-part of the survey area is depicted in the line HH02_076 (Fig. 6.18) that crosses the southern shoulder of the Deep. The N–S trending graben separates the southern shoulder of the Kebrit Deep (see also Fig. 6.8). The fault that caused this graben affected the S-Reflector high and the Plio-Quaternary sequence. The appearance of the deeper structures on both sides of the graben is different in terms of the inclination angle of the S-Reflector and the thickness of the overlying sediments.

On the eastern part of the shoulder, the internal structure of the uppermost Plio-Quaternary sediments is disturbed by a slump (Fig. 6.18), like it is already shown on line HH02_074 (Fig. 6.16). Line HH02_067 (Fig. 6.19) shows the slump head that terminates towards the N–S graben very well. The subsurface structure of this cross section reveals a change similar to line g_99_076 (Fig. 6.18). The N–S graben crosses the Deep and feathers up on the northern side of the Deep. Line HH02_063 (Fig. 6.20) is a cross section of the northern shoulder of the Kebrit Deep and shows again an asymmetric subsurface structure that is separated by the N–S trending graben. This is a pattern that could be expected by a strike-slip fault, therefore the N–S graben is most probably related to a strike-slip fault.

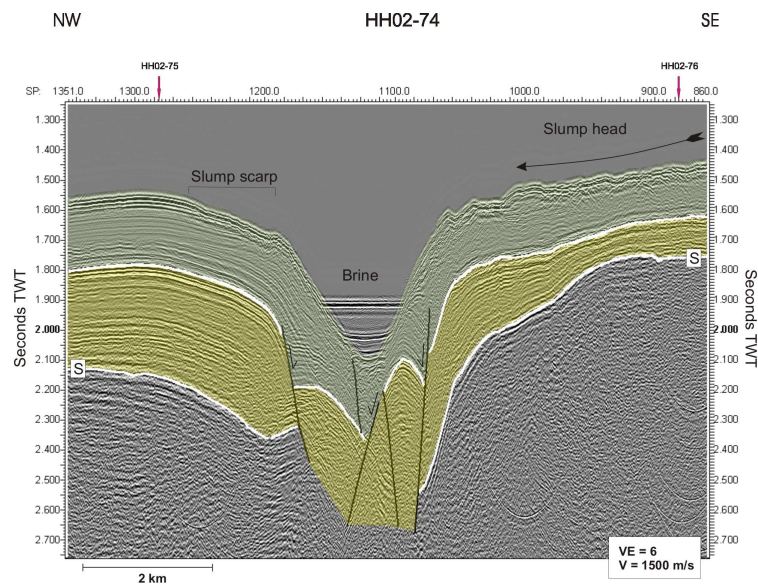


Fig. 6.16: HH02_074, NW–SE cross section (see Fig. 6.8): The slopes of the Kebrit Deep show a continuous subsidence of the entire resolved sedimentary cover, including the evaporites and Plio-Quaternary sediments. Within the Deep, normal faults accommodate the considerable amount of subsidence.

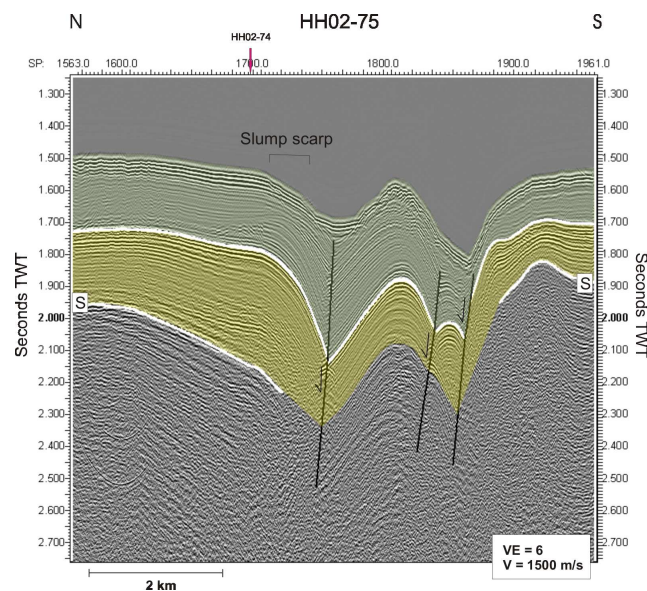


Fig. 6.17: HH02_075, N–S cross section (see Fig. 6.8): The NE-part of the Kebrit Deep reveals huge amounts of Plio-Quaternary sediments. South of the two normal faults the sediments terminate against a high of the S-Reflector.

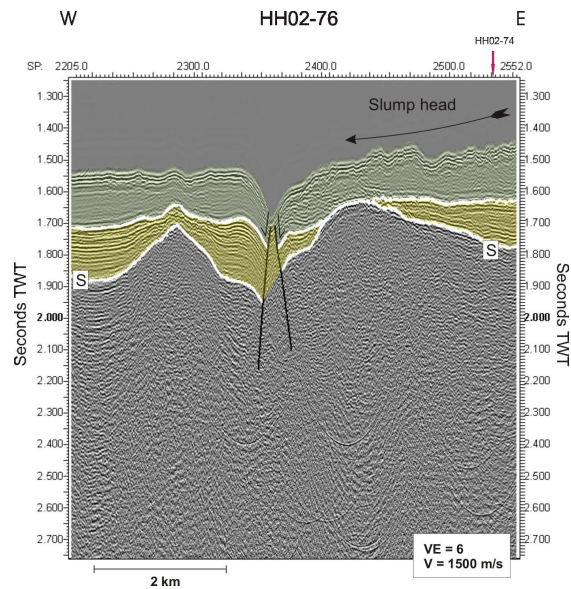


Fig. 6.18: HH02.076, W–E cross section (see Fig. 6.8): The S-Reflector forms a high that is bisected by the N–S trending strike-slip fault. Whereas the Plio-Quaternary cover is layered on the western side, its structure is disturbed by a slump on the eastern side.

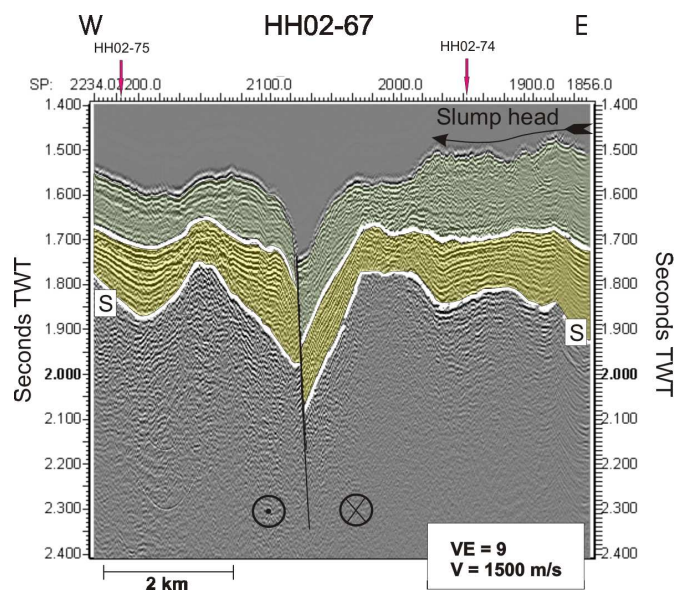


Fig. 6.19: HH02.067, W–E cross section (see Fig. 6.8): The eastern side of the line shows the slump head that terminates close to the strike-slip fault.

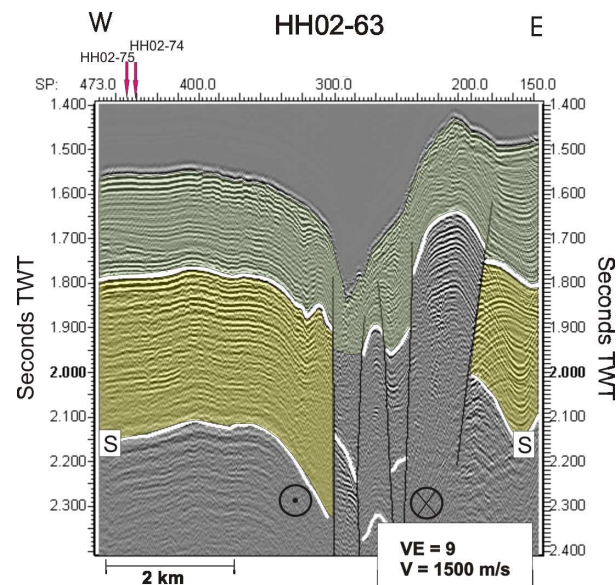


Fig. 6.20: HH02_063, W–E cross section (see Fig. 6.8): A strike–slip fault system separated the eastern and western parts that reveal different inherent structures of the Plio-Quaternary sediments and the S-Reflector.

6.5 Discussion

Using the morphology, internal structure, associated magnetic anomalies and the location of the Deeps, we are able to divide them into two groups, regarding their development. The first group is assembled out of the Conrad- and Shaban Deeps, representing deeps out of the NW–SE segment of the northern Red Sea, and the second is based on the Kebrit Deep that is located in the N–S segment of the northern Red Sea (see Fig. 6.3). The main parameters of the Deeps are summarized in Table 6.3.

6.5.1 Conrad– and Shaban Deeps

Despite the differences in the shape of the individual deeps, the Conrad- and Shaban Deeps have a bunch of analogies:

(a) Both are located in the NW–SE segment of the northern Red Sea, (b) they are affected by magmatic intrusions and extrusions, respectively, (c) the thicknesses of the Plio-Quaternary sequence are similar and (d) faults are present in or around the Deeps. The development of the Conrad Deep has been studied in detail by Ehrhardt et al. (submitted 2004). They correlated the conspicuous

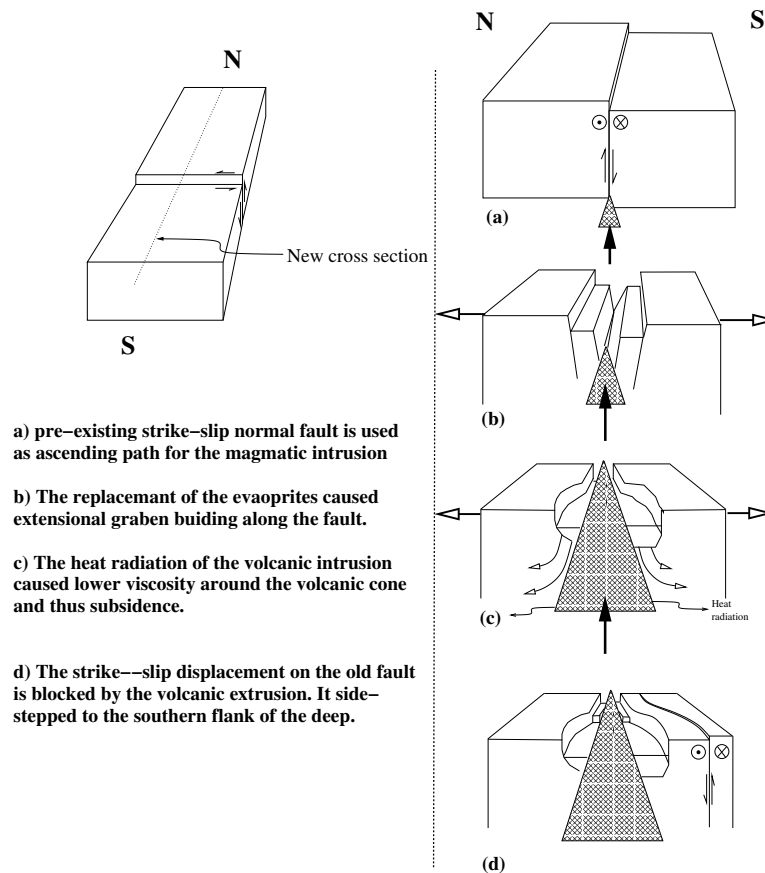


Fig. 6.21: Sketch of the Shaban Deep development: Left hand side: The observation area before the rise of the volcanic extrusion, only affected by the SW-NE fault. Right hand side (New perspective): The rise of the hot magmatic body is the main causative process for the development of the deep. The superposed tectonics are responsible for the fault zones in the south of the basin.

elongated shape of the Conrad Deep with the fact that it is accompanied by two magmatic intrusions, located at the top ends of the Deep. The superposed heat flow that radiated from the intrusions formed an elongated heat flow high between the intrusions where the Conrad Deep developed. The associated reduction of the viscosity of the Miocene evaporites led to a low viscosity zone and, thus, a zone of weakness. Oblique to the strike of this zone the continuous extension of the Red Sea, caused a transtensional regime at the low viscosity zone that led to the opening of the Conrad Deep. As the top of the Miocene evaporites and the Plio-Quaternary sediments reacted in a brittle style, classical pull-apart related structures like the en-echelon distributed pattern of the slope developed and characterize the Conrad Deep.

The Shaban Deep is larger and seems to be further developed than the Conrad

Deep. It is affected only by one extrusion, but this extrusion forms a huge volcano that overtops even the axial depression by about 200 m (Fig. 6.7). This volcano controlled the development process of the Shaban Deep. Additionally, the pre-existing SW–NE trending graben plays a vital part which is depicted in a sketch (Fig. 6.21). The left hand side shows the observation area before the onset of the magmatic activity. The SW–NE orientated fault zone was most probably a strike slip fault with additional normal component (in order to explain the difference in altitude between the northern and southern parts). The right hand side shows a sequence of snapshots that illustrate the development of the Shaban Deep in the successive stages of the ascent of the magmatic body. The intrusion used the pre-existing fault for its rise (Fig. 6.21a). Because of the lateral replacement of the sediments by the magmatic cone, an extensional regime perpendicular to the strike of the fault, i.e. in NW–SE direction was initiated (Fig. 6.21b). The radial heat transfer of the hot magmatic material lowered the viscosity of the surrounding evaporites significantly. In combination with the continuous ascent of the intrusion, the direction of the particle trajectory of the replaced sediments is downward and outward, which led to subsidence of the overburden and to the effective basin formation (Fig. 6.21c). The strike–slip displacement along the pre-existing fault is now blocked by the volcano, thus it is side–stepped to the south around the barrier (Fig. 6.21d). This scenario explains the SW–NE striking fault that is separated from the volcano, the circular shape of the Deep and the faulted SE-part of the survey area. In correlation to the Conrad Deep, the emplacement of magmatic intrusion/extrusion is the main causative process for the basin development.

6.5.2 Kebrit Deep

The Kebrit Deep is not associated by magnetic anomalies and thus most probably neither by magmatic intrusions (Fig. 6.4, Table 6.3). Its internal structure points to a development of the collapse structure type, as already assumed by Bäcker et al. (1975). The most conspicuous difference, in comparison to the other deeps described above, are the smooth and continuously dipping slopes without scarps. The entire Plio-Quaternary sequence and the top of the evaporites are affected by the subsidence. The causative process of the subsidence is linked with subsidence of the Miocene evaporites, because of hydrothermal circulation. A deep reaching fault system like the N–S graben could have initiated the

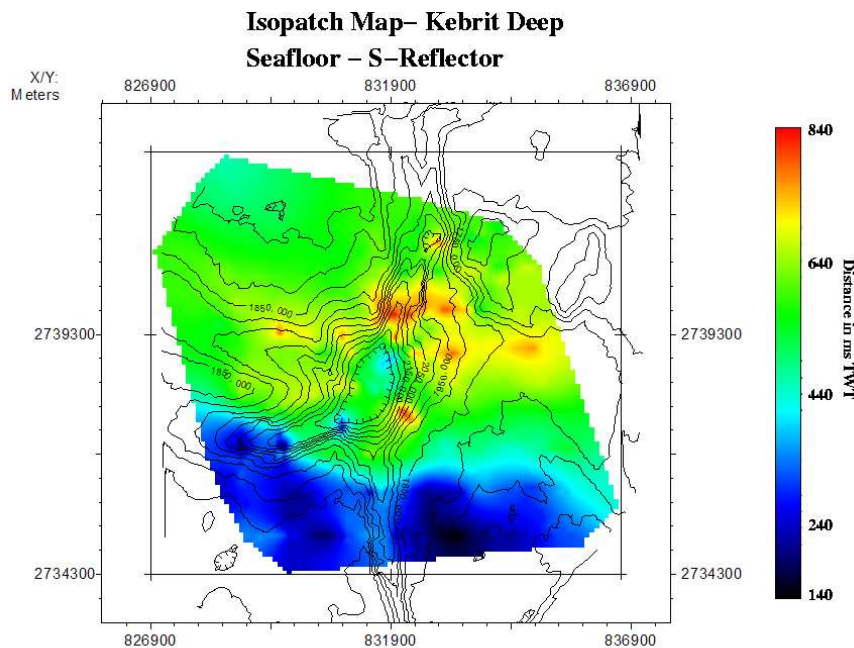


Fig. 6.22: Isopach map of seafloor and S-Reflector in the area of the Kebrit Deep. Note the abrupt thinning of the sediments towards the south. The thickness is given in seconds TWT; for a better orientation, the bathymetric contours are superimposed.

thermal activity. The circulation of sea water dissolved the evaporites beneath the Deep and caused continuous collapsing of the overlying sedimentary cover. Hydrothermal circulation and the absence of a magmatic body is also assumed by Blum and Puchelt (1991) who analyzed the deposits of the Kebrit Deep to be of low temperature origin. These facts point to subsidence as causative process for the development of the Kebrit Deep without any significant alteration of the ductile properties of the evaporites. The location of the Kebrit Deep correlates with several anomalies that could be responsible for the initiation of the hydrothermal circulation and thus the location of the Deep. To the south a high in the evaporites limits the extension of the Kebrit Deep. The isopach map of the Plio-Quaternary sequence shows the discrepancy in the amount of sediments covering the evaporites (Fig. 6.22). This clarifies that the area north of the high developed as a sedimentary basin which is supported also by the divergent reflection pattern in the Plio-Quaternary sequence to the south (Fig. 6.16, 6.17). The eastern boundary of the Kebrit Deep is build out of the N–S trending graben that is most probably formed by a strike–slip fault. The results of the Kebrit Deep point to the fact that, although the development of the deep

is independent from the emplacement of magmatic intrusions, some anomalies are needed to trigger the hydrothermal circulation.

6.5.3 Segmentation controlled development

The investigated Red Sea Deeps were grouped into intrusion related Deeps (Conrad- and Shaban Deeps) and the collapse-type deeps (Kebrit Deep). This classification correlates with the location of the deeps. The intrusion related deeps are settled in the NW-SE segment of the northern Red Sea and the collapse-type Kebrit Deep is representing the N-S segment. The magnetic anomaly map (Fig. 6.4) shows more anomalies in the NW-SE segment, and the anomaly at $26^{\circ}31'/35^{\circ}00'$ is associated with the so far unnamed deep that was mapped by Martinez and Cochran (1988). It is likely that this Deep developed in a similar manner as the Conrad- and Shaban Deeps. The N-S segment does not reveal any significant anomaly that would point to any magmatic activity. This is in agreement with the collapse-type development of the Kebrit Deep. Other deeps, like the Vema Deep that is located at the southern end of the N-S segment (Fig. 6.3) exhibits similar patterns as the Kebrit Deep, like e.g. the scarpless slopes and the continuous dipping sediments (Fig. 4 in Guennoc et al., 1988).

Further to the south, a NW-SE segment adjoins the studied N-S segment. It exhibits well developed ocean deeps as the Nereus Deep that forms already a 40 km long trough with a central ridge from which tholeiitic basalt were recovered (Antonini et al., 1998). This segment comprises deeps that are associated with magmatic activity, like in the northern NW-SE segment, but the deeps are further developed, in agreement with the assumption of a propagating rift from north to south (Bonatti, 1985; Martinez and Cochran, 1988). Thus, a correlation between the type of the deeps with their location exists. Intrusion related deeps seem to be limited the NW-SE segments of the Red Sea.

6.6 Conclusions

The development of the northern Red Sea Deeps was classified into intrusion/extrusion related deeps and collapse type deeps. This classification correlates also with the geographical allocation of the deeps (see Table 6.4). It is

conspicuous that the magmatic activity and thus the development of the intrusion related type of deeps is restricted to the NW–SE segment thus to the segment where the Red Sea extension is normal to the strike of the axial depression. The collapse type deeps were found in the N–S segment, but this type is not necessarily limited to this area as they are only dependent on hydrothermal circulation and this process exists in both segments. The N–S segment is orientated oblique to the Red Sea extension and causes extension and strike–slip displacement (see Fig. 6.23). The significant strike–slip component is probably compensated by the apparent strike–slip fault that crosses the Kebrit Deep. As a matter of fact, the N–S fault reveals no extension. It is reasonable that the extension is compensated by lateral salt flow.

After the classification of the deeps in direct and indirect rift-related structures, it is possible in the next step to extract information about the rift. The NW–SE segment is orientated normal to the Red Sea extension. After the extension was concentrated to the axial depression (Cochran et al., 1991), the NW–SE segment was pierced by magmatic intrusions and Ocean Deeps developed between or around them. This is in agreement with the model from Bonatti (1985)

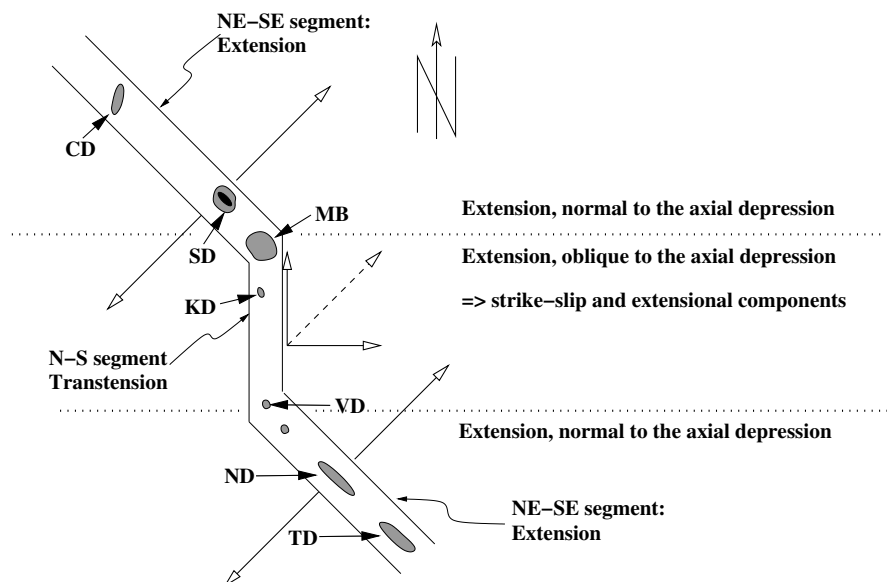


Fig. 6.23: Sketch of the axial depression and Ocean Deeps of the northern Red Sea. The NW-SE segment experiences pure extension normal to its strike. The N-S segment is orientated oblique to the extension between the African- and Arabian Plates, thus it encompasses extension and strike–slip displacement. CD: Conrad Deep, SD: Shaban Deep, MD: Mahahiss Deep, KD: Kebrit Deep, VD: Vema Deep, ND: Nereus Deep, TD: Thetis Deep.

	Magmatic Intrusion	Faulting	Hydrothermal Circulation	Segment
Conrad Deep	Yes between 2 Intr.	Yes Transtension	Yes	NW–SE
unnamed Deep	Yes probab. 2 Intr.			NW–SE
Shaban Deep	Yes, 1 central Intr. 1 central Intr.	local restricted restricted	No, or less	NW–SE
Kebrit Deep	No	less	Yes main process	N–S
Vema Deep	No			N–S

Table 6.4: Correlations of the northern Red Sea Deeps, because of their development and their location within the Red Sea.

who correlated the conspicuous constant spacing of the magnetic anomalies with Raleigh–Taylor instabilities according to density/viscosity inversions in the upper mantle. In contrast, the N–S segment of the northern Red Sea has no prominent magnetic anomaly and seems to be unaffected by magmatic intrusions. It is unlikely that the intrusive bodies are present but have temperatures above the magnetic blocking temperature. Although high heatflow values were reported from the northern Red Sea (Martinez and Cochran, 1989), the temperature rises gently because of the good thermal conductivity of the evaporites ($5.5 \text{ W K}^{-1} \text{ m}^{-1}$) (Cochran and Martinez, 1988). The temperature at the sediment-basement interface is calculated to be about 300°C , using a three layer model and representative parameters for heatflow, thermal coefficient and layer thickness (see also Cochran and Martinez, 1988). The deeps that were discovered so far in the N–S segment have the topographic characteristics of collapse structures caused by subsidence of the Miocene evaporites from below. Probably, the oblique orientation of the N–S segment lowered the effective extension and hinders the emplacement of magmatic intrusions. Thus, the N–S segment as a magmatic ‘passive’ segment may link the magmatic ‘active’ NW–SE segments. As a result of this work, we concluded that magmatic intrusions and extrusions, respectively, do provoke the development of deeps at the surface. On the other hand, collapse type deeps are not linked to magmatic activity and are not limited to the ‘passive’ segments of the Red Sea. This is supported by the existence of the unnamed deep north of the Conrad Deep (Guennoc et al., 1988) that reveals evidence for a collapse type deep. In addition, the processing of the bathymetric

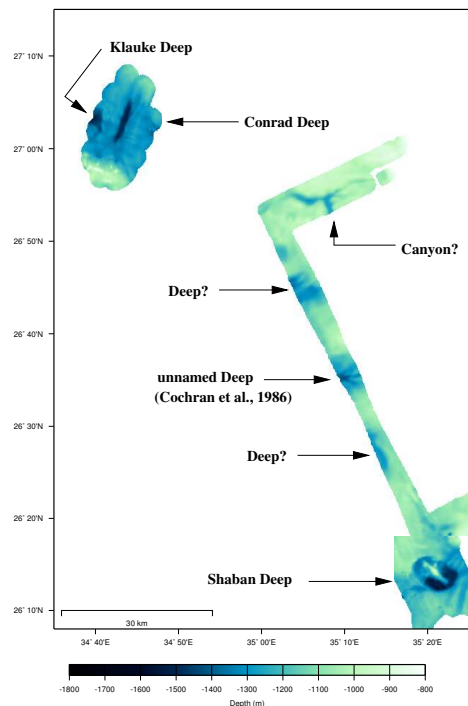


Fig. 6.24: Bathymetric map of the Conrad- and Shaban Deeps extended with the transits of cruise M44/3. Between the Shaban and Conrad Deeps, the location of an already published, but still unnamed deep is confirmed, but other deeper parts that may be parts of more deeps are present.

data of the transits of R/V Meteor cruise M44/3 points to some more deeps in the NW–SE segment as so far known. This map (Fig. 6.24) illustrates the combined swath echosounder data from the cruises M44/3, M52/3 and transits. At 26°35'N/35°11'E the unnamed deep that is already mentioned above could be identified (Cochran et al., 1986), besides other depressions that point to deeps with water depths of more than 1350 m to 1400 m. Not all depressions are associated with magnetic anomalies so that the collapse type is present most probably in the NW–SE segment as well. It is reasonable that deeps are more widespread in the Red Sea as previously suggested. In order to broaden the knowledge of the Red Sea Deeps and their relation to the rifting, extended detailed bathymetric datasets must be acquired and added with seismic sections at crucial locations, as e.g. the different deeps. This would be helpful for the understanding of the Red Sea rifting process and to understand the complex behavior of evaporites in tectonically active regions like as Red Sea.

6.7 Acknowledgements

We would like to thank Jürgen Pätzold (University of Bremen) for providing the bathymetric data. Thanks also goes to Volkard Spiess (University of Bremen) for providing the seismic acquisition equipment and Mohammed Salem (University of Bremen) for editing of the bathymetric data. We would like to thank Klaus Reicherter for his valuable suggestions. We are grateful to the crew of the RV Meteor for the technical assistance provided during cruise M44/3. The interpretation was supported by the utilization of the KingdomSuite – software. All maps were produced with GMT. This work was founded by the German Research Foundation (DFG) grant HU698/4.

7 Summary and Conclusions

During the R/V Meteor cruises M44/3 and M52/3 in 1999 and 2002, the northern Gulf of Aqaba (Elat) and the Conrad-, Shaban- and Kebrit Deeps were investigated by means of 2D multichannel seismic and hydroacoustic data acquisition. In these particular areas, the rifting process between the African- and Arabian Plates has induced the development of basins within the sedimentary infill. In the northern Gulf of Aqaba, the Elat Deep developed as a pull-apart basin, because of a left step over of the left lateral Dead Sea Transform fault. In the northern Red Sea, the Conrad-, Shaban- and Kebrit Deeps developed above the central axis of the Red Sea, where the maximum extension between the African- and Arabian Plates is assumed.

In the following, the main observations of the individual survey areas were summarized briefly. The derived evolutionary scheme will be discussed in the context of its relation to the Red Sea- Dead Sea rift system and the importance of salt layers within the sediments.

Northern Gulf of Aqaba:

Four en-echelon distributed pull-apart basins, the Tiran-, Dakar-, Aragonese- and Elat Deeps form the Gulf of Aqaba, the marine part of the Dead Sea Transform. The Elat Deep is the northernmost deep. North of it, the Gulf's Head constitutes the transition between the marine Elat Deep and the onland Arava Valley. The survey area covers the northern extension of the Elat Deep and the Gulf's Head, including the surficial expression of the left step over of the Dead Sea Transform. The mapping of the fault system and the sedimentary pattern has led to the following results:

- The transition of the surficial branch of the Dead Sea Transform takes place in the Gulf's Head in the southern prolongation of the pre-existing Shlomo Graben. However, the step over is much smoother than expected and forms a continuous strike-slip fault between the eastern side of the Elat Deep and the western side of the Gulf's Head.
- A single branch of the Dead Sea Transform remains on the eastern side, bends to the right and forms a newly discovered thrust fault at the Jordan coast.
- The sediments within the northern Gulf of Aqaba yield two main sedimentary

units, separated by an unconformity representing a major change in the displacement history of the Dead Sea Transform. The lower (prekinematic¹) unit reveals an asymmetric pattern with an inclination towards the eastern (active) side of the Elat Deep. In the Gulf's Head (north of the left stepping Dead Sea Transform) the lower unit shows no asymmetry. The upper unit shows divergent reflection patterns and onlap structures, indicating the synkinematic deposition.

– The pre- and synkinematic sedimentary units dip almost continuously below the Elat Deep, without any major extensional structures. The correlation of these results with published single channel lines south of our survey area lead to the assumption that the pre- and synkinematic units persist below the entire Elat Deep, only separated by one major crossing fault.

As this is not the classical pattern of a pull-apart basin, the observed structures were compared with results of published analogue models. The analogue model setup was designed in order to investigate pull-apart basin development including a special ductile sedimentary bed that forms a décollement layer and decouples the sedimentary overburden from the basement. The good fit between the seismic image of the northern Gulf of Aqaba with the results of the analogue model led to the conclusion that the Elat Deep and the adjacent Arava Valley belong to a common crustal pull-apart basin that is decoupled from the sedimentary overburden, possibly by a salt layer. This crustal pull-apart basin is located below the transition zone at the Gulf's Head, at the southward prolongation of the Shlomo Graben. The décollement layer was not observed within the limits of the seismic signal penetration, but precipitated salt layers are abundant in the Red Sea and Dead Sea areas, so it is conceivable that salt layers exist within the sediments of the Gulf of Aqaba. Thus, the sedimentary basin of the Elat Deep has developed as a consequence of the left step over of the Dead Sea Transform, but does not consequently trace limits and shape of the crustal pull-apart basin.

Northern Red Sea:

The main trough of the northern Red Sea is filled with several kilometers of Miocene evaporites that are covered, in general, by about 200 – 300 m of Plio-Quaternary hemipelagic sediments. The main trough, about 1000 m deep, is bisected by an axial depression that comprises water depths of about 1200 m. The extension between the Arabian- and African Plates is assumed to be con-

¹concerning the latest development of the Elat Deep

centrated to the axial depression. Within that axial depression, several isolated Ocean Deeps with maximum depths of more than 1500 m are partly associated by magnetic anomalies, indicating magmatic bodies that have intruded into the upper crust and into the sediments. The northern Red Sea can be separated into two segments, the northern NW–SE trending segment and the southern N–S trending segment. The Conrad– and Shaban Deeps are situated in the NW–SE segment whereas the Kebrit Deep represents the N–S segment. The Conrad– and Shaban Deeps are associated with magmatic intrusions and extrusions, respectively; the Kebrit Deep shows no indication for magmatic activity in its vicinity.

Of all surveyed deeps the Conrad Deep stands out because of its special elongated shape. It is 10 km long and 2 km wide and strikes in N20°E direction, oblique to the strike of the axial depression. It runs almost parallel to the strike of the Gulf of Aqaba, which is slightly shifted in its NE prolongation. The Conrad Deep is associated with two dipole type magnetic anomalies that are located at the top ends of the Deep. These anomalies were most probably caused by magmatic intrusions ascending along the faulted slopes of the axial depression. The interpretation of the 2D-seismic and hydroacoustic data set led to the following results:

- The Conrad Deep is a composition of two subbasins that were offset to the left. The basins are filled by a newly discovered small brine body.
- The slopes of the Deep are segmented into several N34°E parts that are linked by N–S orientated segments. These segments form an en-echelon distributed pattern.
- West of the Conrad Deep, a second deep was identified for the first time. This Deep was discovered after the combination of published bathymetric data with the recent acquired dataset, and named *Klauke Deep*. The NW shoulder of the Deep reveals a randomly distributed topography, whereas the SE shoulder is characterized by two elongated anticlinals, parallel and subparallel to the strike of the Deep. From our seismic data, these structures were identified as a rise in the Miocene evaporites and a salt wall that pierced the Plio-Quaternary overburden. The subparallel salt wall strikes almost parallel to the expected Red Sea extension and forms a part of the slope of the Deep.
- The Plio-Quaternary sediments that cover the Miocene evaporites have a thickness corresponding to 200 - 300 ms TWT, typical for the Red Sea. They

can be separated into pre- and synkinematic² sedimentary units. According to the thickness of the synkinematic unit in combination with recently calculated sedimentation rates, the onset of the development of the Conrad Deep began 75 000 years ago.

The development of the Conrad Deep is linked with the emplacement of the magmatic bodies at the slopes of the axial depression. This caused a locally limited transtensional regime. The enhanced heat flow radiation of these magmatic bodies has induced heat flow highs around them and between them, where the heat flow was superposed. This formed an elongated heat flow high that fits the position and strike of the recent Conrad Deep. The enhanced heat transfer has reduced the viscosity of the Miocene evaporites significantly and has caused a low-viscosity zone. Because of the oblique orientation of the low-viscosity zone to the Red Sea extension, the transtensional regime has initiated the enhanced subsidence, and thus, the development of the deep. As the top of the evaporites and the Plio-Quaternary sediments reacted brittle to the transtension, the typical pull-apart related structures are found in the area of the Conrad Deep. The Conrad Deep is a basin within the sediments of the Red Sea. It has been formed because of the ongoing Red Sea extension in combination with the emplacement of magmatic bodies that have lowered the viscosity of the evaporites, but it does not necessarily reflect basement structures, as the evaporites decouple the basement from the sedimentary overburden.

The Shaban Deep is located about 100 km southeast of the Conrad Deep within the axial depression. It is accompanied by only one magmatic extrusion, but seems further developed than the Conrad Deep. The following conclusions were derived from the seismic and hydroacoustic data:

- The magmatic extrusion has formed a ridge within the deep that overtops the axial depression by ca. 200 m. It trends parallel to the strike of the axial depression. The volcanic ridge crosses a smaller SW–NE trending ridge. These structures separate the Shaban Deep in four distinct subbasins. In agreement with the general trend, the southern subbasins are significantly lower (and deeper) than the northern basins.
- A SW–NE striking extensional fault runs through the deep, forming the hinge zone between the higher northern and the lower southern parts. As this fault is cut by the magmatic extrusion, it is likely that this fault is a pre-existing

²concerning to the development of the Conrad Deep

structure, pre-dating the development of the Shaban Deep.

– The Miocene evaporites are covered by an amount of Plio-Quaternary sediments corresponding to 200 - 300 ms TWT. The topography of the surrounding is regular with exception of the SE part and the SW–NE trending fault zone. In the regular areas the evaporites terminate against the slopes of the deep, whereas they are bent down in the SE part. This part is affected by a SW–NE trending strike–slip fault, oblique to the extensional fault.

The development of the Shaban Deep has been dominated by the rise of the magmatic body and the formation of the volcanic ridge. Similar to the Conrad Deep, the reduction of the viscosity of the Miocene evaporites caused the faster reaction of the evaporites to the Red Sea extension and the replacement of the material, because of the rise of the magmatic intrusion/extrusion body. The general difference in depth between the northern and southern part of the Shaban Deep point to a pre-existing W–E striking fault that separates the deep. This fault was probably used for the ascent of the magmatic body.

The dense grid of 2D-seismic lines over the Kebrit Deep in combination with hydroacoustic measurements illustrates the topography and the subsurface structure of this area. The following results were derived from this detailed dataset:

– The top of the Miocene evaporites and the Plio-Quaternary sediments dip below the deep, and although the slopes are steep, they do not form escarpment like structures as at the Conrad– and Shaban Deeps.

– The oval shape of the Deep does not show a preferential direction that would point to a tectonic induced development. Hydrothermal circulation is observed at the Kebrit Deep that can cause subsrosion of the evaporites below the Deep.

– Unusually large amounts of Plio-Quaternary sediments cover the Miocene evaporites north of a high of the S-Reflector, about twice the typical amount of sediments compared to other Red Sea regions. Divergent reflection patterns and onlap structures on the S-Reflector high indicate a pre-existing sediment basin that was affected by the subsidence of the Kebrit Deep.

– A N–S trending strike–slip fault runs through the Deep and cuts the Plio-Quaternary sediments and the top of the evaporites. Because the Kebrit Deep is located in the N–S segment of the northern Red Sea, a significant strike–slip displacement must be compensated within the axial depression. This strike–slip fault could be the surficial expression of the displacement.

The Kebrit Deep shows all symptoms of a collapse structure. Affected by hy-

drothermal circulation and the resulting subsidence, the top of the Miocene evaporites and the Plio-Quaternary cover subsides and forms concordantly stratified slopes that dip into the deep. The location of the Kebrit Deep is possibly determined by the coincidence of the sedimentary basin and the N–S strike slip fault. No deep crustal process, like the emplacement of intrusions, could be identified in the area of the Kebrit Deep, thus its presence and location is not directly controlled by the transition of continental rifting to seafloor spreading.

The development of the four studied basins, the Elat Deep in the northern Gulf of Aqaba, and the Conrad-, Shaban- and Kebrit Deeps in the northern Red Sea are related to the rifting between the Arabian- and African Plates. With the exception of the Kebrit Deep, the development of the deeps is a direct consequence of irregularities within the basement. A left step over of the Dead Sea Transform is responsible for the formation of the Elat Deep. Magmatic intrusions into the upper crust and sediments are the causative processes in the northern Red Sea. All basins have in common that they do not necessarily reflect basement structures, but only point to the irregularities in the basement. In all cases, salt³ plays a vital part as a lubricant that decouples the basement from the overburden. Surficial structures in the sediments are thus the consequence of the ductile deformation of the salt layers. It is important to distinguish between surficial structures that have developed because of a direct response to tectonic stress and strain, and indirectly linked structures. The decoupling of the sediments from the basement causes surficial basins, ridges and fault systems that could conceal the underlying geologic stress system. The understanding of the mechanism of detached sediments in tectonic regimes is a precondition in order to deduce crustal structures and dynamics from surficial sediment tectonics. As most of the main tectonic fault zones are covered with sediments, the derivation of models from topographic or bathymetric data is a powerful tool, because exhaustive datasets are available.

The analysis of the four deeps in the northern Red Sea and the Gulf of Aqaba has led to new insights into the status of the rift system. Especially an explanation for the development of surficial basins was provided. In the northern Gulf of Aqaba, the interpretation of the Elat Deep as the conjugate surficial basin to the

³assumed in the northern Gulf of Aqaba

Arava Valley with a common crustal pull-apart basin has severe consequences for the reconstruction of the displacement of the DST. Within this new context less displacement is needed to explain the extension of the Elat Deep.

In the northern Red Sea the Conrad-, Shaban- and Kebrit Deeps were classified into intrusion related deeps and collapse-type deeps. The intrusion related class of deeps (Conrad- and Shaban Deeps) is restricted to the NW-SE segment of the northern Red Sea. The adjacent N-S segment reveals only collapse-type deeps (Kebrit Deep and probably the Vema Deep). Thus, the northern Red Sea could be subdivided into a 'magmatic active' NW-SE segment and a 'magmatic passive' N-S segment. Therefore, the interpretation of the northern Red Sea Deeps allows continuative conclusions about the basement dynamics in this complex area.

This work has shown that the sophisticated analysis of detailed seismic and hydroacoustic data provides information beyond the surficial structural interpretation. The inherent structure of the studied basins has led to conclusions regarding their development and further to evidences regarding the basement dynamics that initiated their formation.

Following this approach, the data base of continuous seismic and hydroacoustic data should be extended in order to enlarge the prospect of success for solving the geological and geodynamical tasks with geophysical methods. It would be a great asset for the research in the Middle East to enlarge the data base independently of political borders. This would open new perspectives to learn more about the unique structural setting of the Red Sea Rift and the Dead Sea Transform Fault.

References

- Abu-Ouf M., Al-Hazmi Y.M., Al-Rousan S., Arz H.W., Donner B., Felis T., Kadi K.A., Kuhlmann H., Lützeler T., Moammar M.O., Moos C., 2000, Meteor Berichte, Cruise No. 44, edited by Pätzold J., Halbach P.E., Hempel G., Weikert H., Leitstelle Meteor, Institut für Meereskunde der Universität Hamburg.
- Arz, H. W., F.P. Lamy, J. Pätzold, P.J. Müller, and M. Prins, Mediterranean Moisture Source for an Early–Holocene Humid Period in the Northern Red Sea, *Science*, 300, 118–121, 2003.
- Alamri, M. A., F. R. Schult, and C. G. Bufe, Seismicity and Aeromagnetic Features of the Gulf of Aqaba (Elat) Region, *Journal of Geophysical Research*, 96, B12, 20,179–20,185, 1991.
- Al-Zoubi, A., and U. S. ten Brink, Salt diapirs in the Dead Sea basin and their relationship to Quaternary extensional tectonics, *Marine and Petroleum Geology*, 18, 779–797, 2001.
- Antonini P., Petrini R. and Cotin G., A segment of seafloor-spreading in the central Red Sea: Basalts from the Nereus Deep (23°00'–23°20'N), *Journ. of Afr. Earth Sc.*, 27, 107–114, 1998
- Bäcker H., Lange K and Richter H., Morphology of the Red Sea central graben between subair island and Abul Kizaan, *Geol. Jahrb.*, D13, 79–123, 1975
- Barjous, M., and S. Mikbel, Tectonic evolution of the Gulf of Aqaba–Dead Sea transform fault system, *Tectonophysics*, 180, 49–59, 1990.
- Bartov, Y., G. Steinitz, M. Eyal, and Y. Eyal, Sinistral movement along the Gulf of Aqaba – its age and relation to the opening of the Red Sea, *Nature*, 285, 220–221, 1980.
- Ben-Avraham, Z., Structural Framework of the Gulf of Elat (Aqaba), Northern Red Sea, *Journal of Geophysical Research*, 90B1, 703–726, 1985.

- Ben-Avraham, Z., G. Almagor, and Z. Garfunkel, Sediments and Structure of the Gulf of Elat (Aqaba) - Northern Red Sea, *Sedimentary Geology*, *23*, 239–267, 1979.
- Ben-Avraham, Z., and Z. Garfunkel, Character of Transverse Faults in the Elat–Pull–Apart Basin, *Tectonics*, *5*, 1161–1169, 1986.
- Ben-Avraham, Z., and G. Tibor, The northern edge of the Gulf of Elat, *Tectonophysics*, *226*, 319–331, 1993.
- Blum N., and Puchelt H., Sedimentary hosted poly-metallic massive sulfid deposits of the Kebrit and Shaban Deeps, Red Sea, *Mineral. Deposita*, *26*, 217–227, 1991
- Bonatti E. Punctiform initiation of seafloor spreading in the Red Sea during transition from a continental to an oceanic rift, *Nature*, *316*, 33–37, 1985
- Christie–Blick, N., and K. T. Biddle, Deformation and Basin Formation along Strike–Slip Faults, *Soc. Econ. Paleontol. Mineral Spec. Publ.*, *37*, 1–34, 1985.
- Cochran J.R., A model for the development for the Red Sea, *Am. Assoc. Petrol. Geol. Bull.*, *67*, 41–69, 1983.
- Cochran J., Martinez F., Steckler M.S. and Hobart M.A., Conrad Deep: a northern Red Sea deep. Origin and implication for continental rifting, *Earth and Planetary Science Letters*, *78* 18–32, 1986.
- Cochran J. and Martinez F., Evidence from the northern Red Sea on the transition from continental to oceanic rifting, *Tectonophysics*, *153*, 25–53, 1988.
- Cochran J., Gaulier, J-M, and LePichon, X, Crustal Structure and the Mechanism of Extension in the Northern Red Sea: Constraints from Gravity Anomalies, *Tectonics*, *10*, 1018–1037, 1991
- Cocherie A., Calvez J.Y. and Oudin-Dunlop E., Hydrothermal activity as recorded by Red Sea sediments: Sr–Nd isotopes and REE signatures, *Marine Geology*, *118*, 291–302, 1994
- Coutelle A., Pautot G., and Guennoc P., The structural setting of the Red Sea axial valley and deeps: implications for crustal thinning process, *Tectonophysics*, *198*, 395–409, 1991

- Courtilot, V., R. Armijo, and P. Tapponnier, Kinematics of the Sinai triple junction and a two phase model of the Arabia–Africa rifting, in *Continental Extensional Tectonics* from Coward, M.P., Dewey, J.F. and Hancock, P.L. (eds), Geological Society Special Publication No.28, 559–573, 1987.
- Ehrhardt A. & Hübscher C., *Meteor Berichte 003*, Cruise No. 52, edited by Pätzold J., Halbach P. E., Hempel G., and Weikert H., 2003
- Ehrhardt A., Hübscher C. and Gajewski D., Conrad Ocean Deep, northern Red Sea: transtension basin within the axial depression, *Tectonophysics*, submitted.
- El-Isa, Z. H., H. M. Merghelani, and M. A. Bazzari, The Gulf of Aqaba earthquake swarm of 1983 January–April, *J.R. astr. Soc.*, 78, 711–722, 1984.
- Eyal, M., Y. Eyal, Y. Bartov, and G. Steinitz, The Tectonic Development of the Western Margin of the Gulf of Elat (Aqaba) Rift, *Tectonophysics*, 80, 39–66, 1981.
- Freund, R., I. Zak, and Z. Garfunkel, Age and rate of the sinistral movement along the Dead Sea Rift, *Nature*, 220, 253–255, 1968.
- Garfunkel, Z., Internal structure of the Dead Sea leaky transform (rift) in relation to plate kinematics, *Tectonophysics*, 80, 81–108, 1981.
- Garfunkel, Z., I. Zak, and R. Freund, Active Faulting in the Dead Sea Rift, *Tectonophysics*, 80, 1–26, 1981.
- Garfunkel, Z., and Z. Ben-Avraham., The structure of the Dead Sea basin, *Tectonophysics*, 226, 155–176, 1996.
- Gaulier J.M., LePichon X., Lyberis N., Avedik F., Geli L., Moretti I., Deschamps A., and Salah Hafez, Seismic study of the crust of the northern Red Sea and Gulf of Suez, *Tectonophysics*, 153, 55–88, 1988
- Gebco, General Bathymetric Chart of the Ocean, <http://www.ngdc.noaa.gov/mgg/gebco/gebco.html>, 2004
- Girdler R.W., Problems concerning the evolution of oceanic lithosphere in the northern Red Sea, *Tectonophysics*, 116, 109–122, 1985

- Girdler R.W. and Styles P., Two Stage Red Sea Floor Spreading, *Nature*, *247*, 7–11, 1974.
- Girdler, R.W., and C. Southren, Structure and evolution of the northern Red Sea, *Nature*, *330*, 716–721, 1987
- GMT–Generic Mapping Tool, <http://gmt.soest.hawaii.edu>
- Guennoc P., Pautot G., and Coutelle A., Surficial structures of the northern Red Sea axial valley from 23°N to 28°N: time and space evolution of neo–oceanic structures, *Tectonophysics*, *153*, 1–23, 1988.
- Hartmann M., Scholten J.C., Stoffers P. and Wehner F., Hydrographic structure of brine–filled deeps in the Red Sea–New results from the Shaban, Kebrit, Atlantis II, and Discovery Deep, *Marine Geology*, *144*, 311–330, 1998.
- Hofstetter, A., Seismic observations of the 22/11/1995 Gulf of Aqaba earthquake sequence, *Tectonophysics*, *369*, 21–36, 2003.
- Horowitz, A., Palynological evidence for the age and rate of sedimentation along the Dead Sea Rift, and structural implications, *Tectonophysics*, *141*, 107–115, 1987.
- Horowitz, A., Palynological evidence for the Quaternary rates of accumulation along the Dead Sea Rift, and structural implications, *Tectonophysics*, *164*, 63–71, 1989.
- Hübscher C., Böke W., Gutowski M., Kästener R., and Salem M., Meteor Berichte 003, Cruise No. 44, edited by Pätzold J., Halbach P. E., Hempel G., and Weikert H., 2000
- Jackson M.P.A. and Talbot C.J., Advances in Salt Tectonics, Chapter 8 in Continental Deformation edited by P.L. Hancock, *Pergamon Press, Oxford, New York, Seoul, Tokyo*, 159–179, 1999
- Joffe S., and Z. Garfunkel, Plate Kinematics of the circum Red Sea – a re-evaluation, *Tectonophysics*, *141*, 5–22, 1987.
- Karaki, N. A., L. Dorbath, and H. Haessler, La crise sismique du golfe d’Aqaba de 1983: implications tectoniques, *C.R.Acad.Sci.Paris, Série II*, t. 317, 1411–1416, 1993.

- Kertz, W. Einführung in die Geophysik I, B.I. Wissenschaftsverlag, 1992.
- Khalek, A., A. Wahed, and A. Sehim, Wrenching Deformation and Tectonic Setting of the Northwestern Part of the Gulf of Aqaba, *Geol. Soc. Egypt, Sec. Publ. No 1*, 409–444, 1993.
- Klinger, Y., L. Rivera, H. Haessler, and J.-C. Maurin, Active Faulting in the Gulf of Aqaba: Knowledge from the M_w 7.3 Earthquake of 22 November 1995, *Bull. Seis. Soc. Am.*, *89*, 1025–1036, 1999.
- Klinger, Y., R. Michel, and J.-P. Avonac, Co-seismic Deformation during the $M_w = 7.3$ Aqaba Earthquake (1995) from ERS-SAR interferometry, *Geophysical Research Letters*, *27*, 3651–3654, 2000.
- Lowell J.D. and Genik G.J., Sea-floor spreading and structural evolution of the southern Red Sea, *Am. Assoc. Petrol. Geol. Bull.*, *56*, 247–259, 1972.
- Makris J. and Rihm R., Shear-controlled evolution of the Red Sea: pull-apart model, *Tectonophysics*, *198*, 441–466, 1991.
- Makris J., Tsironidis J., and Richter H., Heatflow density distribution in the Red Sea, *Tectonophysics* *198*, 383–393, 1991
- Makris J., Henke C.H., Egloff F. and Akamaluk T., The gravity field of the Red Sea and East Africa, *Tectonophysics*, *198*, 369–381, 1991
- Makris J. and Henke C.H., Pull-Apart Evolution of the Red Sea, *Journal of Petroleum Geology*, *15*, 127–134, 1992.
- Manheim F.T., Red Sea geochemistry, in: R.B. Whitmarsh, O.E. Weser, D.A. Ross (Eds.), Initial Reports of Deep Sea Drilling Project, Vol. 23., *US Government Printing Office, Washington D.C.*, 975–998, 1974.
- Martinez F. and Cochran J.R., Structure and tectonics in the northern Red Sea: catching a continental margin between rifting and drifting, *Tectonophysics*, *150*, 1–32, 1988.
- Martinez F. and Cochran J.R., Geothermal Measurements in the Northern Red Sea: Implications for Lithospheric Thermal Structure and Mode of Extension During Continental Rifting, *Journal of Geophysical Research*, *94*, 12239–12265, 1989

- Mart Y. and Hall J., Structural trends in the northern Red Sea, *Journal of Geophysical Research*, 89, 11352–11364, 1984.
- Plate Tectonics of the Red Sea and East Africa, *Nature*, 226, 243–246, 1970.
- Tectonostratigraphic Framework and Hydrocarbon Potential of the Red Sea, *Journal of Petroleum Geology*, 15, 187–210, 1992
- NEIC Earthquake Catalogue, 2004 <http://neic.usgs.gov/>
- Pautot G., Guennoc, P., Coutelle A., and Lyberis N., Discovery of a large brine deep in the northern Red Sea, *Nature*, 310, 133–136, 1984.
- The Elat (Aqaba)–Dead Sea–Jordan subgraben system, *Tectonophysics*, 141, 23–32, 1987
- Pinar, A., and N. Türkelli, Source inversion of the 1993 and 1995 Gulf of Aqaba earthquakes, *Tectonophysics*, 283, 279–288, 1997.
- Quennell, A. M., Tectonics of the Dead Sea Rift, *Int. Geol. Congr.*, 20, 384–405, 1959.
- Reches, Z., J. Erez, and Z. Garfunkel, Sedimentary and tectonic features in the northwestern Gulf of Elat, Israel, *Tectonophysics* 141, 169–180, 1987.
- Rihm R., Die Entwicklung des Roten Meeres abgeleitet aus geophysikalischen Messungen, Hamburger Geophysikalische Einzelschriften, Universität Hamburg, Heft 94, 1989.
- Röser, H.A., A detailed geomagnetic survey of the southern Red Sea, *Geol. Jahrbuch*, 13, 131–153, 1975.
- Sandwell and Smith, http://topex.ucsd.edu/marine_topo/mar_topo.html 1999
- Searle, R. C. and D. A. Ross, A Geophysical Study of the Red Sea Axial Trough between 20.5° and 22°N, *Geophys. J. R. astr. Soc.*, 43, 555–572, 1975.
- Sims, D., D. A. Ferrill, and J. A. Stamatakos, Role of a ductile décollement in the development of pull-apart basins: Experimental results and natural examples, *Journal of Structural Geology*, 21, 533–554, 1999.
- Talbot C. J., Halokinesis and thermal convection, *Nature*, 273, 739–741, 1978

-
- Warren, John, *Evaporites, their evolution and economics.*, blackwell science, 1999
- Wdowinski, S., and E. Zilberman, Kinematic modelling of large-scale structural asymmetry across the Dead Sea Rift, *Tectonophysics*, 266, 187–201, 1996.
- Whitmarsh R.B., Weser O.E., Ross D.A., et al., *Initial Reports of the Deep Sea Drilling Projects, 23B*, U.S. Government Printing Office, Washington D.C., 1974.
- Winckler G., Aeschbach–Hertig W., Kipfer R., Botz R., Rübél A.P., Bayer R. and Stoffers P., Constraints on origin and evolution of Red Sea brines from helium and argon isotops, *Earth and Planetary Science Letters*, 184, 671–683, 2001.

Acknowledgements

I thank Prof. Dr. Dirk Gajewski for the opportunity to do this dissertation, for his support and valuable suggestions.

I would like to thank my supervisor Dr. Christian Hübscher for his steady support and backing through the whole time and his confidence in my work. For his funded and helpful remarks that always showed me the right way and for having good and fruitful times on expeditions and meetings.

I thank Prof. Dr. Dirk Gajewski for the opportunity to do this dissertation, for his support, valuable suggestions and his confidence in my work.

I am grateful for the inspiring cooperation with Prof. Dr. Zvi Ben-Avraham during the work on the Gulf of Aqaba (Elat) data.

I want to express my gratefulness to all members and former members of the Institut of Geophysics of the University of Hamburg, who helped me to get through all this stuff I struggled with.

I owe thanks to Dr. Klaus Reicherter for his valuable support and his nonchalant way to explain complex geologic facts.

I want to thank my family for their support through all the years of my studying and PhD times.

Financial support of this work was provided through the Deutsche Forschungsgemeinschaft (DFG) (Grants HU698-4)